THE UNLUBRICATED SLIDING WEAR BEHAVIOUR OF AUSTEMPERED DUCTILE IRONS

by
E.P. FORDYCE

A Thesis Submitted to the Faculty of Engineering, University of Cape Town for the Degree of Master of Science in Engineering

Department of Materials Engineering, University of Cape Town, November 1988

ACKNOWLEDGEMENTS

I would like to thank the following people who assisted me in producing this thesis.

Professor C. Allen, my supervisor, for his guidance and support in making this project possible.

Mr. B. Greeves for his photographic expertise.

Mr. N. Dreze for his help in the development and building of the testing equipment.

Mr. G. Newins for his help in the machining of the testing specimens.

Mr. D. Dean for his electronic expertise and help in the development of the testing equipment.

Mrs. H. Böhm and Mrs. S. Betz for their help in the preparing the graphics used in the thesis.

Miss U. Scholtz, Mr. J.D. Fordyce and Mr. G. Gatzanis for their assistance in the preparation of this thesis.

I would like to thank the BOART RESEARCH CENTRE for the financial support given for this project.

ABSTRACT

A study has been made of the unlubricated sliding wear behaviour of austempered ductile irons under conditions of sliding velocity and load. The load was varied between 0.9 and 2.8 MPa, whilst the sliding velocity range was between 0.5 and 2.0 ms^{-1}. Two commercial grades of spheroidal graphite irons, SG42 and SG60 were austempered between 250°C and 400°C.

A distinction in the wear behaviour was found with metallic type wear dominating at the lower sliding velocities and an oxidative type wear being evident at the higher sliding velocities. It was however found that an increase in the load resulted in an earlier onset of the oxidative type wear regime, for a specific sliding velocity.

On austempering these spheroidal graphite irons the mechanical properties as well as the sliding wear resistance increased dramatically. Furthermore, the austempered irons outperformed a series of steels of much higher hardness by factors between 2 and 28 times under the same conditions.

At the lower velocity of testing the outstanding wear resistance is attributed to the austempered iron's unique microstructure of acicular ferrite and retained austenite and a partial transformation of austenite to martensite. However, at the higher sliding velocity the exceptional wear resistance is derived from a development of an tribologically protective oxide film together with the formation of a hardened white layer. The development of the work hardened layer is linked to the high carbon in the matrix of these irons. The work hardened layer leads to a similar wear rate prevailing for all irons austempered from a specific parent iron.

The synergism of variation in load, sliding velocity and wear counterface together with the effect of initial microstructure has been explain in terms of simple wear models.

CONTENTS

Chapter I

INTRODUCTION

AIMS AND OBJECTIVES

During the past decade **Austempered Spheroidal Cast Iron or Austempered Ductile Iron** (ADI) has become increasingly important as an engineering material, particularly in the automotive industry [25]. There have been many reported cases where ADI has successfully replaced components such as gears, cams, brake blocks and suspension links. This is not surprising in view of the high strength levels that can be achieved with these materials which range from 800 to 1600 Nmm^{-2} with elongation values of 14% to 1% respectively. Furthermore, large cost benefits can be achieved by reduction in energy output and machineability in addition to producing a lighter end product compared to machined and forged steels.

Prior work has shown that these materials exhibit excellent abrasive wear resistance [62]. However, there appears to be little quantitative work published on the unlubricated sliding wear behaviour of these alloys. This work is an attempt to address this imbalance by examining the dry sliding wear behaviour of two commercial ADI alloys.

The specific aims and objectives of the work were to:-

a. Determine the dry sliding wear resistance of ADI subjected to conditions of varying load and sliding velocity.
b. Analyse the mechanisms of wear which predominate under these conditions.
c. Correlate the wear resistance with surface and microstructural parameters.
d. Compare the performance of ADI to hardened steels.
e. Determine if a correlation exists between the martensitic transformations occurring in abrasive wear and wear subjected to rubbing under unlubricated conditions.

Chapter II

A REVIEW OF AUSTEMPERED DUCTILE IRON

2.1 BACKGROUND ON CAST IRON

Cast iron is defined as an alloy of iron and other elements, chiefly carbon, phosphorus, silicon and manganese. These elements can be present to a total of about 10%, with carbon being the primary alloying element.

Cast iron is a crystalline metal which is easily melted and capable of being cast. Traditionally it is brittle and poor in tension although excellent in compression, being able to withstand crushing loads. In recent years through special treatments cast irons can be produced with one or more of several special properties not present in traditional cast iron.

Several varieties of cast iron can be produced through the selection of different pig irons, by variation of melting conditions and alloying (FIGURE 2.1). There are three main groups, firstly White Irons which have no free graphite and consist of cementite and pearlite, being extremely hard and unmachineable. The second group Malleable Iron, is derived from the first by annealing white iron. Thirdly Grey or Machineable Iron consisting of free graphite in a flake or spheroidal form. This latter iron is known for excellent machineability attributed to the free graphite in the structure.

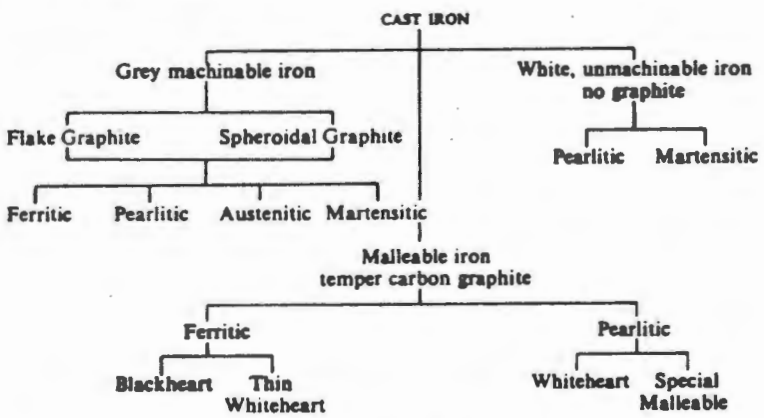

Figure 2.1: The Family of Cast Iron (after Rollason)

The latest addition to the cast iron family has been **Austempered Ductile Iron** (ADI). This iron is derived from the spheroidal graphite grey iron and has a high tensile strength and toughness unlike any of the other cast irons. It is this material on which the present study centres.

2.1.1 Spheroidal Graphite Cast Iron (SGI)

Grey Cast Irons differ from steel in that they always contain carbon precipitates, which takes the form of pure crystalline graphite. Ordinarily the graphite assumes the shape of flakes, but can be modified to form crystallised graphite in the form of spheroids or nodules.

Spheroidal Graphite Cast Iron (SGI) is defined as a high carbon iron-base alloy in which the graphite is present in compact spherical shapes rather than than the traditional flakes. SGI is essentially a ternary alloy of iron, carbon and silicon of near eutectic composition containing carbon in excess of 1.5% (usually in excess of 3%) and silicon between 1% and 4 %.

The importance of the graphite geometry lies in it's ability to resist crack propagation. The flake graphite geometry is such that it acts as a stress concentration, enhancing crack growth and propagation, while the spherical nature of nodular graphite tends to reduce the stress concentration as well as acting as a "crack arrestor" (FIGURE 2.2). The result is a vast improvement in the tensile strength and toughness over that of a normal flake grey iron.

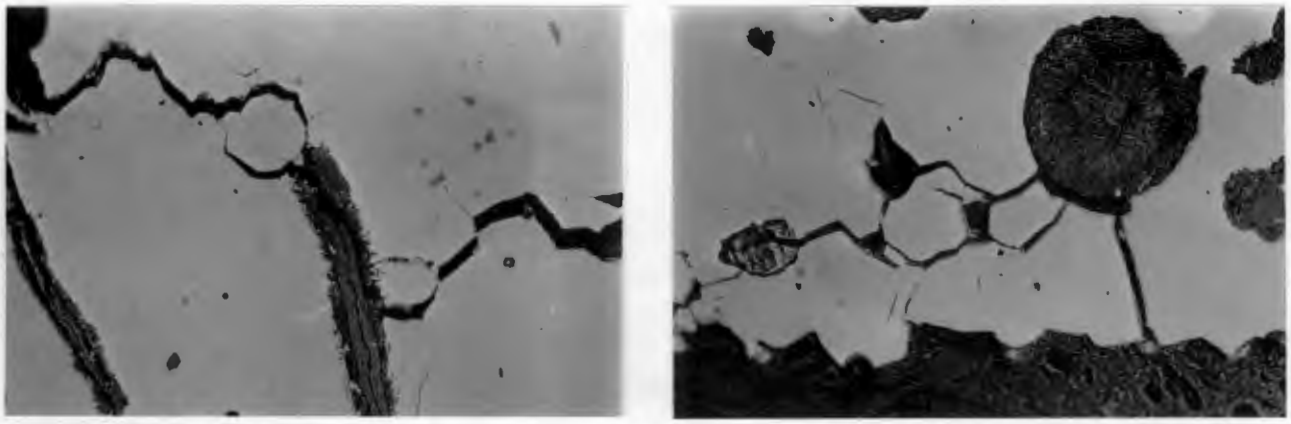

a] Effect of flake graphite in promoting crack propagation.

b] Effect of spheroidal graphite in resisting crack propagation.

Figure 2.2: Effect of Graphite Geometry on the Ability to Promote Crack Growth (after Karsay).

The spheroids are produced by inducing additions of magnesium or cerium to the molten iron prior to casting. This controls the form in which the graphite phase is precipitated during solidification, producing spheroids of free graphite. Since these elements have strong carbide forming tendencies, the silicon content in the iron must be high enough (at least 2.5%) to prevent formation (by chilling) of white iron in thin sections.

The nodule count, i.e. the number of graphite spheroids per square millimetre, is a critical factor in the microstructure. It is the most sensitive indicator of the ductile iron quality. A high nodule count above 100, minimises segregation effects as well as tends to improve tensile strength and elongation. Toughness and fatigue properties are also dependent on the nodule count [25].

2.2 AUSTEMPERED DUCTILE IRON (ADI)

ADI is derived from SGI through an austempering heat treatment. This heat treatment produces a duplex ferritic/austenitic matrix in the iron, which has a high tensile strength with the added advantage of good toughness and ductility.

To ensure successful ADI, the base material SGI must have a high degree of graphite nodulity (min. 80%) and a high nodule count - (min. 100 nodules/mm^2). A high nodule count is an assurance of good properties in the parent material and also reduces solute segregation effects [25].

The significance of ADI as an engineering material can be best viewed when compared with comparative materials (FIGURE 2.3).

Figure 2.3 : Comparison of Properties of ADI (after Forrest)

	CAST IRON				STEEL	
	Malleable Iron	Grey Iron	Ductile Iron	ADI	Forged	Cast
ASTM Specification	A602	A48	A536	-	A290	A27
Tensile Strength MPa	345-724	138-414	380-690	890-1380	552-1172	470-483
Yield Strength MPa	221-586	-	276-483	780-965	310-1000	207-276
Elongation %	10-1	<1	18-3	10-2	22-10	24-22

The above Table clearly illustrates the difference in mechanical properties between the flake and spheroidal graphite irons. It can be seen that the tensile strength of grey iron shows an improvement from 138-414 MPa to 380-690 MPA, and very significant ductility and toughness are achieved as the graphite changes from a flake to a spheroidal form.

Applying an isothermal heat treatment to the SGI, the tensile strength doubles with a slight decrease in toughness. It is important to note that at the same elongation value the forged steel has only a 25% higher strength level. The significance of this emerges when the manufacturing methods and cost factors are considered, revealing ADI to be very competitive with forged steel.

2.2.1 Heat Treatment Of Austempered Ductile Iron

The ADI is manufactured by applying a special heat treatment. To maximise the properties it is important to have an understanding of this process.

2.2.1.1 Austenitisation

The importance of austenitising is that it determines the amount of carbon that can and will be dissolved in the austenite matrix. The greater the carbon content of the austenite, the higher the hardenability and the lower the critical cooling rate to avoid pearlite formation. The carbon content of the austenite also determines how austenite will be stabilised following austempering. The higher the carbon content of the austenite, the greater the depression of the M_s temperature. The M_s temperature can be depressed to well below room temperature resulting in a substantial quantity of austenite being retained on cooling to room temperature [62].

It is important to note that the austempering reaction also affects the carbon content of the austenite. Thus the final amount of carbon in the austenite is dependent on both the austenitising as well as the austempering temperature and time.

Austenitising Temperature

Austenitising is performed in the range of 840-950°C (above the A_{c3}). Harris and Maitland (1970) found that by increasing the austenitising temperature the amount of carbon dissolved in the austenite matrix increases. This resulted in a greater amount of stabilised austenite after a set austempering time [61]. In addition to the carbon content increasing, the austenite grain size also increases, leading to an increased hardenability.

Shepperson (1987) found that the amount of retained austenite in the structure tended to a maximum with increasing austenitising temperature. For the material tested this was found to be approximately 900°C (FIGURE 2.4).

Since Shepperson's work dealt in detail with the effects of the austenitising times and temperatures on similar grades of the SGI as used in this work, particular attention will be given to his results. The two grades being SG42 a fully ferritic matrix and SG60 with a ferritic and pearlitic matrix.

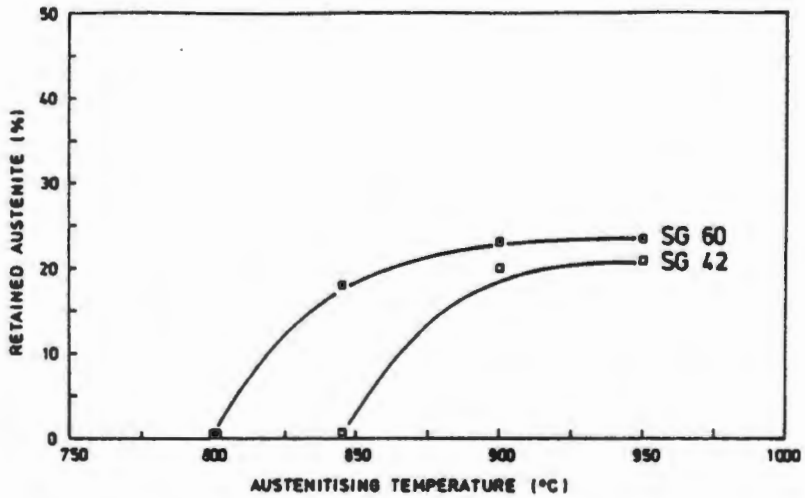

Figure 2.4 : Effect of Austenitising Temperature on the Amount of Retained Austenite, for a Fixed Austenitising Time of 60 minutes and Austempered at 250°C for 30 minutes (after Shepperson).

Austenitising Time

The longer the austenitising time the greater the amount of austenite present in the structure after austempering. This is due to the increase of carbon in the austenite with increasing austenitising time [62].

The diffusion of carbon into the austenite is time dependent and with longer soaking times more carbon is able to diffuse into the austenite matrix. Eventually the carbon saturation will reach a limit. This tends towards a maximum which Shepperson found to be around 60 minutes for the commercial grades he tested (FIGURE 2.5).

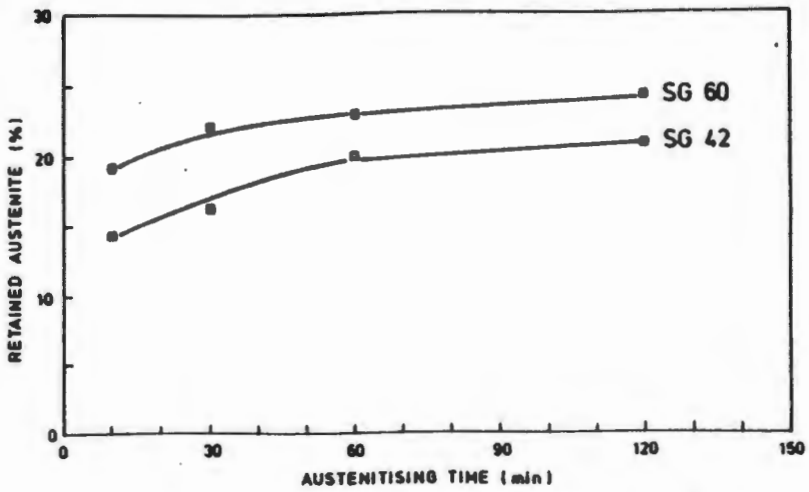

Figure 2.5: The Effect Of Austenitising Time For Two Commercial Grades SGI, Austenitised at 900°C and Austempered at 250°C for 30 minutes (after Shepperson).

2.2.1.2 Austempering

There is a distinct difference between the resulting structures from the austempering process used for steels and for SGI. In steels a complete bainitic structure is produced, whereas in SGI varying quantities of acicular ferrite and austenite are present [31].

Austempering occurs between the temperature range of 205-450°C, i.e. above the M_s and below the pearlite/ferrite formation curve (FIGURE 2.6). The metal is quenched and held isothermally for a predetermined time. The quench must be sufficiently fast so that ferrite and pearlite formation is avoided, while being above the M_s to prevent brittle martensite formation [20].

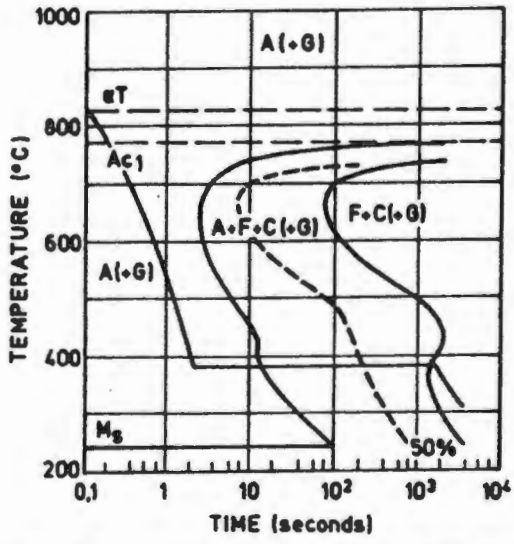

Figure 2.6: Illustration of a Typical Austempering Heat Treatment (after Karsay).

The austempering temperature and time appear to have an important effect on the final nature of the heat treated material. Austempering conditions determine the microstructures, the quantities of stabilised austenite as well as the mechanical properties of the material [63].

Austempering Temperature

Shepperson used a austenitising temperature and time of 900°C and 60 minutes, (this condition allowed satisfactory austenitising) to perform work on the dependence of austempering temperature [62].

Shepperson found that as the austempering temperature is raised from 250°C the amount of retained austenite increased from 15% to a maximum of 45-50% for the grade SG60 at a temperature of 420°C. A similar effect was found for SG42, with a maximum retained austenite content of 35% at 350°C. As the temperature increased above where the maximum austenite content was reached, nodules of fine pearlite started to form at which point the amount of retained austenite tended sharply towards zero (FIGURE 2.7).

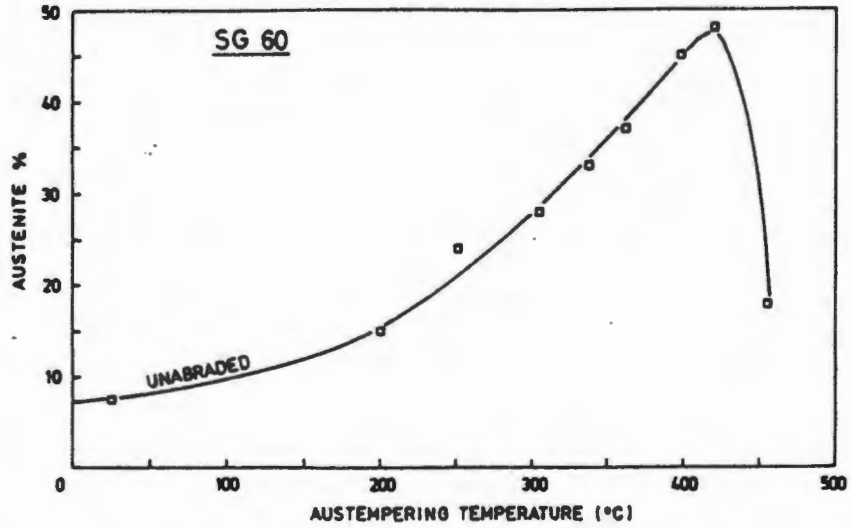

Figure 2.7: Effect of Austempering on Retained Austenite Content for SG60, Austenitised at 900°C for 60 Minutes and Austempered for 30 Minutes (after Shepperson).

Shepperson also noted that as the austempering temperature was lowered, the ferrite plates became finer and more acicular and the amount of retained austenite was lowered with a resultant increase in strength and hardness [62].

Austempering Time

The basic acicular ferrite/austenite matrix is modified for short austempering times by the appearance of fine martensitic needles. The amount of martensite decreases with increasing austempering times. As the length of austempering time increases the volume of acicular platelets increases (FIGURE 2.8). The amount of retained austenite reached a peak after 30 minutes.

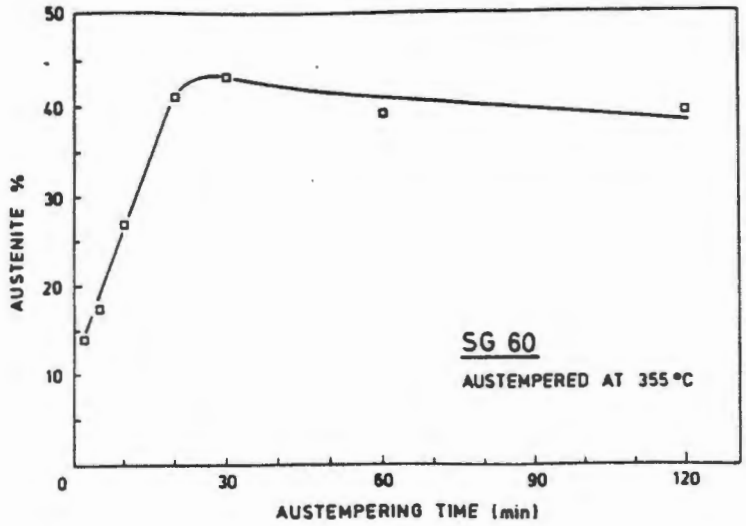

Figure 2.8 : Effect of Austempering Time on Amount of Retained Austenite, Austenitised 900 °C for 60 Minutes (after Shepperson).

2.2.2 Austempering Reaction

The matrix of ADI consist of a two phase mixture of austenite and ferrite. During the austempering process acicular ferrite precipitates and grows into the austenite matrix. This growth is unaccompanied by the formation of cementite (FIGURE 2.9).

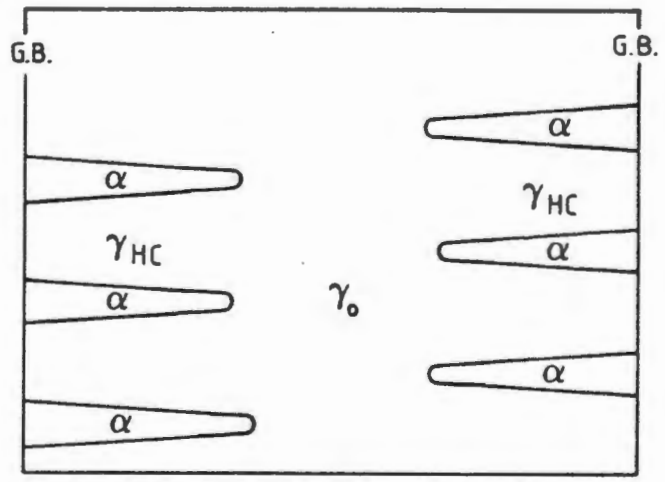

Figure 2.9: Formation of Acicular Ferrite Plate (after Janowak and Grunlach).
Ferrite Platelets (α), *Grain boundary (G.B.), Original austenite* (γ_o) *and High carbon austenite* (γ_{HC}).

The carbon that is rejected from the growing acicular ferrite plates enriches the surrounding austenite. The austenite is able to continue absorbing this carbon due to the high silicon content of the ductile iron. The silicon suppresses the cementite phase associated with bainitic transformation [36].

The richer the austenite becomes in carbon the more inhibited the ferrite reaction becomes until it stops altogether. Johansson (1977) has shown that the carbon content of the austenite can be as high as 2% and that the austenite is stable to below -120°C. At sufficiently long austempering time this austenite breaks down into ferrite and carbides.

The Austempering process can be broken down into two reactions :-

1. The decomposition of the austenite to acicular ferrite and carbon enriched austenite. This reaction is sometimes called the "toughening" reaction due to the high toughness attributed to the austenite/ferrite structure produced.

Heheman reported that the bainitic reaction in high silicon steels is notably different to that of normal steels, in that the ferrite plates are unaccompanied by iron carbide. Hence the term acicular ferrite is used rather than bainitic ferrite or bainite [50].

2. The decomposition of the carbon enriched austenite to ferrite and carbides. This is an undesirable reaction due to the embrittlement caused by the carbides (FIGURE 2.10).

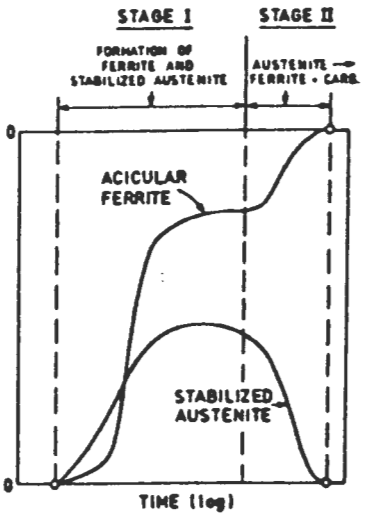

Figure 2.10 : Illustration of the Formation of Ferrite, Austenite and Carbide During Austempering (after Morton).

Reaction 1 : Toughening

$$\gamma_o \rightarrow \alpha + \gamma_{HC}$$

The austempering time and temperature largely determines the morphology of the matrix and the relative amounts of acicular ferrite and austenite present.

The lower range of austempering temperatures (205-350°C) produces a much finer structure. The acicular ferrite needles are finer and closer together (the ferrite/austenite spacing decreases). The higher range of austempering temperatures (350-450°C) produces coarse acicular ferrite needles in the austenite matrix.

Above 350°C the mechanism of transformation changes. Carbon diffusion is more rapid and carbon is therefore able to diffuse out at the growing acicular ferrite plates (FIGURE 2.11), thereby enriching the austenite, especially between the ferrite plates. The level of carbon in the retained austenite will gradually increase and can reach up to 2% [37]. At this level of carbon the ferrite reaction stops and the increase in the carbon content of the austenite serves to stabilise the austenite upon quenching. Retained austenite levels of up to 50% can be achieved.

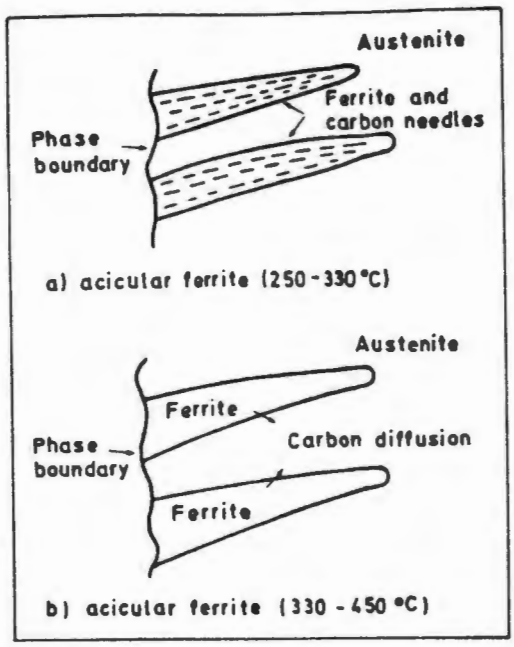

Figure 2.11: Formation of Lower and Upper Acicular Ferrite (after Harding).

If this first reaction is interrupted before the retained austenite is sufficiently stabilised, then there will be martensite in the matrix upon cooling. The martensite affects the properties of iron by increasing hardness but reducing toughness and ductility.

Reaction 2. Embrittlement

$$\gamma_{HC} \rightarrow \alpha + carbides$$

The second reaction is undesirable because it results in embrittlement. The onset of this second reaction occurs if the material is held for long enough at the austempering temperature (FIGURE 2.12). The carbide precipitation takes place in the carbon enriched austenite phase. As the quantity of austenite is lowered, further transformation to acicular ferrite occurs [27]. The microstructure at room temperature will be ferrite plates, carbides and a small percentage of retained austenite.

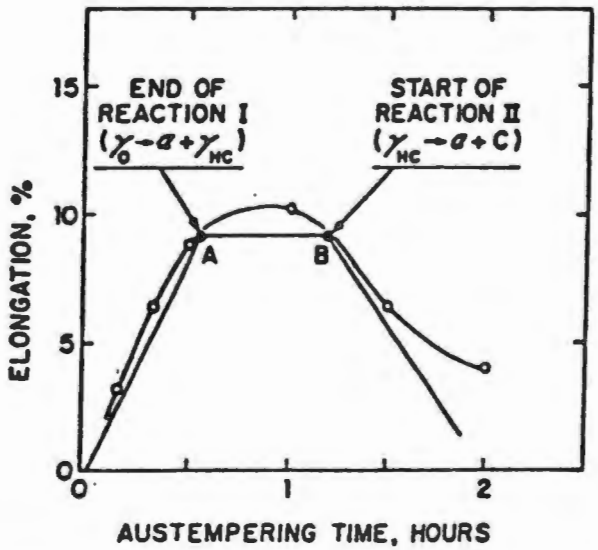

Figure 2.12: Idealised Characterisation of the Influence of the Two Acicular Reactions on Ductility (after Janowak).

2.2.3 Segregation Of Alloying Elements

Segregation of alloying elements during solidification is known to occur in ductile iron. Silicon will segregate to the graphite nodules and therefore it will have a lower concentration at the cell boundary. Manganese and molybdenum have the opposite effect (FIGURE 2.13).

The degree of segregation increases as the section size increases due to slower solidification rate - this creates more time and longer freezing distances for the segregation to occur. Cell boundaries would tend to become rich in carbon, manganese, chromium and molybdenum and low in nickel and silicon.

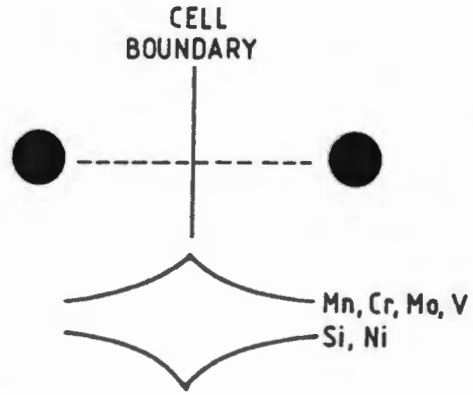

Figure 2.13: Representation of Relative Segregation of Some Elements In ADI (after Forrest).

As manganese is a strong austenite stabiliser, the time for completion of the first reaction would be very long and therefore the bulk of the material would have reached the embrittling stage before the reaction is complete at the cell boundary.

Segregation can therefore seriously limit the commercialisation of the ADI as martensite and/or retained austenite can preferentially occur at the cell boundaries. Mechanical properties would, as a result be significantly reduced (FIGURE 2.14).

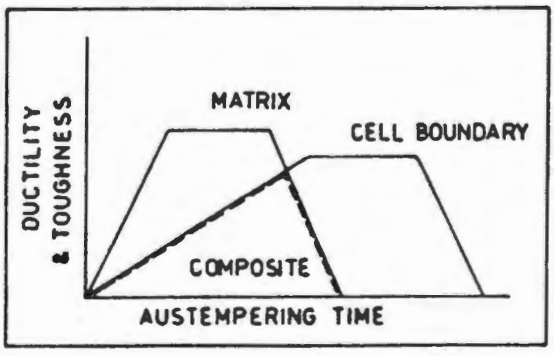

Figure 2.14: Illustration of the Effects of Segregation on the Development of Toughness with Austempering Time (after Forrest).

To try and avoid segregation a high nodule count is required. High nodularity results in a decrease in interdendritic spacing which in turn reduces alloy segregation and it's effects.

2.2.4 Effect Of Elevated Temperature On ADI

In an application of ADI where the structure or component is subjected to some form of heat e.g. a friction wearing process, it is important to know how the structure is going to behave. It is therefore important to have some comprehension of the stability of the acicular ferrite and retained austenite at elevated temperature.

Ishihara conducted tensile tests on one grade of ADI at elevated temperatures of 100, 200, 300, 400 and 500°C. The elongation remained unchanged up to 300°C, while the tensile strength began to lower at 400°C (FIGURE 2.15).

The quantity of retained austenite began to decrease from 300°C and attained 0% at 500°C, although when once heated and cooled, then tested, this change occurred at 400°C and decreased to 0% at 500°C (FIGURE 2.15).

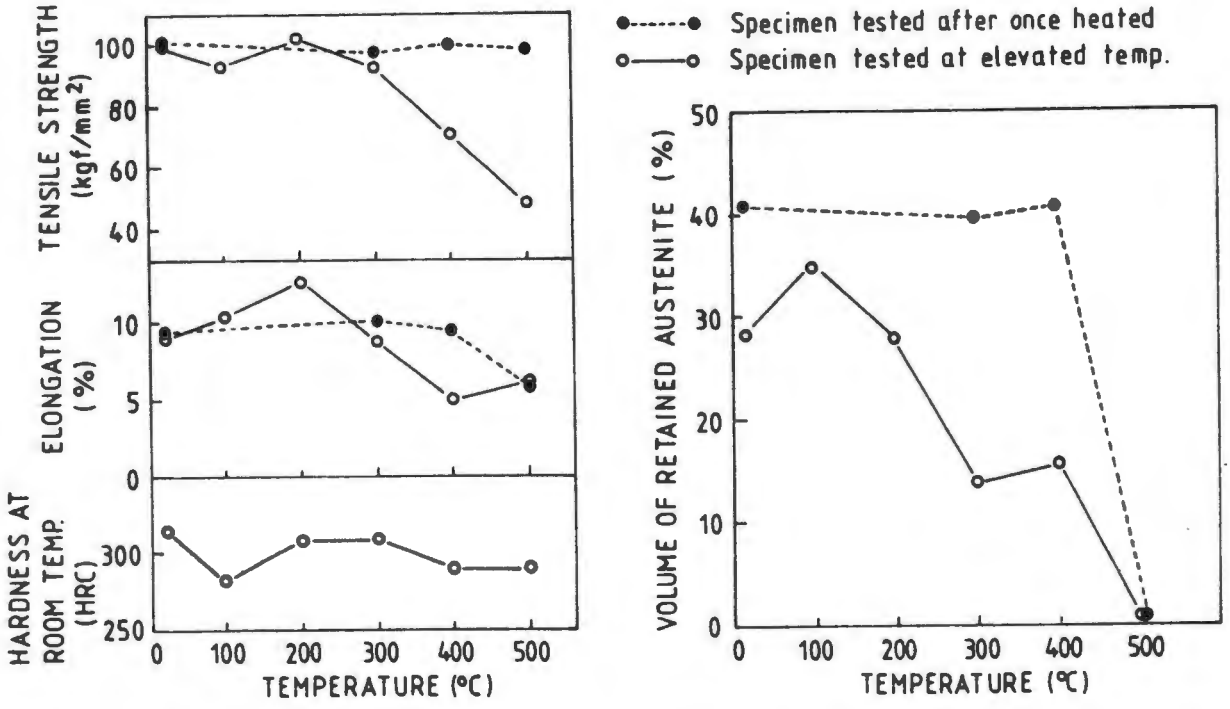

a] Relationship Between Heating Temperature and Mechanical Properties

b] Relationship Between Temperature and Retained Austenite Content

Figure 2.15: The Behaviour of Temperature on the Properties of ADI (after Ishihara).

The decrease in the retained austenite signifies that a transformation has occurred resulting in a different structure. It is supposed that the retained austenite transforms to martensite above 200°C (M_s point 200°C), while the retained austenite transforms to ferrite and carbide above 400°C.

2.2.5 Transformation Effects Of Retained Austenite

Shepperson attributed the high abrasive resistance of ADI to the changing morphology of the ferrite/austenite matrix with austempering temperature, as well as to the high stress that can be accommodated before material is lost from the surface. This capacity for

accommodating strain is provided by the strain associated with the stress induced transformation of the austenite to the martensite, and the high work hardening rate of the resulting product.

Stress induced martensitic transformations have a distinct advantage in improving wear resistance. Shepperson maintains that these transformations lead to high work hardening capacity in the resultant product and a high strain to fracture. The maximum advantage will be gained when an optimum amount of martensite forms during abrasion to give a high work hardening rate. The maximum amount of transformation that can be suffered by the material is dependent on the strain undergone by the material and the maximum martensitic deformation temperature (M_d) at which the transformation of the austenite to martensite can be mechanically induced. The M_d temperature is related to the M_s temperature, which is in turn related to the composition of the austenite.

Two factors appear to be paramount in contributing to the abrasion resistance of the ADI, namely the morphology of the structure and the amount of austenite that transforms during abrasion (FIGURE 2.16). Below 300°C the ferrite/austenite matrix contains fine epsilon carbide and appears to dominate the abrasion resistance. However, above 300°C large quantities of stress induced austenite to martensite transformation occurs during abrasion, which results in a product that is strongly abrasion resistant.

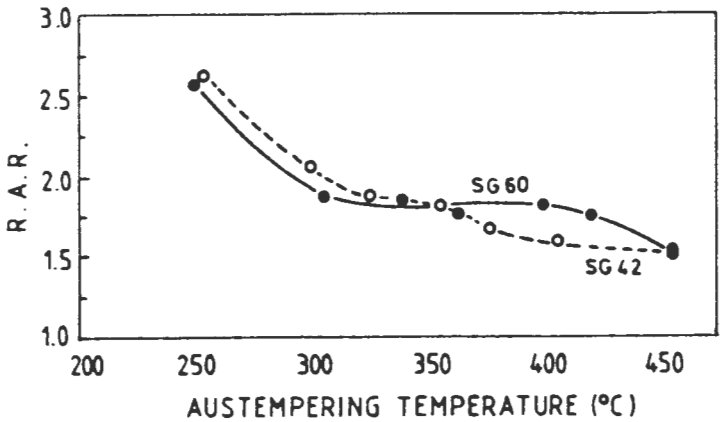

Figure 2.16: The Relative Abrasion Resistance of ADI (after Shepperson).

In this study the grade SG42 was found to be superior to that of grade SG60, despite it's lower hardness and mechanical properties at each austempering temperature. Shepperson attributed the superior wear resistance of SG42 to an increased amount of austenite transforming to martensite.

In spite of both grades having a similar austenite content initially, for a specific austempering condition, SG42 had a 5-10% greater austenite to martensite transformation after abrasion. It was further suggested that this is a result of the M_d temperature of SG42 being higher, resulting in a less stable austenite which more readily transforms to martensite.

This less stable austenite was thought to be related to the austenite in SG42 having a lower carbon content. Thus as the as-cast SG42 has a ferritic matrix, it would be expected to take longer at austenitising temperature to reach a maximum carbon saturation, compared with the iron carbon in the ferritic/pearlitic matrix of SG60.

Chapter III

A REVIEW OF SLIDING WEAR

3.1 INTRODUCTION TO SLIDING WEAR

Sliding wear involves the sliding of surfaces relative to each other. This study of wear is generally termed **Tribology,** and is derived from the Greek word *tribos* meaning rubbing [55]. Hence tribology is defined as the study of the science and technology of interacting surfaces in relative motion.

The interaction of surfaces in relative motion involves a complexity of friction, adhesion, shearing of junctions and the behaviour of the substrate material with possible abrasion by debris. The wear rate and degree of surface damage is a result of a synergism of the above variables influenced by the interaction of the surfaces in relative motion.

Wear is furthermore affected by the chemical composition of the surfaces and the mechanical properties of the surface and substrate material. The effect of oxidation of both surface and debris as well as fatiguing of the surface, have an influence on the interaction between the surfaces.

The frictional forces between sliding surfaces are manifest in the form of plastic and elastic deformation of the surface and subsurfaces [10]. Changes in surface temperatures arising from frictional heating results in changes in the surface and subsurface characteristics. This frictional heat is dependent on the surface topography, thermal conductivity as well as external parameters such as load, speed and atmospheric conditions. Temperature has an influence on the oxidation rate of the surface material in conjunction with its influence on surface and subsurface strength which controls the ability to resist junction shearing.

3.2 MODELS OF SLIDING WEAR

Before examining models of wear behaviour it is necessary to introduce a few concepts in sliding wear :-

Wear

The most general definition of wear is taken as "the progressive loss of substance" from the surface of a body as a result of relative motion at the surface [18].

Real Area of Contact

For contact between two surfaces we must distinguish between the apparent contact area A_o and real area of contact A_r (FIGURE 3.1). The real area of contact is the sum of the separate contact areas at which the asperities are in contact. The surface asperities are solid bodies in static contact that deform elastically or plastically.

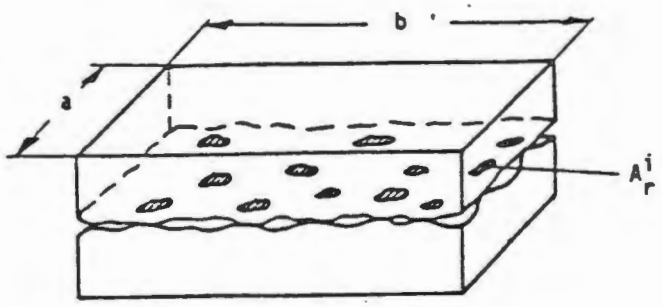

$$A_0 = a \cdot b \gg A_r = \sum_{i=1}^{n} A_r^i \quad \text{(n: number of contacts)}$$

Figure 3.1 : Nominal and Real Area of Contact (after Czichos 1978).

Friction

When sliding two surfaces relative to each other there is a general resistance to this action. This resistance parallel to the direction of motion is the "frictional force".

It is important to note that a distinction in friction exists between the tangential force required to initiate the sliding, "static" (or initial force) and the force required to maintain sliding being the "kinetic" (or dynamic) frictional force (Moore 1972).

The macroscopic frictional force is the sum of all the microscopic forces at the individual contact areas and the energy dissipated may be expressed as the sum of the corresponding elementary dissipative processes. In the different stages of the formation and separation of the micro-contact, the following main processes are involved (Czichos 1978).

1. Elastic asperity deformation
2. Plastic asperity deformation
3. Ploughing
4. Shearing of adhesive junctions

For unlubricated surfaces in relative motion, the different contributions to the overall friction may be broadly classified into two groups :-

1. Adhesion processes
2. Deformation processes

As an approximation friction may be defined as

$$F = F_{adhesion} + F_{deformation}$$

3.2.1 Basic Laws Of Tribology

These laws have been derived as a result of general experience and represent a concise description of the general behaviour of surfaces interacting during sliding. The laws are macroscopic in nature and any hypothesis regarding the interactions of sliding surfaces must satisfy these experimentally based laws [55]. They are generally written in the form:-

1. $F_{kin} \propto W$
2. $\omega \propto W$, *provided the nature of the surfaces does not change*
3. F_{kin} and ω *are independent of the "apparent area of contact"*

Where F_{kin} = *force of friction whilst sliding*

ω = *wear rate*

W = *normally applied load*

wear rate = volume of material removed per sliding distance.

A number of general theories have been proposed to explain the nature of dry friction between metal surfaces (Moore 1972).

Amontons and De La Hire in 1699 proposed that metallic friction could be attributed to a mechanical interlocking of the surface roughness elements.

Tomilison in 1929 and Hardy in 1936 attributed frictional forces to energy dissipation when atoms of one material are "plucked" out of the attractive range of their counterparts on the mating surface.

According to theories of electrostatic forces presented as early as 1961, slip-stick phenomena between rubbing metals can be explained by the initiation of a nett flow of electrons. This produces clusters of charges of opposite polarity at the interface. These charges are assumed to hold the surface together by electostatic attraction.

Welding, shearing and ploughing, being amongst recent theories was proposed by Bowden in 1950. High pressures developed at the asperity contact spots cause localised welding and the junctions formed are subsequently sheared by the relative motion of the surfaces. Ploughing of the softer surface by the harder surface asperities contributes to the deformation component. Thus friction occurs through the asperity interaction and through a dissipative process involving the joining and separation of welded junctions (FIGURE 3.2).

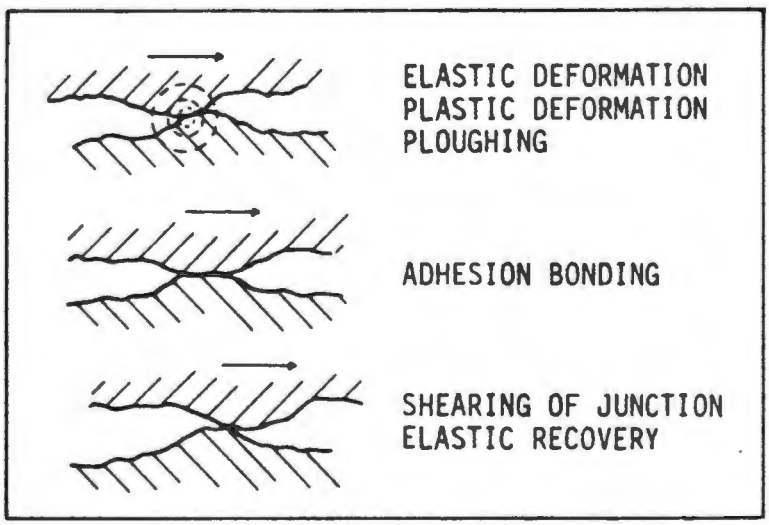

Figure 3.2: A Schematic Representation of an Unit Event in the Friction Process (after Czichos 1978).

The most recent attempts to explain friction have been in two main directions. Bowden has attempted to explain this in terms of a plastic deformation of the surface whilst Archard proposes an elastic deformation hypothesis.

3.2.2 The Plastic Deformation Of Surfaces

The basic deformation hypothesis arose from work performed by Bowden et al. The following is a summary of a review of their ideas regarding friction and wear.

The Area of single Contact

Any hypothesis of friction must take into account that an ideally smooth surface does not exist. There are so called "hills and valleys" which enable only a few contact points where asperities of both surfaces touch.

Considering an idealised contact, a single point of contact of a hemispherical particle against a smooth flat surface [55].

Let E_1 and E_2 be Young's modulus for the asperity and the flat surface respectively. Assume that the flat surface is softer. Apply load W to the asperity so it deforms elastically according to

$$a = 1.1\left\{W\frac{R}{2}\frac{1}{E_1}+\frac{1}{E_2}\right\}^{\frac{1}{3}} \text{----------1.1}$$

a = radius of the circle bounding the region of contact

R = radius of the asperity

From EQUATION [1.1] we can see that the contact due to the elastic deformation only is proportional to $W^{2/3}$ i.e.:-

$$(A_2)_s = \pi a^2 \propto W^{\frac{2}{3}} \text{----------1.2}$$

$(A_2)_s$ = area of a single elastic deformed contact

For plastic deformation hypothesis, we need to know the mean pressure p_m across the interface which is given by :-

$$p_m = \frac{W}{\pi \cdot a^2} \text{----------1.3}$$

and from EQUATION [1.2]

$$p_m \propto W^{\frac{1}{3}} \text{----------1.4}$$

This gives a form of dependence of the mean pressure on the load for complete elastic deformation. According to Timoshenko (1934), if we increase the load until $p_m = 1.1Y$ the elastic limit of the softer material is exceeded and the surface then deforms plastically at a point (0.6a) below the surface. If the load is increased further the material around this point becomes plastic and yields irreversibly until the whole region around the original point of contact deforms plastically. This occurs to such an extent that the new area of contact supports the load. Then

$$p_m \sim 3Y \text{----------1.5}$$

This is the condition for fully plastic flow. Note that p_m is independent of the load once fully plastically deformed, i.e. an increase above $3Y$ will cause the new area of contact to increase such that p_m is constant.

Essentially it is difficult to verify, as the softer material work hardens and Y increases, however, Bowden and Tabor were essentially correct and verified this by using heavily worked flats and steel spheres [12].

The Area of Multiple Contact

Bowden and Tabor (1954) made the following assumptions when relating the single contact model to a multiple contact one :-

a] The theory of a spherical asperity on a flat surface holds true for a case of multiple contacts of asperities of arbitrary geometry.

b] The material around the contacting surface asperities is subjected to stresses well above the elastic limit.

c] The value of p_m for which plastic flow is obtained (for a real surface) is the mean pressure over the deformed areas of contact.

$$p_m = \frac{W}{(A_1)_m} \text{----------1.6}$$

A_1 = Real Area of multiple plastic contacts
m = *multiple contacts*

$$(A_1)_m = \frac{W}{p_m} \text{----------1.7}$$

From EQUATION [1.5] the mean yield pressure p_m of a single point is independent of the load W once plasticity has been obtained. Considering that the assumptions [a] and [b] are valid, then for multiple contacting conditions the real area of contact is inversely proportional to the mean yield pressure of the softer material. Hence when two surfaces come into contact the harder material sinks into the softer material until the real contact area is sufficient to support the load W. Under stationary conditions this entails "cold welding" of the mating materials in contact. Bowden and Tabor maintain that the force required to shear these welded junctions is directly related to the static frictional force, F_{stat} [12].

They also claim that the junctions still weld together when the surfaces are sliding over one another under the normal conditions of sliding contact between specimens.

The force required to maintain a constant sliding speed whilst making and breaking the welded asperities is the kinetic friction F_{kin}, provided one assumes that the force required to "plough" out the softer material ("the plough term") is negligible. This last assumption is probably valid for harder metals.

Then the shearing stress s, is the stress required to shear the welded junctions and hence :-

$$F_{kin} = (a_1)_m s \text{----------1.8}$$

Combining EQUATION [1.8] and [1.9]

$$F_{kin} = W \cdot \frac{s}{p_m} \text{----------1.9}$$

EQUATION [1.9] embodies the empirical laws of friction, namely that friction is proportional to the applied load W and is independent of apparent area of contact. Considering the coefficient from EQUATION [1.9].

$$\mu_{kin} = \frac{F_{kin}}{W} = \frac{s}{p_m} \text{ ---------- 1.10a}$$

i.e.

$$\mu_{kin} = \frac{\textit{shear strength of junction}}{\textit{yield pressure of softer material}} \text{ ---- 1.10b}$$

Since shearing usually takes place in the softer material, Bowden and Tabor suggest that we take s to be the shear strength of the softer material.
Thus we may write

$$\mu_{kin} = \frac{\textit{shear strength of the softer material}}{\textit{yield pressure of softer material}} \text{ ---- 1.11}$$

Note that EQUATION [1.11] is a ratio of two strength properties of the same material. Hence, if the hypothesis is correct one would expect μ_{kin} to be approximately the same for a wide range of materials. In this way Bowden and Tabor are able to explain why μ_{kin} lies within a fairly narrow range for materials; for example metals $0.6 < \mu < 1.2$. They also point out that the shear strength and yield pressure will vary together, as the temperature is raised or lowered, hence one would expect the coefficient would remain constant with changing temperature, a prediction often confirmed by experimentation.

Recent Modifications To Simple Theory Of Friction

Bowden and Tabor (1964)[13] re-examined their assumptions that lead to EQUATION [1.9b]. They maintain that the interface is not usually one between metal and metal and it is incorrect to take the critical shear stress of the underlying material s_m and s_i. This interface may consist of a boundary lubricant, an oxide film, or even some contaminant. Provided that it retains its integrity, they maintain that the following equation is essentially the same as given by EQUATION [1.10b].

$$\mu_{kin} = \frac{\textit{shear strength at the interface}}{\textit{yield pressure of softer material}} \text{ --------- 1.12}$$

When the surface is no longer homogeneous and uniform, i.e. when it becomes damaged, then the situation becomes one in which there is a mixture of contacts between regions where the critical shear stress is s_i (undamaged film material) and where it is s_m (small metallic junctions). It is then not easy to specify the way in which yielding will occur.

3.2.3 The Elastic Deformation Of Surfaces And Relation to Basic Laws

The hypothesis was first made by Archard (1953)[1]. In order to show that the first law of friction ($F = \mu W$) can be explained in terms of complete elastic deformation Archard makes plausible assumptions. These assumptions regard the distribution of contacting asperities and

the application of the theory of single elastic spherical contact on a flat surface. This area of contact has generally been discounted on the grounds that simple contact theory gives the area of contact proportional to $W^{2/3}$ [see EQUATION [1.2]].

This would mean that the kinetic frictional force should also be proportional to $W^{2/3}$ which is in contrast to the direct proportionality of the first law. On the other hand, Archard et al., obtained experimental evidence indicating that the plastic deformation and cold welding hypothesis could not be valid for all conditions of sliding between surfaces.

Archard's Hypothesis On The Role Of Elastic Deformation

Archard (1953) represented a flat multiple contacting surface by means of a reasonably valid but simple model. He assumed that at the lightest loads such surfaces touch over only three small areas. As the load increases these areas increase in size and some of the asperities, hitherto separated, approach and touch to form new areas of contact. It automatically follows that these contact areas have a size distribution. This model shown in FIGURE 3.3 incorporates all these features. It consists of a perfectly flat non-deformable surface and a nominally flat deformable surface containing large numbers of spherical asperities of equal radii of curvature R_1.

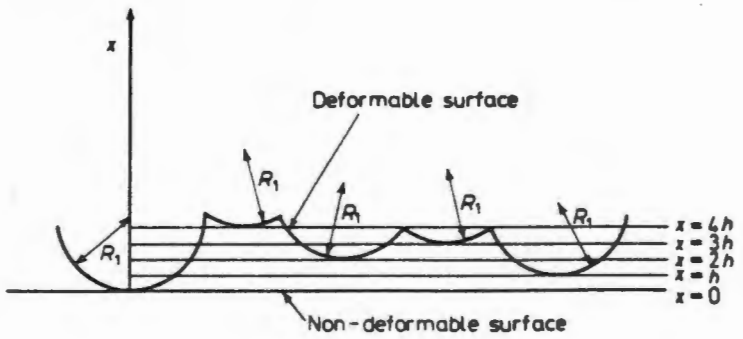

Figure 3.3 : Multiple Area of Contact Model (after Quinn).

It is assumed that the asperities are evenly distributed in depth (in x-direction) i.e. there is one asperity at each x co-ordinate x=0, h, 2h, 3h, ...etc. When a load is applied, the total contact area $(A_2)_m$ resulting from a movement of the non-deformable surface through a distance x = Nh (i.e. such as to bring N asperities into contact) is given by

$$(A_2)_m = \sum_{r=1}^{r=N} \delta A_r \text{ ---------- } 1.13a$$

where δA_r is the contribution to the load contact area formed by multiple contacts which have been deformed elastically. When a spherical asperity of radius R_1 is deformed elastically through a distance rH, the area of contact is given by

$$\delta A_r = 2\pi R_1 r h \text{ ---------- } 1.13b$$

This relation arises from an application of the well know **saggital formula** $(2R_1 - rh)rh = a_r^2$ where $rh \ll 2R_1$ and a_r is the radius of area of contact from EQUATION [1.13a] and [1.13b]

$$(A_2)_m = 2\pi R_1 h \sum_{r=1}^{r=N} r \text{ ---------- } 1.13c$$

For large values of N, EQUATION [1.13c] becomes

$$(A_2)_m = \pi R_1 h N^2 = \frac{\pi R_1 x^2}{h} \text{ ---------- } 1.13d$$

Archard now introduces the number of asperities per unit depth M which is equal to $1/h$, so that EQUATION [1.13d] becomes

$$(A_2)_m = M\pi R_1 x^2 = Bx^2 \text{ ---------- } 1.13e$$

where $B = M\pi R_1$

Using EQUATION [1.1] and an analysis similar to that detailed above, it is possible to deduce an expression for the load $(W_2)_m$ which can be supported elastically by multiple contact area $(A_2)_m$, namely

$$(W_2)_m = 0.86 E R_1^{\frac{1}{2}} M x^{\frac{5}{2}} = C x^{\frac{5}{2}} \text{ ---------- } 1.14$$

where

$$C = 0.86 E R_1^{\frac{1}{2}} M \quad \text{and} \quad E = E_1 = E_2$$

From EQUATION [1.13c] and [1.14] it is possible to obtain a relation between $(W_2)_m$ and $(A_2)_m$ namely

$$(A_2)_m \propto (W_2)_m^{\frac{4}{5}} \text{ ---------- } 1.15a$$

In a later paper, Archard (1957) considered surfaces of increasingly more complex topography. By assuming that each protuberance of radius R_1 in figure [1.1] is itself covered with protuberance of R_2, ($R_2 << R_1$) he showed that the relation between the area of contact and the load which the area was capable of supporting elastically was as follows

$$(A_2)_m \propto (W_2)_m^{\frac{14}{15}} \text{ ---------- } 1.15b$$

By considering that each of the proturberances of radius R_2 was itself covered with a spherical proturberance of radius R_3 , where $R_3 << R_2$. Archard showed that

$$(A_2)_m \propto (W_2)_m^{\frac{44}{45}} \text{ ---------- } 1.15c$$

The more Archard's "flat surface model" approaches the surface revealed by microscopic techniques, the closer the relationship between the calculated area of contact and load approach direct proportionality.

Accepting that the frictional force should always be proportional to the real contact area, then Archard's hypothetical but realistic surface model and analysis leads to the possibility that the frictional force between real surfaces will still be proportional to the load, even if all the deformations were elastic.

3.2.4 Discussion Of The Plastic And Elastic Hypotheses Of Friction

The elastic theory shows that it is possible to explain proportionality between load and frictional force provided an assumption of a realistic surface model is made. It should be noted that the hypothesis assumes that the force of friction is proportional to the real area of contact. According to Archard's hypothesis, the frictional force between sliding surfaces is associated with the energy required to deform the real contact area elastically.

This must be compared with the plastic deformation hypothesis, which says that the force of friction is in part due to the force required to break the welds formed between such surfaces.

Either or both hypotheses, which are probably relevant to explain the frictional behaviour of sliding metal surfaces. The hypothesis depends on the condition of surfaces during sliding, which in turn depends primarily on the way in which surfaces are wearing.

Quinn [55] discusses various conditions for the relevancy of elastic and plastic hypotheses. For instance, under conditions of severe wear, in which rubbing surfaces are metallic and rough and the debris consist mainly of metallic particles, it may be expected that plastic deformation followed by rupture of welded junctions will occur.

Under conditions of mild wear, in which the rubbing surfaces are obviously oxidised and smooth with the wear debris consisting mainly of oxidised particles, the elastic deformation hypothesis could possibly be more applicable.

3.2.5 Archard's Wear Hypothesis

Archard (1953) makes the following assumptions in order to deduce theoretical wear laws from first principles.

i] *multiple areas of contact* : Instead of spherical asperities rubbing on flat surfaces he makes the more realistic assumption that both surfaces consist of spherical asperities with a distribution as shown in FIGURE 3.3. He does not, however, consider the effect of smaller scale protuberances on these asperities.

ii] *Time of contact* (t_c) between mating asperities : Archard assumed that this is the time for two areas forming a fully established circular contact of radius a to move (relatively) such that zero contact area is obtained (FIGURE 3.4). Thus, in the case of a circular contact of radius a the time of contact t_c is given by $2a/V$ where V is the sliding speed. In addition, it is also assumed that a new similar contact of radius a has just become fully established elsewhere on the surface at the time the original contact becomes zero, and so on.

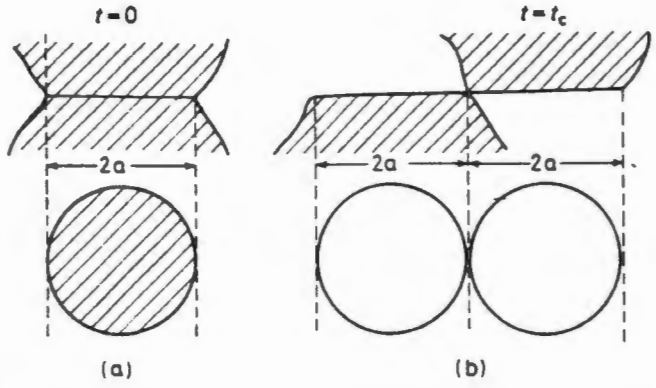

a) Fully established contact *b) Zero contact just attained*

Figure 3.4: Schematic Illustration of an Asperity Interaction

iii] *The shape of the wear fragments* : The volume V of a given wear particle is assumed either to be proportional to the square of the contact radius **a** for layer removal, or proportional to the cube of the contact radius for a lump removal. Thus we have

for layer removal $V = \beta a^2$ ------[1.17]

for lump removal $V = \gamma a^3$ ------[1.18]

where β and γ are constants.

iv] *The probability of forming a wear particle* : This is the most important part of Archard's hypothesis. He suggests that not every contact results in the formation of a wear particle - only a proportion K of the total asperities will do so i.e. $1/K$ total encounters will produce a wear particle.

Using these four assumptions, Archard (1953) was able to obtain a rather complicated expression for the wear rate ω, namely

$$\omega = K\left\{\frac{M}{1+q}\right\}e\left\{\frac{W(1+p)}{Mc}\right\}^{\left(\frac{1-q}{1-p}\right)} \text{----------1.19}$$

where K = proportional constant

W = load

M = number of asperities per unit depth

p, q, e and c are constants dependent on fragment shape and type of deformation

Keeping EQUATION [1.19] in mind, let us first examine the phenomenon of mild to severe wear.

3.3 MILD AND SEVERE WEAR

The overall sliding wear phenomenon may be separated into two regimes, "mild" and "severe" which are not mutually exclusive. It is an experimental fact that wear is either of a "mild" form or of a "severe" form. Archard and Hirst (1956) reported this fact as a result of countless wear experiments with many combinations of materials.

Mild wear leads to severe or metallic wear at higher loads with either a gradual or a sharp transition between them. A reversal from severe wear at even higher loads has also been reported by Welsh (1964). Prior conditioning of the surface through plastic deformation has been observed to affect the mild to severe wear transition. The mild to severe transition has been ascribed to a change from a predominantly elastic to plastic interaction between asperities in sliding contact. The transition from mild to severe wear in air is usually accompanied by a change in the nature of the wear particles from predominantly oxide to metallic with an increase in the roughness of the surface. The oxide is generated through a chemical interaction of the wearing surfaces with the environment (air) and is aided by the high temperature conditions prevailing at the asperity contact regions [55].

3.3.1 Archard's Hypothesis with Relevance to Mild And Severe Wear

Following numerous experimentation, Archard was able to characterise the features of mild and severe wear. These characterisations of mild and severe wear are described in Table 3.0.

Table 3.0: The characteristic features of mild and severe wear (after Quinn).

Feature	Severe Wear	Mild Wear
Type of contact	Metallic (low contact resistance)	Oxide film (high contact resistance)
Surface Topography	Deeply torn	Relatively smooth
Wear debris	Large, metallic particles	Smooth oxide (or oxidised) particles

Examining Archard's Hypothesis [3.2.5] and applying EQUATION [1.19] and setting a number of the variables of this equation, mild and severe wear can be related as follows :-

a) For plastic deformation ; set $p = 1$ and $c = 2\pi R p_m$, where R is the radius of the hemispherical asperities assumed in the simple model of the interacting surfaces and p_m is the flow pressure of the material forming the surfaces (for simplicity both surfaces are assumed to be made of the same material).

b) For elastic deformation ; one assumes that elastic deformation will occur and cause the removal of wear fragments (perhaps a fatigue process), then set $p = 3/2$ and $c = 4.25ER^{1/2}$, E is the Young's modulus for both surfaces.

c) Particle shape ; for layer removal set $q = 1/2$ and $e = R^{1/2}B/2$]
for lump removal set $q = 1$ and $e = R_Y$

Considering the various possibilities in TABLE 3.1.

Table 3.1: Relationship Between Wear Rate and Load (after Quinn).

DEFORMATION	PARTICLE SHAPE	RELATIONSHIP BETWEEN WEAR RATE AND LOAD
Elastic	layer	$\omega \propto W^{\frac{3}{5}}$
	lump	$\omega \propto W^{\frac{4}{5}}$
Plastic	layer	$\omega \propto W^{\frac{3}{4}}$
	lump	$\omega \propto W$

From TABLE 3.0 and 3.1, Quinn (1971) assumed that severe wear occurs by the removal of lumps of plastically deformed material. Mild wear, on the other hand being characterised by smooth often heavily oxidised surfaces, could not be caused by such a drastic process. It seems more probable that mild wear should involve the removal of parts of the surfaces by some elastic fatigue mechanism occurring with each contact. There is plenty of experimental evidence for both types of wear mechanisms.

According to Archard's hypothesis (TABLE 3.0) the mild wear is expected to be proportional to $^4/_5$th power of the load, with the severe wear rate directly proportional to the load. This is not in accordance with the results of Archard and Hirst (1956), who found that both mild and severe wear rates were directly proportional to the load.

Quinn (1971) re-examined Archard's hypothesis and recalled that a very simple distortion of asperity heights was assumed for Archard's model of a wearing surface. It was shown that when one used a more realistic surface geometry (an extension of Archard's (1953) analysis of real area of multiple elastic contact [section 3.2.4]), it was probable that $(A_2)_m \propto W$ for the complex geometry expected from real surfaces. Hence, if a system is probably wearing by some mechanism involving elastic fatigue of the surfaces, it would be expected that the amount of wear ω_2 will be proportional to the real area of multiple elastic contact, $(A_2)_m$ so that

$$\omega_2 \propto (A_2)_m \propto W \text{ ---------- } 1.20a$$

However, if the system is wearing by removal of lumps by plastic deformation, it can be expected that the wear rate ω_1 will be related to the real contact area of multiple plastic contact $(A_1)_m$, which according to [section 3.2.3] is also proportional to the load. So that for this system we have

$$\omega_1 \propto (A_1)_m \propto W \text{ ---------- } 1.20b$$

Thus regardless of whether or not the total area of contact is comprised entirely of multiple elastic or multiple plastic contacts, the wear rate will be proportional to the applied load for both types of contact. Archard in fact proposed this in his equation

$$\omega = K A \text{ ---------- } 1.21$$

where A is the real area of contact, plastic or elastic
and K is the proportion of such contact producing a wear particle

In order to get an "order of magnitude" estimate for K, put $A = W/P_m$ from Bowden and Tabor's plastic elastic deformation hypothesis. This procedure is probably only valid for severe wear. Thus the K-factor for several systems can be calculated, see TABLE 3.2. Note how the K-factor can vary by over 3 or 4 orders of magnitude whilst the coefficient remains relatively constant.

Table 3.2: Wear Rates, Coefficients of Friction and K-Values using a Pin and Ring Wear Machine with Speed 1800 mm/s and 4N Load (after Quinn).

Materials	Wear Rate (10^{-8} mm^3m^{-1})	Coefficient of friction (μ)	K-Factor
Mild steel pin on mild steel ring	1570	0.62	7×10^{-3}
60/40 leaded brass on a tool steel ring	240	0.24	6×10^{-4}
PTFE pin on tool steel ring	20	0.18	2.5×10^{-5}
Stellite pin on tool steel ring	3.2	0.60	5.5×10^{-5}
Polyethylene pin on tool steel ring	0.3	0.65	1.3×10^{-7}

According to Archard (1931), rubbing between two surfaces involves many encounters between protuberances. All these encounters contribute to the friction, but only a small proportion contribute to wear. Friction is therefore dominated by the behaviour of the undamaged contacts and is practically independent of what happens at the small number of encounters contributing to wear. However, this small proportion dominates the wear behaviour; if for example it changes from one in a million to one in a hundred thousand, the wear increases ten fold but the friction is practically unchanged. This theory is consistent with small ranges of friction and the widely varying magnitudes of wear found in wear studies.

3.3.2 Influence Of Load And Speed

Kenridge (1955) and Archard (1957) used a combination of radioactive tracer techniques and conventional methods of wear measurement to follow the history of the wear process.

Kenridge's studies of soft steels sliding against hard steels showed that the initial wear mode was severe and associated with material transfer from the softer to the harder material. The transferred fragments built up an agglomerate film thickness before becoming detached to form a wear particle. All metallic debris produced during the initial stages of sliding was formed in this way. Subsequent stages of sliding consisted of transformation or hardening of the soft steel surface and oxidation of the metallic transfer layer to form a hard protective film. In this stage of wear, debris again originated from the now oxidized layer to be replaced by further transferred material. In contrast to this for hard steel sliding on hard steel little transfer occurred with subsequent abrasive removal of the oxide film leading to low wear rates.

Perhaps the most definitive work in the separating of modes of dry wear of steel was that of Welsh. Welsh produced a series of curves, the general pattern of which bears his name. The curves show that large changes in the wear rate can result from small changes in applied load and sliding speed.

Effect of Load

In FIGURE 3.5 the schematic wear of an annealed carbon steel pin rubbing against a similar material for increasing load is shown. The Welsh curve has three distinct regions apparent, the transitions between these regions have been explained in terms of sub-surface transformations.

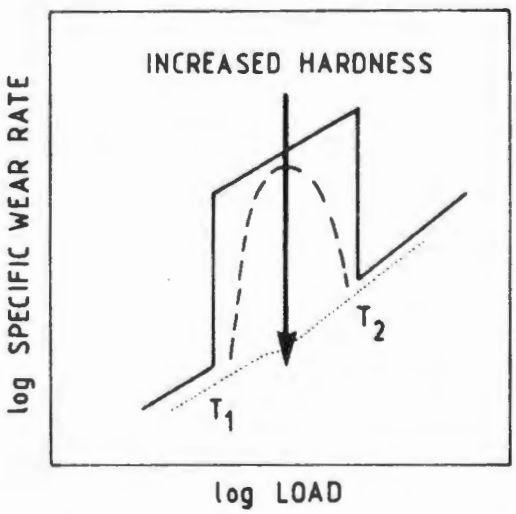

Figure 3.5 : Illustration of the Mild / Severe Wear Transition with Increasing Load.

At loads below T_1 the wear is relatively low, with "mild" wear surface conditions. In the region between T_1 and T_2 the wear rate increases by orders of magnitude, and the surface condition is related to that of severe wear [TABLE 3.1]. In this region plastic deformation

causes the oxide to break resulting in severe wear. Above transition T_2 the surface temperatures are high enough to produce martensitic phase transformation and hence hard surfaces which are capable of supporting the oxide film.

Eyre (1972) confirmed that the temperatures of the asperities were sufficient to cause the steel to change structure and harden, which may mislead workers into believing that they are a necessary prerequisite for oxidative wear. Sullivan cites Athwal in that if the surface temperature is high enough in mild wear of steels, a strong protective oxide film can be formed and maintained without a hard supportive layer. However, if the oxide and metallic layers are well matched the oxide film will be more stable.

A further important result of this work has been the establishment of two critical hardness ranges. The first is a minimum hardness value between 340HV and 425HV which is required to support an oxide film. Secondly, a hardness value of between 550HV and 775HV, where no oxide film is necessary to produce wear rates comparable with mild oxidative wear [65].

Effect of Speed

Fein [5], showed that the regime of severe metallic wear operates over a central range of speeds. At the two extremes of speed the wear rate falls by two orders of magnitude and the mechanism of wear is reduced to mild wear regime.

At the lower speeds this occurs because the time between asperity contacts is sufficiently long to allow the regeneration of the protective oxide film. As the speed increases the time for the asperities to reoxidise is insufficient and a great number of asperity interactions are metallic. At higher speeds the oxide essentially regenerates itself, but in this case it arises from the consequential higher chemical reaction rates due to increased temperatures as a result of increased frictional heating.

In general the severe regime between T_1 and T_2 can be suppressed or eliminated by hardening of the rubbing surfaces (reducing the adhesion effects). This severe wear regime can be brought forward or delayed by altering the speed or partial pressure of the oxygen.

3.4 INFLUENCE OF EXTERNAL PARAMETERS ON WEAR BEHAVIOUR

The effects of wear have been examined in terms of friction arising from elastic and plastic deformation of the interacting asperities, as well as the phenomenon of mild-severe wear. From this we have seen that oxidation as well as temperature plays a major role in the extent of the severity of the wear process. Thus, it is a logical progression to examine these effects.

3.4.1 Oxidation Effects In Sliding Wear

Fink in 1930 published the first paper in which the importance of oxidation in the reduction of wear and friction in the sliding surfaces was recognised. Following this Rosenberg and Jordan (1935), showed that steel exhibited a wear rate in hydrogen which was 50 times greater than in air. They were the first to analyse the wear debris using XRD and found only Iron (Fe) debris in the experiment conducted in hydrogen. In the

experiment conducted in air the debris consisted mainly of oxides haematite (Fe_2O_3) and magnetite (Fe_3O_4). Further observations of oxide films to reduce metallic contact and hence modify friction and wear were reported by Sullivan [65].

Oxidative wear can be classified into two processes namely the formation of oxide at the interface and its separation from the surface. Oxide formation is dependent on both temperature and the partial pressure of oxygen.

Logarithmic oxidation rates usually apply at low temperatures (up to 200-300°C) and the rate governing physical mechanisms are variously described as absorbtion, chemical absorbtion and electric field induced ionic transport [55]. At higher temperatures ionic dissolution rates and diffusion rates through comparatively thick oxide layers lead to parabolic or cubic oxidation kinetics.

With further increase in temperature debonding of the oxide film occurs, probably due to direct coalescence of the oxide/metal interface sometimes leading to linear oxidation rates. It is generally found that as the temperature increases a more rapid oxidation occurs and provided that the oxide film remains adherent to the substrate, the wear resistance increases.

Oxide removal from the surface during oxidative wear has generally been ascribed to the abrasive action of the asperities on an opposite surface as well as the cyclic disruption of the oxide film [42]. Bill (1982) suggests the following factors are important in determining whether the film will inhibit or accelerate wear; adherence of oxide to substrate, mechanical properties of oxide, thickness, rate of growth, composition of oxide film.

3.4.1.1 Mechanisms of Growth of Tribological Oxide Films

A wide number of mechanisms have been proposed for the growth of tribological oxide films and their subsequent removal to form wear particles.

Yoshimoto and Tsukizoe (1957), assumed that an oxide film grows and is removed between each asperity contact and that this is the source of the debris.

Quinn (1962) proposed two mechanisms. Firstly, bulk oxidation occurs at the instant that the "virgin" metal is exposed and that further surface to surface contact causes shearing at the metal/oxide boundary. Secondly, that a critical oxide film thickness is necessary before the film becomes detached to form a wear particle.

Toa (1969) considered two models similar to Quinn, one in which time of oxide growth is negligible compared with the time taken to remove the oxide layer, and a further model where he assumed a gradual growth of an oxide which is only removed when a critical thickness is attained.

Molgaard (1975) also postulated a gradual growth to a critical thickness, but suggested that this thickness is maintained by abrasive removal of the surface oxide film.

Models which suggest the continuous removal of thin oxide layers without the build up of a film of critical film thickness are not supported by experimental evidence, which suggests that the production of a relatively thick oxide or oxidation plateau is necessary if mild wear is to ensure [65].

3.4.1.2 An Oxidational Hypothesis of the Wear of Steels

Quinn [55] in a development of his oxidational wear theory assumed that the second of his proposals is more likely, and developed a hypothesis for the oxidation of surfaces.

This hypothesis arose from a review of the published literature on oxidation of iron and steels, and a similar review of papers in which the wear of iron and steels was described, in which the wear debris had been reliably analysed. It was found (Quinn,1962) that there was a correlation between the temperatures of oxidation indicated by the presence of certain oxides in the wear debris and the temperatures expected to occur at the contacting asperities. This correlation depends on the assumption that the oxidation of a metal surface at a given temperature was the same irrespective of how that temperature arose.

It is expected that a change in oxide results in a change in wear rate characteristics [41]. The presence of wüstite (FeO) in the wear debris was taken to indicate a contact temperature of greater than 570°C, whilst the presence of the spinel oxide (Fe_3O_4) was taken to indicate a contact temperature greater than approximately 200°C, and Fe_2O_3 at temperatures below 200°C [55,41].

Obviously the correlation between calculated and experimentally indicated temperatures was only very approximate, since any calculation showing contact temperatures in the range of 500-1450°C would be comparable with the presence of wüstite in the debris. Similarly, the presence of Fe_3O_4 oxide would be comparable with any calculated contact temperatures in the range 200-1450°C. A much more precise indication of the temperature of the wearing contact is provided by the analysis of the proportions of α-Fe, Fe_2O_3, Fe_3O_4 and FeO in the wear debris.

Having demonstrated the existence of a rough correlation between the wear debris and those oxides expected to be present (according to bulk oxidation experiments), Quinn (1967) proposed the following hypothesis of wear through oxidation. It was assumed that, on average, 1/K asperity encounters are necessary (at a given asperity contact) for a critical oxide film thickness ξ to build up before it became detached to form a wear particle. If τ is the duration of a single wearing contact, then the total time t to produce a wear particle of thickness ξ is given by

$$t = \frac{\tau}{K} \text{----------} 1.22a$$

But $\tau = d/V$, where d is the sliding distance along which a wearing contact is made and V is the sliding speed. Hence

$$t = \frac{d}{VK} \text{----------} 1.22b$$

Now the mass per unit area of oxide growth δm depends on the time of oxidation t through the parabolic relation

$$\delta m^2 = k_p t \text{----------} 1.23a$$

where k_p is the parabolic oxidation rate constant. It is reasonable to assume $\delta m = \xi \rho$, where ρ is the density of the oxide so that we get

$$\xi^2 = \frac{k_p t}{\rho^2} \text{----------1.23b}$$

Eliminating t from EQUATIONS [1.22a] and [1.23b] we get an expression for K, namely

$$K = \frac{dk_p}{V\rho^2\xi^2} \text{----------1.24a}$$

It is now generally accepted (Kubascheviski and Hopkins, 1962) that k, is exponetially dependent on the temperature of the oxidation T_o namely,

$$k = dA_o \exp\left(-\frac{Q}{R_c T_o}\right) \text{----------1.24b}$$

Where A_o is the Arrhenius constant, Q is the activation energy and R_c is the gas constant. Combining equations [1.24a] and [1.24b] and writing T_c (the contact temperature) for T_o, we get

$$K = \frac{dA_o \exp\left(-\frac{Q}{R_c T_c}\right)}{\xi^2 \rho^2 V} \text{----------1.25}$$

In this way, the oxidation hypothesis of the wear of steels leads to a new expression for K in terms of basic material properties ρ, Q, A_o and new microscopic parameters of wear ξ and d, the speed V and T_c.

From EQUATION [1.25] the effect of an increase in the critical oxide film thickness ξ, is that the probability of a wear particle forming is reduced as an inverse square of the thickness. Further more note the importance of temperature in the relationship where an increase in temperature results in an increase in K, although this is minor effect since the film thickness increases with a temperature increase.

3.4.2 Effect Temperature On Wear Behaviour

If sliding wear occurs under atmospherical conditions the temperature affects not only the oxidation of the surface, but the interaction of the contact asperities, the strength of junctions, the ease of formation and destruction of adhesive junctions and debris formation as well as the phenomena of transfer and back transfer are effected.

Previous work done on normal Spheroidal Graphite Irons showed that with an increase in velocity the wear rate increased dramatically and with a further increase in the speed the wear rate decreased, the authors related this to a temperature effect (FIGURE 3.6) [39]. Kawamoto and Okabayshi (1979), defined two temperatures involved in the dry sliding wear process, firstly the mean temperature of the apparent sliding surface area (which is not in intimate contact) and secondly the flash temperature (the temperature at the true area of contact) at the asperities.

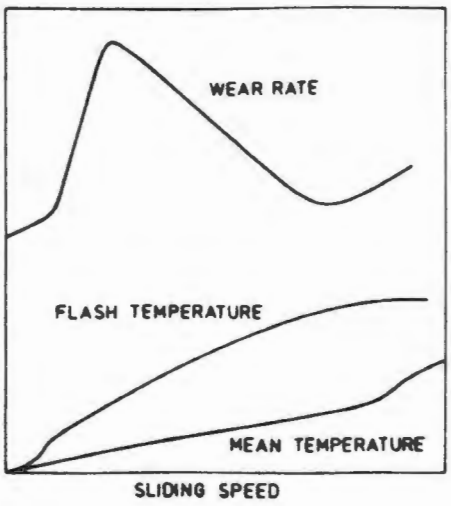

Figure 3.6: The Effect of Temperature on the Wear Behaviour (after Kawamoto).

As the temperature stabilises a limit in the wear rate is reached and in addition the oxidation rate also reaches a constant. Increasing the speed any further will again increase the wear rate, as the time for oxidation to occur decreases. Thus there is less time for asperities to reoxidize and more metal to metal junctions are formed.

Although the above behaviour corresponds to the effects of oxidation on the wear behaviour of the material, it should be noted that temperature affects more than just the friction due to oxidation. The higher temperatures result in the softening of the asperities, the softer asperities deform easier, thus reducing the shear stress as well as increasing the area in contact, both factors reducing wear rates.

Kawamoto (1979), further describes the effect of temperature on the frequency of junction formation and junction strength in relation to the wear rate (FIGURE 3.7).

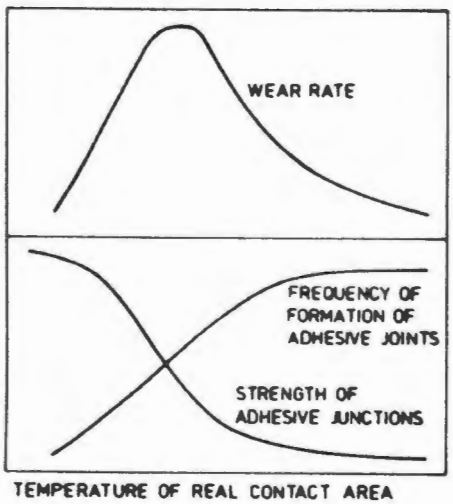

Figure 3.7: The Junction Formation Frequency and Strength (after Kawamoto).

From this it is notable that a maximum wear rate occurs when there is a balance between the strength of adhesive joints and the frequency of formation of adhesive joints i.e. where there is an intermediate number of high strength junctions. A minimum wear rate occurs when there is a large number of weak junctions which reduce the real contact pressure and the required shear stress. An important factor is that although the junctions may be soft and weak, the subsurface material must be strong or else it will result in a higher wear rate.

They further suggest that minimal wear (for cast irons) occurs when the flash temperature is high (in the region of 800°C) and the mean temperature is low (between 200-300°C) i.e. when the interface of contact becomes soft and viscous and the material substrate is kept at a considerable strength. If relative motion occurs only at the interface of the junction, we have a perfect fluid lubrication and wear debris is derived from the transfer of fragments to the mating surface and the peeling-off of fragments from the surface by repeated contact fatiguing. If the mean temperature increases, the substrate becomes weaker and the wear resistance of the material decreases.
A decrease in the flash temperature (in the region of 300-400°C) results in the maximum wear rate, as the asperities are not soft and viscous, thus less asperities are in contact and the lubrication effect of the junction interface does not exist.

It should be noted that as the high flash temperature rise in excess of 1000°C, this high localised temperature produce further effects associated with the formation hard unetched (white) layers on the material surface [39,40].

3.5 VARIABLES IN THE WEAR PROCESS

These are factors which indirectly have a large influence on the wear behaviour. Alongside friction, oxidation and temperature these secondary actions are of major importance in the understanding of dry sliding wear behaviour.

3.5.1 White Layer Formation

The formation of white layers have been mentioned in association with large reductions in wear. The formation of hardened white layers have been reported in many instances; Stead (1912), Trent (1942), Griffiths (1983), Eyre & Baxter (1972), Roger (1969)[65], Allen [8 & 9] and Campany & Wilson (1982).

Although consensus does not exist on the formation of these white layers, they have a number of common features :-

1. They all have hardness values reported between 700 an 1200HV for steels and cast irons. This is far in excess of the hardnesses produced by conventional hardening processes of similar steels.
2. The layers appear amorphous in nature. The structure is very resistant to etching and appears white and featureless under optical examination.
3. They have a high resistance to tempering.

The absence of the acicular morphology normally associated with martensite and the high hardness appear to rule out the possibility of their formation due to normal quenching from austenite.

Rogers [65], described the physical properties of two distinct types of white layers. The first and most common form was termed WII and this was found ón cast iron cylinder liners rubbing against steel surfaces under dry conditions or with a variety of lubricants. It is characterised by the following features :-

1. White, usually featureless appearance when examined optically.
2. The appearance of a thin (10-20 microns) continuous layer having a diffused boundary with the under lying material.
3. A hardness of 700-800$HV_{0.1}$, which gradually decreases with tempering at 300-400°C for 1 hour, at which time tempered carbides are observed to grow within the layer.
4. A structure which when analysed with XRD appears to consist of a mixture of austenite and martensite.

A second form of the white layer WI has also been reported by Rogers on studies of cast iron piston rings, and by Stavitsky & Kogan on steel lubricated with oil. Examples of this layer have been noted only on a few occasions and usually in areas with ready access to carbon. Characteristic properties of this layer are :-

1. An extremely high hardness of 1000-1200$HV_{0.1}$, which does not soften with tempering below 720°C.
2. A completely featureless layer.
3. A distinct boundary with the matrix.
4. It often occurs in isolated patches of 10 microns thick.
5. When analysed with XRD, the structure cannot be indexed according to known patterns.

Campany and Wilson (1982) studied these two distinct white layers with Mossbauer Spectroscopy. They found that the WII revealed a austenite content up to 80% by volume, compared with 5% of the original unworn surface. The original unworn surface contained 95% martensite.

Examining the WI structure using the same technique, they found a large portion of the surface, up to 50%, contained carbides. The austenite content was in the region of 20%.

The suggestion and theories for the formation of these so-called white layers are varied.

Brainin and Seleznoz [65], suggested a mechanism in which diffusion of the carbon to the surface is induced by friction, causing the formation of high carbon martensite. However, Eyre and Baxter (1972) showed that this is unlikely. Electron micrographs and tempering experiments show that the surface is not high carbon martensite. There is general agreement that the properties of the non-etching layers are due to a fine dispersion of second phase particles forming a extremely fine crystalline structure [65].

Theories proposed for the formation of white layers have been divided into three categories Giffiths (1983).

1. A surface reaction with the environment causing nitriding, carburisation or oxidation.

2. Rapid heating and quenching of the surfaces. High localised temperatures 1100°C at surfaces together with a relatively low bulk temperature results in an extremely high cooling rate.
3. Cyclic deformation resulting in a homogenous structure with dispersed carbides

There have been suggestions of high pressures resulting in the formation of white layers [65]. Newcomb and Stobbs (1983)[65] suggest that the white layer is ferrite containing dislocations supersaturated by carbon transferred by the carbides during high pressure pulses near the surface. The dissolution of the carbides in pearlite would produce ferrite supersaturated with carbon, giving rise to deformation twinning.

Eyre and Baxter (1972) suggest that the combined effect of temperature flashes and plastic deformation during asperity contacts would produce the refined structure of martensite. The resultant dislocation substructure would be stable, having been formed at higher temperatures and producing smaller elastic stress fields. In addition to this, dislocations would be pinned by fine carbide precipitates. This pinning would account for the resistance to tempering.

Although no work to-date has been conclusive, it seems most likely that the formation of these white layers is a result of synergistic thermal and mechanical effects.

3.5.2 Effect of Slip-Stick Process

The influence of various tribological processes may lead to the unwanted vibrations of moving parts and to "stick-slip" motion. In any mechanism where the kinetic friction is less than the static there will be a tendency for the motion to be intermittent rather than smooth. The surfaces will stick together until the sliding force reached the static friction value. The surfaces will slip over one another at the lower kinetic friction until once again they stick together [18,53].

The significance of this process in terms of wear behaviour is not only to increase the wear due to higher frictional effects, but the intermittent nature of the process can aid the breakdown and penetration of any protective film formed [53].

3.5.3 Formation Mechanisms Of Debris

The formation of the debris plays an important role in the understanding of the wear process. The resultant geometry of the debris from the wear process plays an important secondary role. It is possible that the harder and more oblique particles might cause secondary abrasive wear effects, whilst uniformly thin flake-like particles might breaking down further and together with further oxidation effects resulting in a coalescence of the oxides.

3.5.3.1 Adhesive Welding and Shearing

When two clean, smooth metal surfaces are brought into contact under load, local welding or adhesion bonding occurs at the tips of the major asperities. The welding process occurs through the action of surface forces, long-range (van der Waals forces) and short-range (metallic, ionic or covalent type) (Czichos,1978).

The strength of the junction formed often has a effect in determining the size and nature of debris formed. It is important to consider the material factors influencing adhesive wear particularly during severe metallic wear.

Material Hardness

In general, a high value of hardness is usually helpful in the reduction of adhesion [5]. Archard suggest that the yield or proof strain of the material, represented by ratio of hardness and Modulus (H/E), is of more significance. However in metals H commonly varies more than E .

Surface Hardness

The hardness of the surface layer which encompasses the majority of the contact stresses is more important than the bulk material hardness [5]. Surface hardening treatments, as well as the development work hardened layers, have been known to reduce the wear by reducing the adhesive bonding [5,26].

Avoidance of Welding

The rubbing of members which are termed compatible should be avoided. For instance, the severity of the wear condition is increased when both members are of a similar material, leading to increased adhesion as a result of increased surface forces [5].

Surface Films

The occurrence of surface films have been known to reduce the adhesive force, by preventing pure metallic contact. In atmospheric conditions, oxide film development plays an important role in the reduction of wear [SECTION 3.2.2]. In grey cast irons the free graphite in the matrix often results in graphite film formation reducing the wear by the action of a film and the inherent lubrication ability of the graphite [47,52,64]. The formation of oxide films in steels and irons are generally known to reduce metallic contact. This aspect will be dealt with at a later stage.

3.5.3.2 Abrasive Effects

In sliding wear this aspect is of importance as a result of direct interaction of asperity ploughing of the softer material by the harder material. In addition to this ploughing effect of the asperities, indirect three body abrasion occurs when large and irregular shaped debris are produced leading to severe metallic adhesive welding and shearing.

Important aspects to consider if debris has secondary abrasive wear effects are:-

Hardness

As the abrasion process is dependent on hardness to a large extent, it would be reasonable to assume that the hardness of the wear particle is a determining factor.

Temperature

At high temperatures, it is likely that the sliding process will deform the particle, rather than the particle cause an abrasive action.

Size and Shape

It is likely that thin and flake-like particles will have little effect on abrading the surface and it is expected that this type of debris will be broken down due to repeated contact. However, it is expected that the angular and less uniform debris formed from welding and shearing will cause secondary abrasive effects due to their geometry. The size of debris also has a significance influence, as small particles below some critical size would be expected to have little effect, irrespective of geometry [60].

3.5.3.3 Delamination Theory and Relevance to Flake-Like Debris

This theory has received much attention and was proposed by Suh [44]. The reason for the interest is the great number of situations where wear particles consist of flakes of material and thus some form of delamination must have occurred. One situation is the removal of an oxide plateaux once a critical thickness has been attained.

The delamination mechanism postulates a coalescence of voids and the propagation of subsurface cracks at a critical depth parallel to and eventually leading up to the surface, resulting in the formation of flake-like debris [42] (FIGURE 3.8).

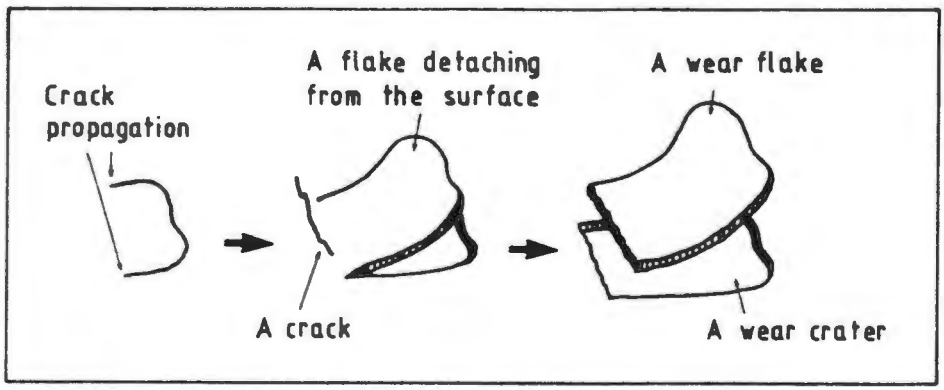

Figure 3.8: A Schematic Representation of the Process Involved in the Formation of Flake-like Debris (after Lim).

Suh [44] assumed that during wear the surface layer of a metal is cold worked less than the sub-surface. This leads to an increase in dislocation density in the sub-surface, the formation of voids and the eventual production of cracks running parallel to the surface. The material between the crack and the surface will then shear and form a wear particle.

Sullivan [66] cites the following, Hirth and Rigney, Rigney and Glaeser and Hsu, Ahn and Rigney for presenting an alternative suggestion for the mechanism of delamination involving crystal plasticity and stacking fault energy.

Kayaba and Iwabuchi (1981) suggest that in delamination wear, flake-like debris is formed according to a process whereby subsurface deformation accelerates crack formation. Kayaba cited Soda stating that the size of fragments are related to the thickness of the plastically deformed substrate layer. Tsuya [66] obtained the result that the site of the crack generated was connected with the thickness of the subsurface fine grain layer. Consequent discussion revealed that the thickness of the debris is related to

the deformed layer. In these cases they considered the surface layer as homogeneity. For oxidative wear, the surface should be regarded as heterogeneity, consistent of an oxide layer and bulk. The delamination theory in this case cannot apply to the formation of a flake-like oxide debris [6].

Suh's [17] delamination theory does not account directly for oxidative wear, but the process could be responsible for the "metallic debris" mechanism, where metallic particles are broken up and reduced in size before becoming oxidised and incorporated into an agglomerate film.

It is thus important to examine the formation of the oxide film as a result of normal film growth and a coalescence of oxidised debris, leading to it's eventual breakdown.

3.6 DEVELOPMENT OF OXIDE FILMS

In the presence of a coherent oxide film the wear rate is known to be reduced. The mechanism of oxide film formation by normal film growth and/or by compaction of oxidised debris leading up to it's eventual breakdown, is of great importance in the reduction of the wear.

3.6.1 Formation And Breakdown Of Compacted Debris

If an oxide is to be protective under tribological conditions it must be compact and non-porous. The conditions for this are stated by the Pilling and Bedworth ratio. These are that

$$\frac{molar\ volume\ of\ oxide}{molar\ volume\ of\ metal} \geq 1$$

For ratio's less than one, the volume of the oxide produced does not compensate for the volume of the metal removed and the film is then porous. If the Pilling Bedworth ratio is greater than one, the oxide film forms in compressive stress. The compressive stresses formed at non-uniform and irregular surfaces increase as the oxide film thickness grows. Thus a critical "film thickness" will be reached when the compressive stresses result in the detachment of the film in these areas [66].

The effect is more pronounced when the oxidation is controlled by anion diffusion. In this case oxide is formed at the metal oxide interface where the expansion of the lattice has the greatest effect on the mechanical integrity of the film.

When cation diffusion predominates, vacancies accumulate at the metal-oxide interface, with the formation of these cavities leading to complete loss of adhesion. In this case lamina removal of the oxide film is more probable than the crazing and cracking which might be expected in anion diffusion controlled oxidation.

Stresses may also develop within an oxide film during heating or cooling due to a difference in thermal expansion coefficients of the metal and oxide.

3.6.2 Relevance to Iron and Steel

When steel or iron oxidises in air the oxide can consist of a multi-layer film of the primary oxides haematite (Fe_2O_3), magnetite (Fe_3O_4) and wüstite (FeO).

Below 570°C iron oxidises to form a two layer film of Fe_3O_4 and Fe_2O_3 with Fe_3O_4 at the interface. Above 570°C the sequence in the film is FeO, Fe_3O_4 and Fe_2O_3 with FeO adjacent to the metal [66]. Mills and Sullivan (1983) found a further constituent in the film; FeOOH, which was found as an outer layer on all oxide particles.

Oxide Critical Film Thickness

In order to assess possible mechanisms responsible for the attainment of critical oxide thickness and subsequent film removal, it is important to consider the properties of these oxide films in relation to each other.

The Pilling Bedworth ratio's for FeO, Fe_3O_4 and Fe_2O_3 are 1.68, 2.10 and 2.14 respectively. Hence all produce compact oxides, the higher the Pilling Bedworth ratio the greater the compressive stresses.

Fe_2O_3 has the highest ratio, but in addition the oxide is produced by anion diffusion. Thus the oxide Fe_2O_3/Fe_3O_4 is formed at the oxide/metal interface and expansion of the lattice is necessary to accommodate growth. The internal compressional stresses will have a more acute effect on the mechanical integrity of the oxide under these circumstances. The stress per unit area produced in this way, increases with increase in film thickness. Thus at a particular thickness the stresses in the film will become sufficient for the loss of adhesion between the film and the metal substrate to occur.

FeO has a relatively low Pillings Bedworth ratio and growth occurs at the gas/oxide interface due to diffusion of cations through the oxide. The combination of these two properties means that the internal stresses in the oxide has little effect on the stability of the film. However, when cations diffusion is responsible for oxide growth, vacancies accumulate at the metal/oxide interface. This results in the formation of cavities which eventually lead to a loss of adhesion.

Fe_3O_4 has growth occurring both by anion and cation diffusion. Hence the oxide film is subjected to the extremes of conditions found in the other two. Thus considering the basic kinetics of formation of these oxides, one would expect Fe_3O_4 to be mechanically more stable.

Oxide Film Thickness in Relation to Tribological Conditions

Goud and Godfrey (1947), Bisson, Johnson and Swibert argue that in the sliding of steel, Fe_3O_4 produces a more protective film than Fe_2O_3, resulting in lower wear rates.

Available evidence on the protective properties of the high temperature oxide FeO is contradictory. Bisson, Johnson and Swibert and Cornelius and Roberts (1961) found FeO to be protective, where and Hurricks (1974) found a distinct increase in wear between 500°C and 600°C where FeO became predominant.

Under static conditions the thickness of the oxide is limited by the various factors discussed above, however, such films grow substantially thicker than those in tribological situations before becoming detached.

Thermal Stress

According to Oxx (1958) a differential thermal effect for these iron oxides would produce relatively negligible stresses for large temperature differences. However, it is possible that if these stresses are very localised, high forces could be produced.

Overall it is probable that differential thermal contraction is not a major factor in limiting film thickness and producing oxide detachment, particularly in Fe_3O_4 and Fe_2O_3.

A fact that supports this view is that the oxide thickness increases with increase in both load and surface interface temperature differentials.

Mechanical Stress

It has been shown that the detachment of the film is not thermally induced. Hence it is most likely that it is due to a mechanical process. The most probable mechanism responsible for delamination of the film to form a lamina wear particle is a fatigue process [41,44,65].

Sullivan [66] supposes that continued cyclic stress due to asperity contact leads to a dislocation build up at the natural boundary between metal and oxide. This leads to delamination and removal of the oxide.

With increasing temperatures and loads, it might be expected that plastic flow within the oxide at the interface could relax some of the internal stresses produced and so allow thicker films to form [66].

Thus it would be expected that the oxide film grows and reaches a critical film thickness due to a combination of growth laws and mechanical effects.

3.7 THE CONNECTION BETWEEN DRY AND LUBRICATED WEAR

The function of a lubricant is, firstly, to prevent direct interaction between surfaces and secondly to provide an easily sheared interfacial film and finally, to carry away heat involved in lubricated asperity contacts.

Unless the surfaces are in relative motion an oil film cannot generally support the load between the surfaces. Furthermore, only when fitted with a copious oil supply will it dissipate heat.

Whenever a system is started from stationary contact the surfaces are in direct contact until the speed has reached the value necessary for oil to support the load. Thus, there exists conditions which are very similar to "dry" running at the start. Most of the solid lubricants such as graphite and molybdenite satisfy the primarily aims of a lubricant with the exception of heat dissipation at all times.

In order to get all three conditions satisfied in the some system, a mixture of solid and liquid lubricant is often used. However, all forms of lubricant can be made to fail provided the conditions of loading, speed etc. are made severe enough. The point when a particular lubricant will fail can only be satisfactorily found out by systematic testing under closely simulated running conditions in the laboratory. Quite often the form of this failure will be catastrophic; e.g. pitting or scuffing or even seizure [55].

Investigation of failures has lead to the conclusion that they originate from failure at one small region of the surface. Normally, some form of fatigue process is said to be the cause of the failure, especially in the case of rolling contact. Similar fatiguing (due to cyclic changes in the thermal and mechanical stresses at a particular contact) must also occur during 'dry' sliding wear whether the motion be sliding, rolling, or a combination of both.

The main difference between the two types of surface failure lies in the fact that a direct surface contact occurs at each cycle of unlubricated contact. This is in contrast to the situation of lubricated contact in which most of the fatigue stresses are transmitted through the thin oil film. It is relevant to note that most real surfaces have a contaminant film of some sort, generally an oxide film, which can often act as a lubricant, if only as an extremely inefficient one. Hence even in the case of a nominally unlubricated ("dry") wear, we have to deal with an interposing film [5].

Wear studies are more likely to discover the causes of high friction and heavy wear in a particular lubricated system. Studies must then first be concentrated on the nominally lubricated behaviour of that system. One hypothesis of "dry" wear involves the disintegration of the oxide film due to possible fatigue cracks originating in the sub-surface material. This is not very different from the fatigue process envisaged for lubricated rolling.

In summary it has been shown that nominally unlubricated ("dry") sliding or rolling is not fundamentally different from lubricated sliding or rolling. To achieve a better understanding of the wear process, the simplicity of testing in important to obtain a initial fundamental understanding. For this reason dry sliding wear test are performed to gain an initial understanding, although the final objective must be the understanding of sliding wear under lubricated conditions.

Chapter IV

EXPERIMENTAL PROCEDURES

4.1 MATERIAL

Two grades of commercial spheroidal cast iron were chosen for this work namely; SG42 with a fully ferritic matrix and SG60 with a ferritic and pearlitic matrix. A high quality iron was ensured by having a high nodule count of in excess of 110 nodules/mm^2.

The composition of the SG Irons and the two steels used for comparative purposes are given in TABLE 4.1.

Table 4.1 :Chemical Composition of Materials Tested

Material	C	Si	Mn	S	P	Cr	Ni	Mo	Cu	Mg
Steel A BS817M40	0.38	0.1	0.71	-	-	0.99	1.45	0.29	-	-
Steel B	1.15	0.17	0.35	0.045	0.045	0.46	-	-	-	-
SG42	3.7	2.2	0.1	0.02	0.05	-	-	-	-	0.37
SG60	3.6	2.1	0.25	0.05	0.05	-	-	-	0.80	0.03

4.2 SAMPLE PREPARATION

The specimens used for testing were machined from cast ingots to a size 20mm long and 6.35mm diameter. Four austempering conditions were chosen for each parent spheroidal graphite iron while for comparative purposes three oil quenched and tempered conditions for Steel B were chosen. Sliding wear tests on the heat treated materials were conducted on two different bases, an oil quenched SG60 iron ($610HV_{30}$) and a hardened steel A ($630HV_{30}$). The material conditions are listed in TABLE 4.2 .

Table 4.2 : Material Testing Conditions

Material	Condition	Hardness HV30
SG42		
OQ	Oil Quenched *martensite with a small percentage austenite*	610
AT 250	Austempered 250°C *very fine acicular ferrite and austenite*	500
AT 300	Austempered 300°C *fine acicular ferrite and austenite*	414
AT 350	Austempered 350°C *coarse acicular ferrite and austenite*	334
SG60		
AT 250	Austempered 250°C *very fine acicular ferrite and austenite*	530
AT 300	Austempered 300°C *fine acicular ferrite and austenite*	467
AT 350	Austempered 350°C *coarse acicular ferrite and austenite*	367
At 400	Austempered 400°C *coarse acicualar ferrite and austenite*	307
Steel B	*Tempered Martensite*	
OQ & T 100	Oil Quenched & Tempered 100°C	850
OQ & T 250	Oil Quenched & Tempered 250°C	630
OQ & T 350	Oil Quenched & Tempered 350°C	480

4.3 HEAT TREATMENTS

All specimens were heat treated in two muffle furnaces, which were purged with dry nitrogen gas at 2cm³/sec during the process. To prevent decarburisation, the specimens were coated with two commercially available protective coatings. A type A silicon base ceramic (resistant up to 850°C) was applied first, followed by a type B zirconia based ceramic (resistant up to 1100°C). Following this process no decarburisation was apparent.

A standard austenitising temperature and time of 900°C and 60 minutes was used throughout. The specimens were either oil quenched or quenched in a salt bath at respective austempering temperature (see TABLE 4.2) for a holding time of 30 minutes before air cooling to room temperature.

4.4 MECHANICAL TESTING

Vickers hardness measurements were made on an Esseway hardness machine using a load of 30kgf.

Tensile tests were performed on a Zwick 100KN tensile testing machine using Hounsfield specimens of 4.51 mm in diameter and a cross head speed of 0.25mms^{-1}. Impact testing was carried out on a Charpy Impact tester.

4.5 UNLUBRICATED PIN-ON-DISC TEST

A standard pin-on-disc configuration was used throughout the testing programme. For this purpose an existing rig was used. Initially this rig produced reproducibility errors of greater than +/- 24 % . This was deemed unsatisfactory and extensive modification to the rig were made. The base holder was redesigned to incorporate a cylindrical thrust bearing (to support the load) with a new monitoring and control system. A reproducibility of well within +/- 5 % was then attained and this was deemed satisfactory for this type of testing (FIGURE 4.1).

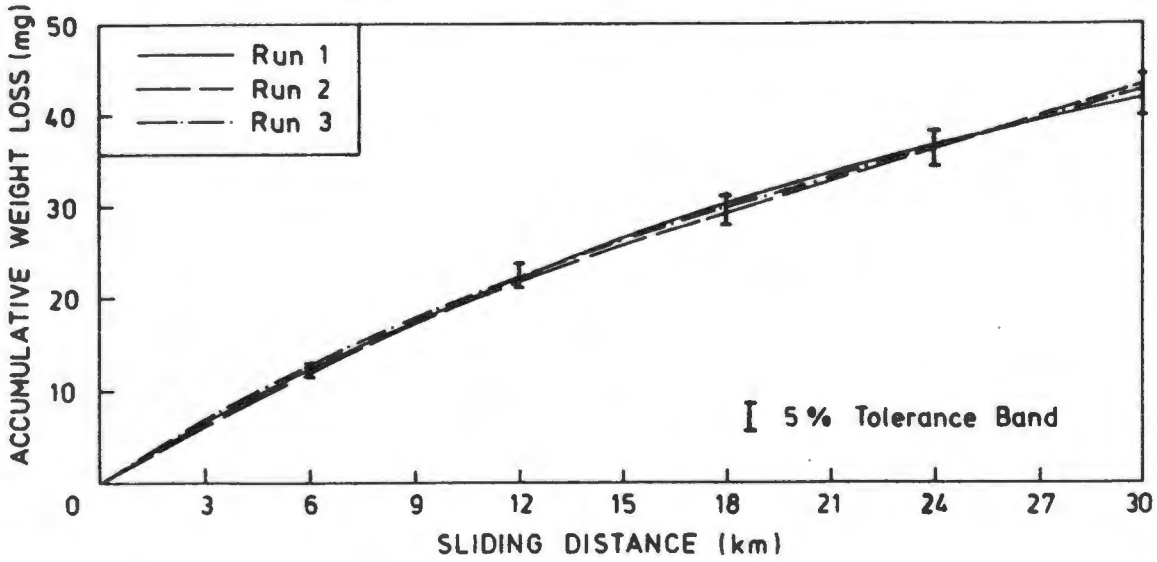

Figure 4.1 : Reproducibility of the Rig

4.5.1 Pin-on-Disc Rig

The pin-on-disc rig (FIGURE 4.2) encompasses a pin (specimen) fixed to a cantilever arm rubbing against a base moving at a constant rotational speed. The sliding velocity is varied by changing the radius of rotation or the rotational speed of the motor.

The load to the pin is applied using a dead weight at the end of the cantilever, which amplifies the load at the pin by a factor of two. The base is supported by a cylindrical thrust bearing giving adequate support for loads up to 20kg at the pin. The rotating base 15mm thick and 90mm diameter is held down on the base holder by four grub screws.

The base holder has 10 vertically milled slots equi-spaced around it's circumference. These milled slots act as non-magnetic pick up points for a 5mm proximity sensor. The signal obtained from the sensor is converted via an electronic box to record the cycles travelled and the speed of travel. An automatic preset counter sends a signal to the AC control relay to stop the motor once the desired distance has been traversed.

A 20 kgf load cell measures the frictional force from the deflection of the cantilever arm. This signal is amplified and recorded continuously on a chart recorder.

The rotational velocity of the base is controlled by an AC control unit. The control unit converts the single phase incoming AC current into a delta three phase AC current and by controlling the frequency of the voltage, the speed of rotation of the motor is varied. A 3:1 reduction pulley reduces the speed to a maximum of 480 r.p.m, while the minimum speed is limited to 150 r.p.m by the available torque.

A sliding velocity of 0.2 to 2.0 ms^{-1} is available by altering the rotational speed of the motor and by varying the radius of rotation.

Figure 4.2: Pin-on-Disc Testing Apparatus.

a. AC control unit
b. 0.75 kw motor
   (1440 r.p.m 3-phase delta)
c. speed dial (r.p.m)
d. preset counter
e. 20 kg load cell
f. electronic control unit
g. chart recorder
h. proximity sensor
i. pin (specimen)
j. base
k. base holder
l. load

4.5.2 Testing Parameters

The testing parameters were chosen as a result of an extensive literature survey on operating parameters of actual components [21,24,31]. The components or applications the ADI material is likely to be used in are gears, pulleys, cams, conrods, camshafts etc. As a result of this survey and bearing the limitations of the rig in mind, the following set of testing parameters was chosen (TABLE 4.3):-

Table 4.3: *Testing parameters*

Load (Nmm^{-2})	0.9	2.0		2.8
Sliding Velocity (ms^{-1})	0.5	1.0	1.5	2.0
Sliding Distance: 28 km				

The sliding distance was chosen after preliminary tests were conducted, in order to establish a minimum of three points from a steady state condition.

To ensure a good matching surface, 280 grid paper was attached to the base and the pin worn in at a speed of 0.4 ms^{-1} while a load of 0.2 Nmm^{-2} was applied. The paper was removed, the pin weighed and the test started. The weight loss was measured to an accuracy of 0.1mg at 4km intervals and this was then converted into volume loss and wear rates.

4.6 MICROSTRUCTURAL EXAMINATION

Optical Microscopy

The heat treated specimens and the 10° taper sections of the worn surfaces were examined using optical microscopy. The specimens were polished down to 0.25 microns, etched in 2.5% nital solution and examined with a Nikon Microscope.

A 10° taper section of the worn specimens was taken to enable a closer examination of the worn surface and subsurface. This section was polished and etched as for optical microscopy. A Shimadzu microhardness tester with a load of 200g was used to determine the hardness of the work hardened layers. It was necessary to nickel plating the worn pins before a taper section of the pin was taken, this enabled a more precise examination of the edge deformation.

The specimens were plated in a nickel chloride and boric acid solution with a nickel anode. A current density of 75 ma/cm^3 was applied until the specimen had reached a sufficient plating thickness of around 1 mm. To ensure a successful nickel plating the following cleaning process was performed on the specimen prior to plating.

1] A general cleaning process using an ultrasonic bath of alcohol (5 min) followed by a rinse in distilled water.

2] An ultrasonic degrease in a 20 % Ammonia solution (2 min) followed by a further rinse in distilled water.

3] The specimen was then nickel plated.

A stereo microscope was used to examine the general surface appearance of the worn specimens at low magnification.

Scanning Electron Microscope (SEM)

The worn surfaces were ultrasonically cleaned and then examined on a Cambridge Stereoscan 200 SEM. The debris resulting from the wear process was collected on a aluminium stub coated with a graphite paste. The graphite paste acted as the binder for the wear debris as well as the conductive medium required for the SEM examination. The stub containing the debris was then splutter coated with gold (Au) prior to examination.

4.7 SURFACE EXAMINATION

4.7.1 X-Ray Diffractometry (XRD)

Prior to testing, XRD was performed on specimens which had been polished and lightly etched. On completion of testing, the specimens were ultrasonically cleaned prior to XRD analysis.

XRD using Molybdenum radiation was carried out on a Phillips diffractometer. The retained austenite measurements were made in accordance to the recommended procedure of the manufacturer (APPENDIX 1). This was done by integrating the intensities of two suitable diffraction peaks. For the austenite-ferrite mixture, the best suited diffraction lines are the (200) of the ferrite and the (220) of the austenite.

4.7.2 X-Ray Photoelectron Spectroscopy (XPS)

XPS was used to analyse the outer surface layer of two worn specimens and their respective debris from sliding velocities of 0.5 and 2.0 ms^{-1}.

XPS is concerned with the measurement of core-binding energies. The sample is radiated with a source of high energy X-rays (MgK), which causes the emission of inner shell electrons. Binding energies unambiguously define a specific atom. The energy of the ejected electron is characteristic of the atom and environment. XPS analysis examines the materials surface layers to a depth of 2-4nm of the surface layers.

The measurements were done using a VG scientific ESCALAB mk II, fitted with a hemispherical photoelectron analyser. The back pressure in the analyser was better than 5 x 10^{-10} mbar, ensuring a good vacuum which is essential for the success of this technique.

Chapter V

RESULTS

5.1 EFFECTS OF AUSTEMPERING TEMPERATURE

5.1.1 Microstructure

The microstructure resulting from austempering consisted of carbon spheroids in a basic matrix of acicular ferrite plates and retained austenite. The actual morphology of the dual phase matrix and relative amounts of ferrite and austenite appear to be largely determined by the austempering temperature. The microstructures produced after austenitising at 900°C for 60 minutes and austempering between 250°C and 350°C for grade SG42 are shown in FIGURE 5.1.

At the lower austempering temperatures, noticeably below 300°C, the structure consists of very fine ferrite needles/platelets interspersed in the retained austenite. As the transformation temperature is raised, the ferrite plates become progressively coarser and more feathery in appearance.

a] Austempered at 250°C

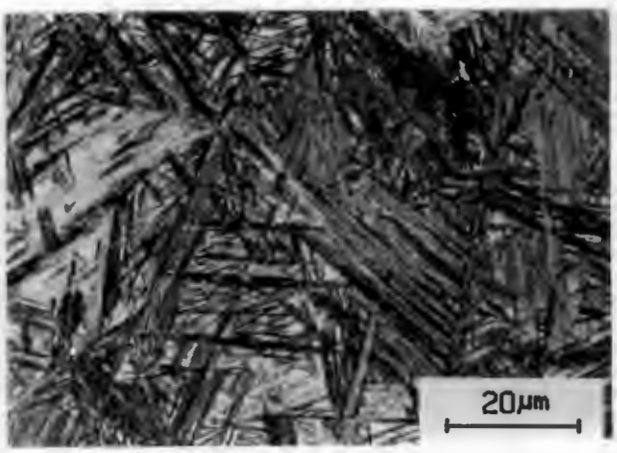

b] Austempered at 300°C

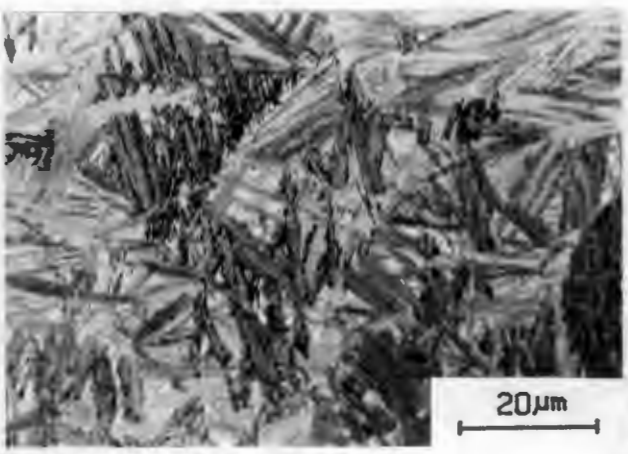

c] Austempered at 325°C

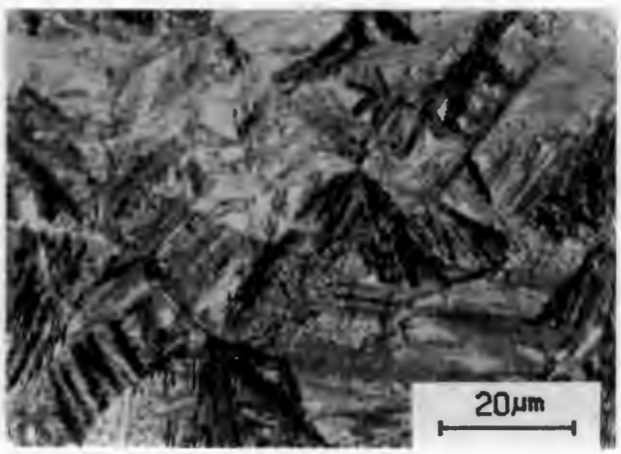

d] Austempered at 350°C

Figure 5.1: Microstructures Produced at Varied Austempering Temperatures for the Grade SG42.

5.1.2 Mechanical Tests

5.1.2.1 Hardness

It is clear that a parallel change in hardness is observed as the morphology and constitution of the austempered microstructures are altered with temperature (FIGURE 5.1).

As the austempering temperature is increased from 250°C to 400°C the hardness falls from approximately 530 HV to 290 HV for SG60, while the hardness of SG42 falls from 500 HV to 334 HV as the austempering temperature is increased from 250°C to 350°C. A further increase in the austempering temperature for both grades results in an increase in the hardness of the structure as pearlite makes it's appearance.

It is notable that the hardness of SG60 was always greater than SG42 for a specific austempering temperature.

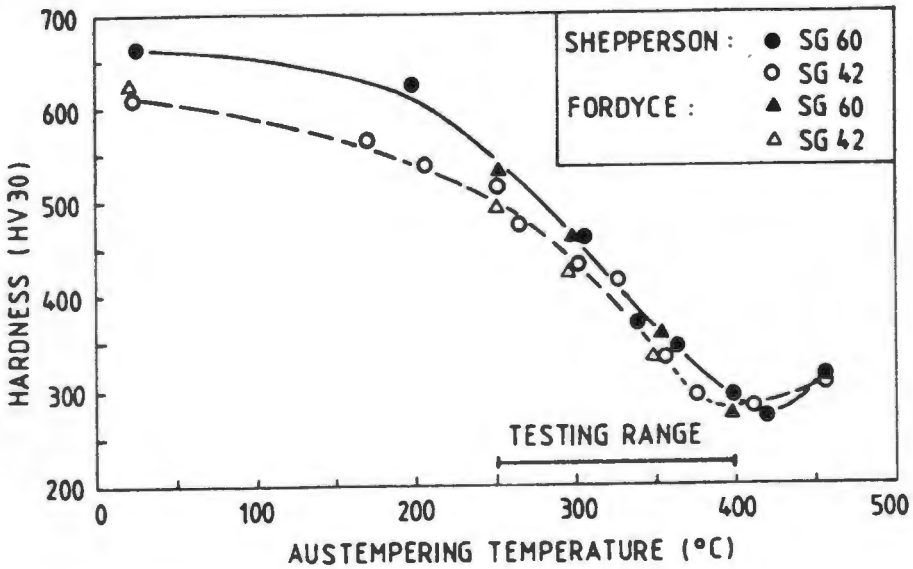

Figure 5.2: Effect of Austempering Temperature on Hardness

5.1.2.2 Table Of Properties

The results of the tensile and toughness tests performed on the SG60 and SG42 for the different austempering temperatures are tabulated in TABLE 5.1.

It is clear that the highest strength levels are associated with the lower austempering time. Tensile strengths of 1300 MPa for SG60 and 1100 MPa a for SG42 are attainable for an austempering temperature of 250°C.

It is notable that the Charpy toughness level for SG60 increases with austempering whilst for SG42 the level decreases. It is apparent that the acicular ferrite and retained austenite structure is less tough than the ferritic structure of SG42, while the ferrite and pearlite matrix of SG60 is less tough than the acicular ferrite and retained austenite matrix.

Table 5.1: Mechanical Properties of SG42 and SG60

GRADE	Austempering Temperature	Hardness Hv30	Notched Charpy J	Tensile strength MPa	Elongation %	Retained Austenite %
SG42	as cast	136	15.0	390	13.0	-
	250°C	500	3.5	1000	6.3	19
	300°C	414	5.0	1090	6.4	26
	350°C	334	6.0	954	6.3	33
SG60	as cast	229	3.0	618	4.2	-
	250°C	530	4.0	1318	6.3	20
	300°C	467	5.0	1236	8.2	28
	350°C	367	9.0	1200	8.0	35
	400°C	307	12.0	1037	11.0	46

5.1.3 XRD

XRD was used to determine the quantity of retained austenite in the matrix of the austempered irons. FIGURE 5.3 shows the variation in retained austenite as a function of temperature.

As the austempering temperature is increased from 250°C to 400°C the amount of retained austenite increases from approximately 20% to 46% for SG60. This maximum for SG60 is reached at approximately 400°C, while SG42 reaches a maximum austenite content around 350°C (FIGURE 5.3). The amount of retained austenite in the SG60 grade was found to be similar to that for SG42 in the temperature range of 250°C to 350°C.

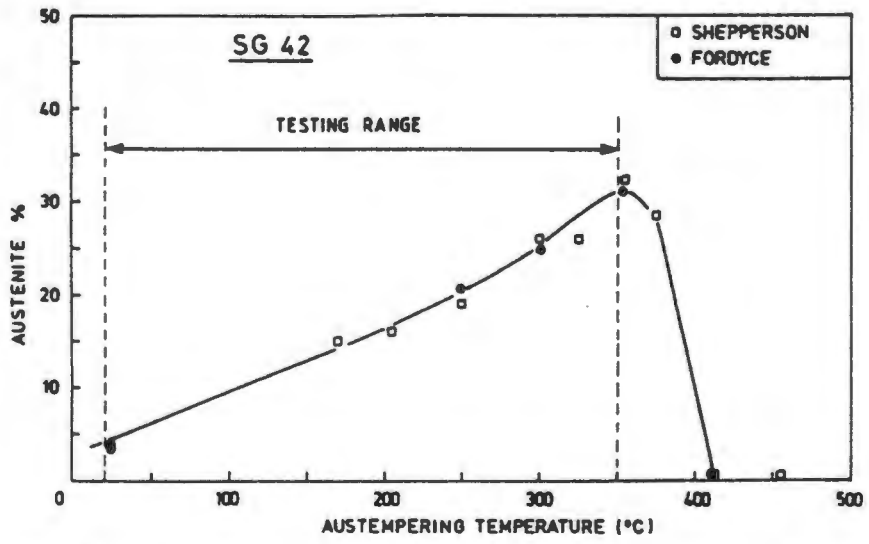

Figure 5.3: Variation in Austenite Content as a Function of Austempering Temperature

5.2 SLIDING VELOCITY

These tests were conducted against a SG60 oil quenched base, with a load of 2.0 MPa, with four grades of each parent grade SG42 and SG60. The sliding velocity was varied from 0.5 ms^{-1}, 1.0 ms^{-1}, 1.5 ms^{-1} and 2.0 ms^{-1}.

5.2.1 Surface Characteristics

Surface Topography

The topography of the worn surfaces was found to vary according to sliding distance rather than microstructure or mechanical properties. An optical examination of the surfaces indicates that as the speed increases from 0.5 ms^{-1} to 2.0 ms^{-1} the uniformity of the wearing surfaces decreases (FIGURE 5.4). At the lower sliding velocities the surfaces appear to be uniformly worn, while at the higher sliding velocities the surface appears smeared and smudged.

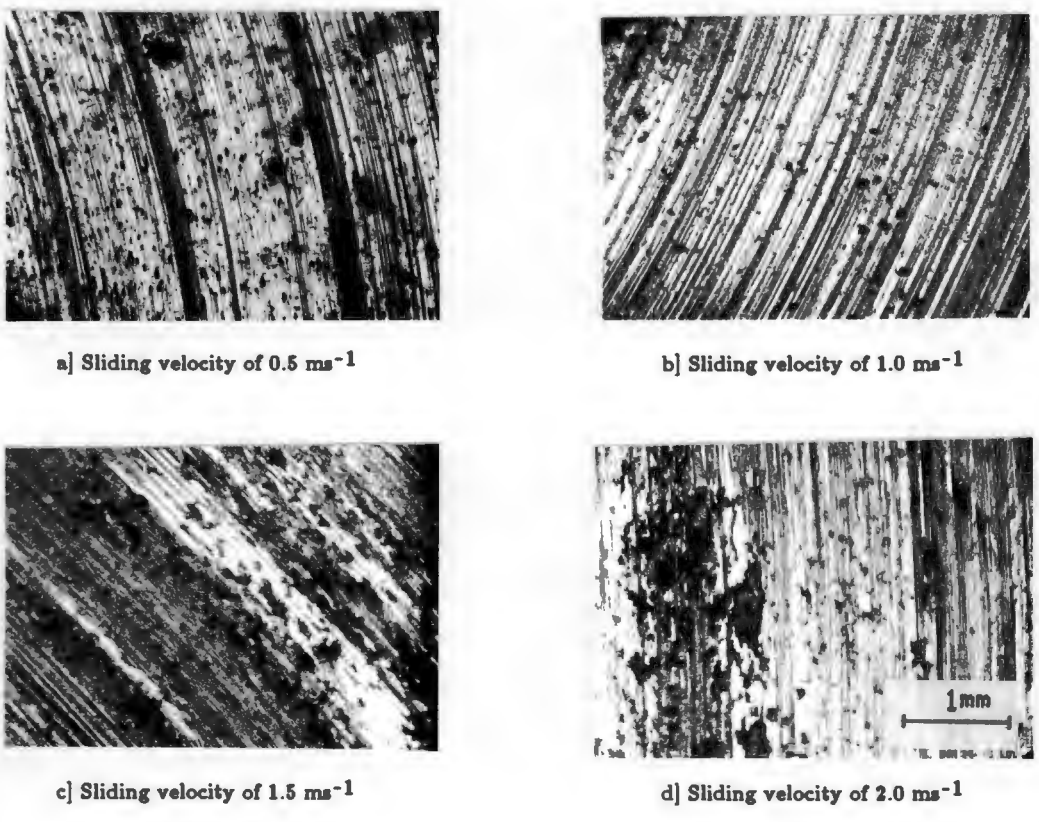

a] Sliding velocity of 0.5 ms^{-1}

b] Sliding velocity of 1.0 ms^{-1}

c] Sliding velocity of 1.5 ms^{-1}

d] Sliding velocity of 2.0 ms^{-1}

Figure 5.4: General Surface of the Worn Pins, Examined Optically

At a velocity of 0.5 ms^{-1} the surface of the worn specimens were oxidised and uniformly worn with wear pits often covering the surface (FIGURE 5.5). The deformed surface layer exhibited wear tracks similar to those found in abrasive wear, which often contained compacted metallic and oxidised debris (FIGURE 5.5). There was also evidence of heavily deformed metallic chips similar to those found in cutting processes (FIGURE 5.6).

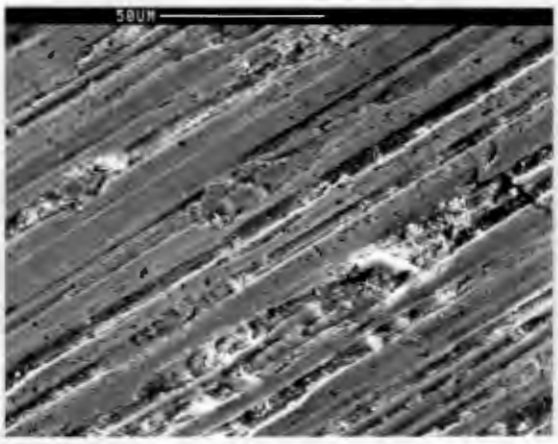

a] Abrasive type wear track showing trapped oxide and metallic debris in the wear track.

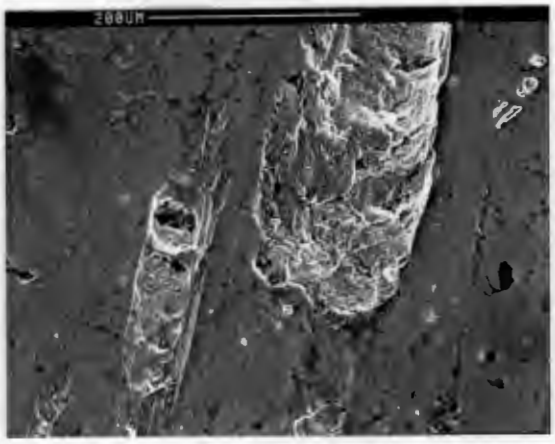

b] wear pits found generally on the surface, exhibiting surface tearing.

Figure 5.5: General Surface Attribute Of 0.5 ms^{-1}.

a] Abrasive wear tracks found at an angle to the wear direction.

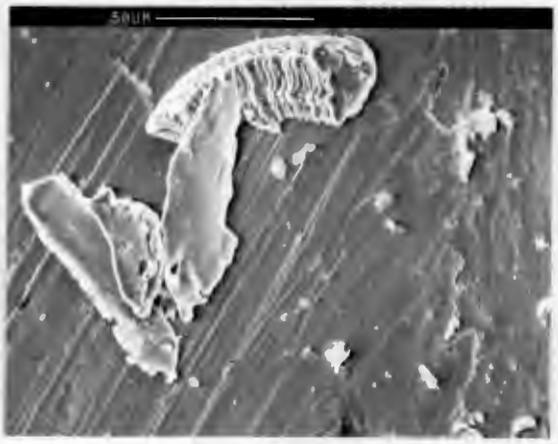

b] Debris with angular type geometry and debris exhibiting the characteristics of a chip formed in a machining process.

Figure 5.6: Evidence of Abrasion and Cutting

Specimens subjected to a sliding velocity of 2.0 ms^{-1} had worn surfaces which were characterised by smooth regions interspersed with areas where the surface layers had been partially removed (FIGURE 5.7). A common feature in the smooth region were cracks in the oxide layer, which eventually lead up to the formation of flake-like particles (FIGURE 5.8). A typical roughened region is shown in FIGURE 5.9, which indicates that there has been a partial removal of the oxide layer, followed by deformation and smearing of the newly exposed surface. Eventually such areas in turn become heavily oxidised smooth regions which eventually crack with resulting loss of the surface material.

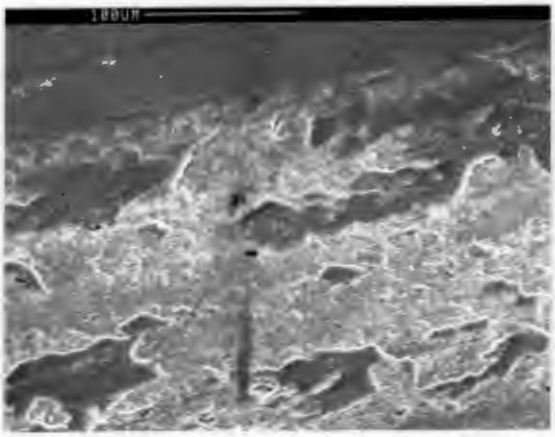

Figure 5.7: Two Distinct Regions Visible at a Sliding Velocity of 2 m/s, a Smooth Surface with a Glazed Appearance and an Area where the Surface Layer has been Removed.

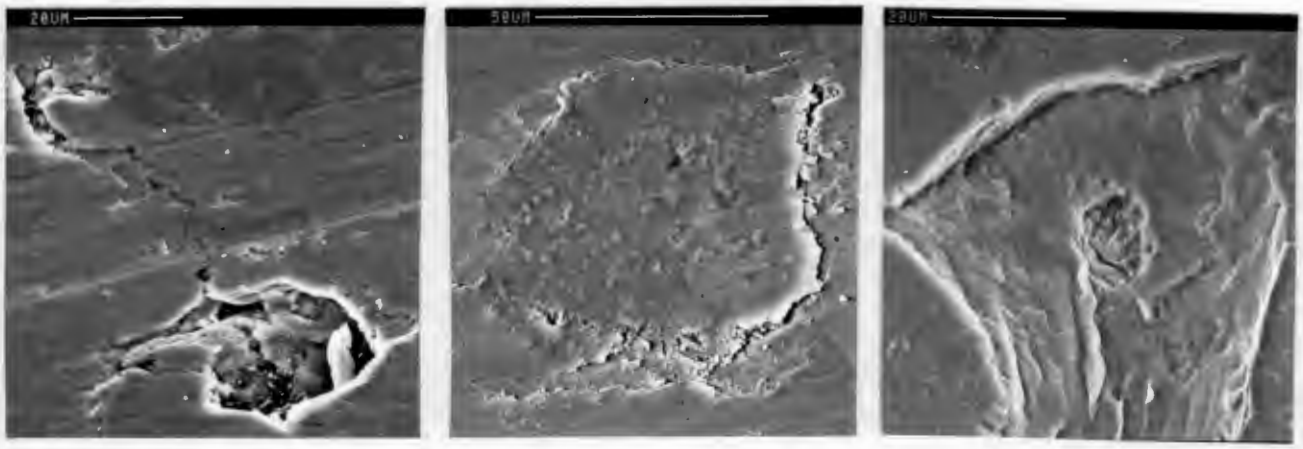

Figure 5.8: Three Stages in the Formation of a *Flake Particle.*

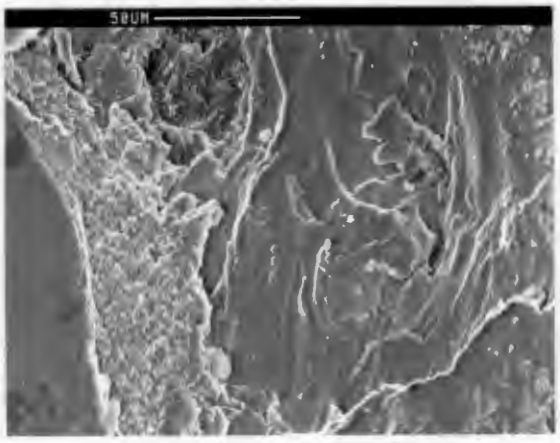

Figure 5.9: Partial Removal of Oxide Film, Showing Cleavage of Oxide and Resmearing of the Surface.

At a sliding velocity of 1.0 ms^{-1} the surface characteristics were similar to those found at 0.5 ms^{-1}. At 1.5 ms^{-1} the surface on the inner radii of the pin (lower sliding velocity) exhibits grooves similar to those found on 1.0 ms^{-1} and 0.5 ms^{-1} (FIGURE 5.10), while the outer edge (higher sliding velocity) exhibit characteristics of 2.0 ms^{-1}, with a smeared appearance (FIGURE 5.11).

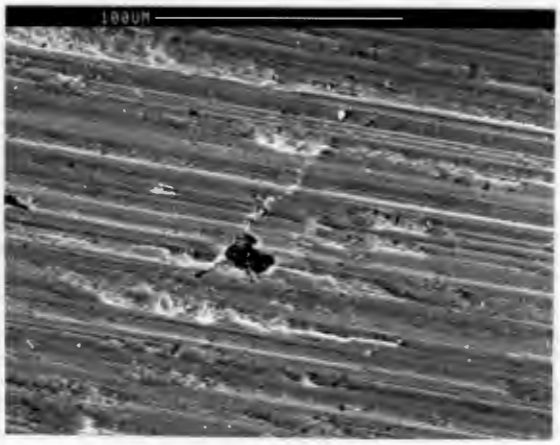

Figure 5.10: Wear Surface at 1.0 m/s Similar to 0.5 m/s Exhibiting Abrasive Type Wear Tracks.

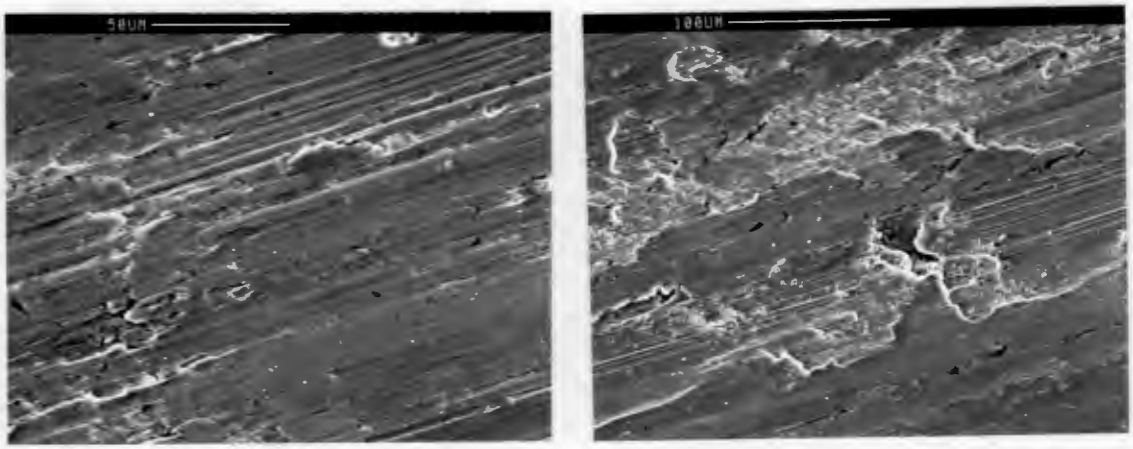

a] Wear surface on inner radii (lower sliding velocity) showing similar wear surface as at 1.0 ms^{-1}, more defined wear tracks.

b] Wear surface on outer radii (higher sliding velocity), with similar wear characteristics as at 2.0 ms^{-1}, evidence of smearing of film.

Figure 5.11: Wear Surface at 1.5 m/s Inner and Outer surfaces of the Pin.

Debris

The debris produced at a velocity of 0.5 ms^{-1} was significantly greater than the amount produced at 2.0 ms^{-1}. The debris consisted of large particles in a matrix of smaller particles.

At a sliding velocity of 0.5 ms^{-1} the larger particles were angular and in excess of 50 microns in length (FIGURE 5.12). The larger debris found at 2.0 ms^{-1} had a flake-like appearance with a particle size of 10 to 50 microns in length and a thickness of approximately 2 microns (FIGURE 5.13).

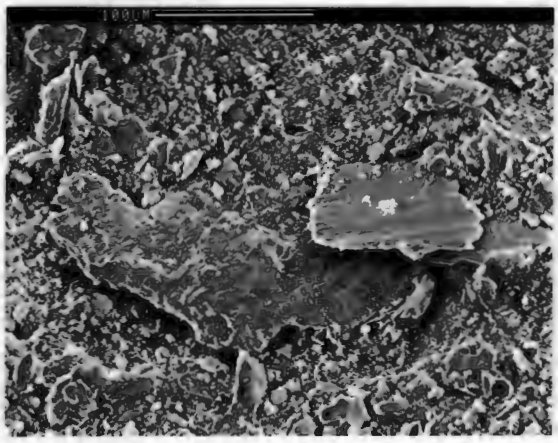

a] Indication of the size of the larger debris found, in a matrix of smaller and more angular particles of 5 to 10 microns.

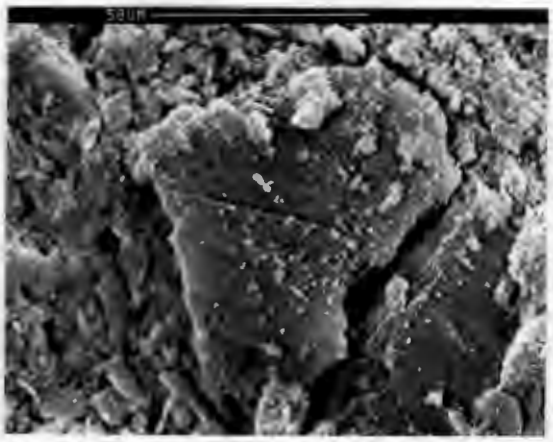

b] An average size debris exhibiting non uniform thickness.

Figure 5.12: Debris Produced at 0.5 ms^{-1}.

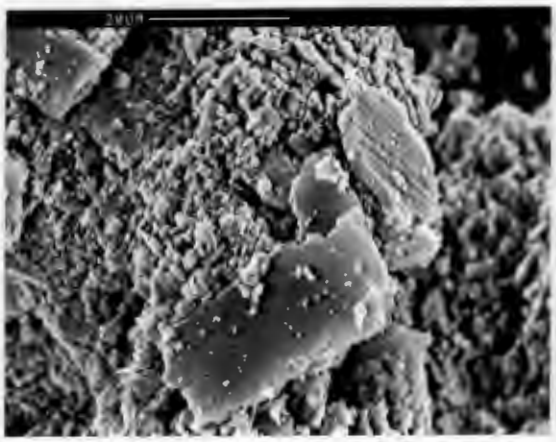

a] Flake-like debris of uniform thickness.

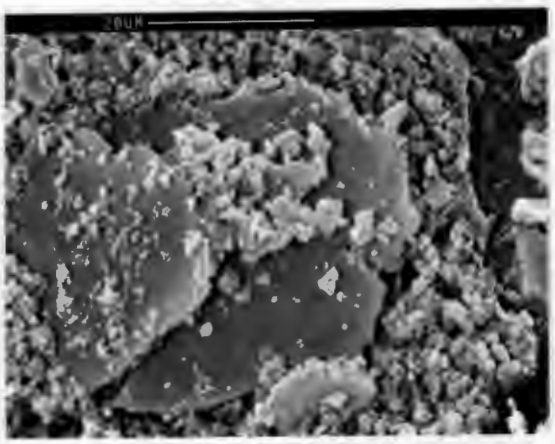

b] The smooth glazed appearance of the debris in a matrix of particles which appear heavily oxidised in the size range of 2 microns.

Figure 5.13: Debris produced at 2.0 ms^{-1}.

Oxides

Similar oxides of wüstite (FeO), haematite (Fe_2O_3) and magnitite (Fe_3O_4) were detected on all worn surfaces regardless of sliding velocity (FIGURE 5.14). In addition to this FeOOH was found on the debris.

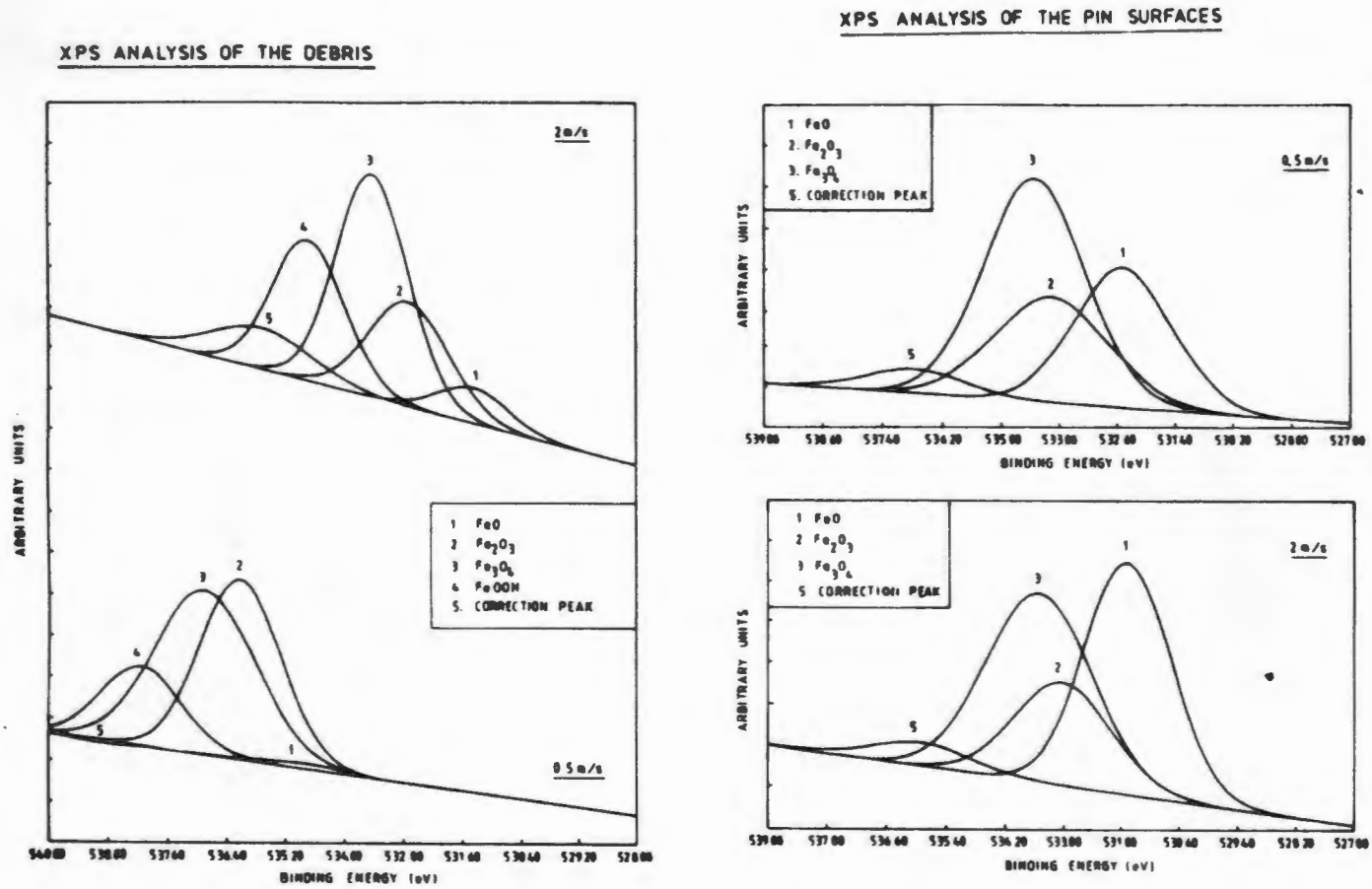

Figure 5.14: XPS Analysis of Two Pins Worn at 0.5 ms^{-1} and 2.0 ms^{-1}

At the lower sliding velocities, the oxide (Fe_3O_4) was predominant, while at 2.0 ms^{-1} the oxide FeO had increased significantly and was predominant.

As FeO forms above 570°C, it would be expected that the temperature (flash temperature of the asperity) is significantly higher at 2.0 ms^{-1}, hence it is likely that higher oxide kinetics prevail at this speed.

The debris produced at 2.0 ms^{-1} has a small amount of FeO, while the FeO content was almost negligible in the debris produced at 0.5ms^{-1}.

It must be noted that it appears that the debris has less FeO than the pin surfaces. This is a result of a probability factor, it is likely that only a proportion of the debris has it's oxidised surface facing for detection purposes. Thus, no significant fact can be deduced when comparing analysis of the debris and the pin surface. Although it

can be noted that FeO is present in the debris and pin surface at 2.0 ms^{-1}, while at 0.5 ms^{-1} the presence of FeO is only noticeable on the pin surface, with the amount of FeO in the debris being negligible.

It appears that the debris produced at 2.0 ms^{-1} is broken down into smaller pieces which are then oxidised further because of higher surface temperatures. It appears that debris particles from 0.5 ms^{-1} do not undergo further oxidation effects. This is as a result of a combination of lower surface temperatures together with the greater difficulty in reducing larger and more angular debris, compared with the thin flake-like debris produced at 2 ms^{-1}.

5.2.2 Subsurface Characteristics

XRD

There was a notable difference in the XRD results between the two extreme sliding speeds of 0.5 ms^{-1} and 2.0 ms^{-1}.

It was established that at the lower speeds (0.5 and 1.0 ms^{-1}), there appeared to be a 20% transformation of austenite to martensite (TABLE 5.2), although some difficulty was experienced in the XRD measurement, possibly due to the presence of an oxide layer.

Table 5.2 : Change in retained austenite content at sliding velocity of 0.5 ms^{-1}

	SG42		SG60	
	before	after	before	after
OQ	4 %	0%	-	-
AT250	18%	13%	19%	14%
AT300	23%	16%	24%	18%
AT350	28%	22%	30%	23%
AT400	-	-	38%	29%

However, at the higher speeds (1.5 and 2.0 ms^{-1}) no retained austenite was detected on any of the specimens. This tended to suggest than all the retained austenite on the surface had transformed to martensite during sliding under these conditions.

Microhardness

There was no distinct change in hardness section beneath the wearing surface layer for the sliding speeds of 0.5 and 1.0 ms^{-1} (FIGURE 5.15). The extent of the deformed layer found at 0.5 ms^{-1} appeared to be confined to the outer few microns (FIGURE 5.16).

However at 1.5 and 2.0 ms^{-1} there was extensive work hardening with three distinct regions visible (FIGURE 5.17):-

i] An outer region which contained non-etching white layers
ii] An intermediate hardened region
iii] The bulk structure

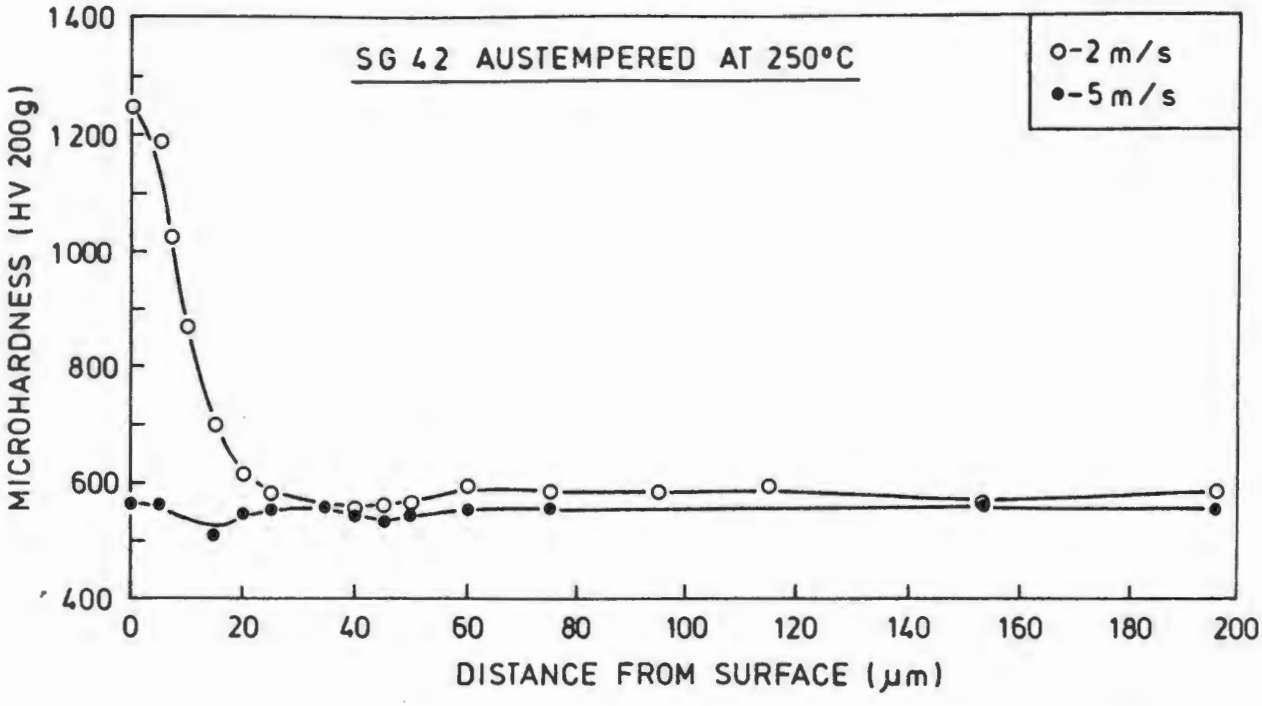

Figure 5.15: Microhardness Section Taken for SG42 Austempered at 250°C at Velocity of 0.5 and 2.0 ms^{-1}.

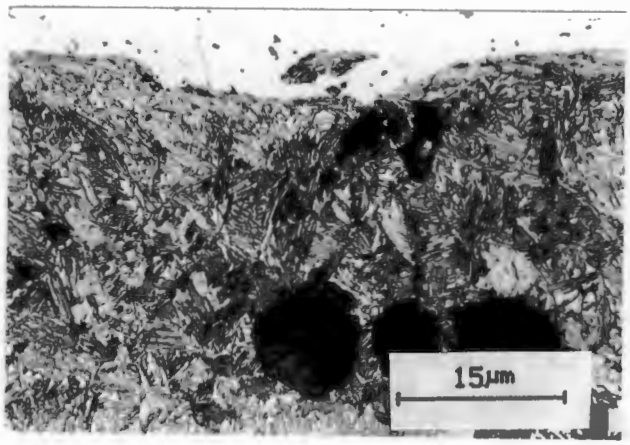

Figure 5.16: Surface Deformation Found Only at the Outer Surface, Speed of 0.5 ms^{-1}.

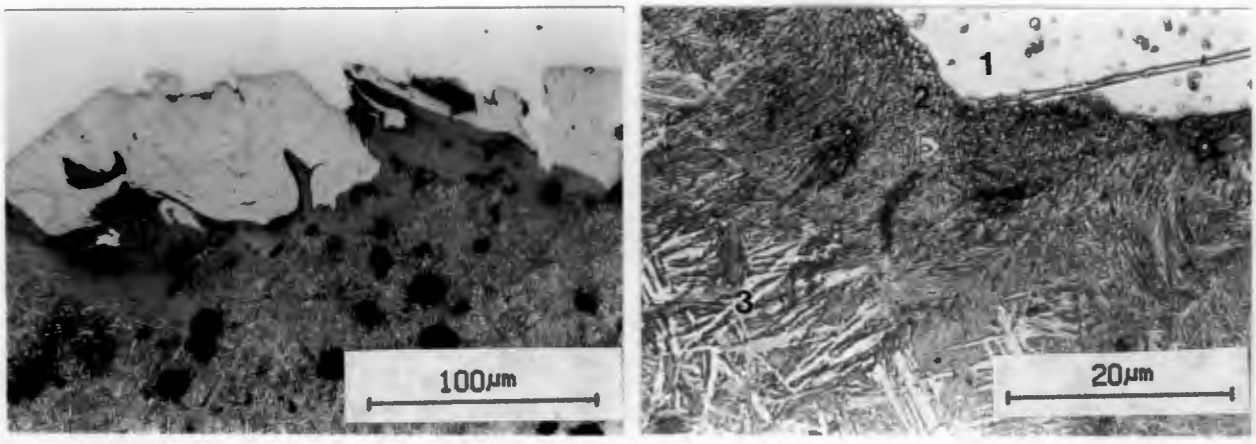

a] Indication of the flow characteristic of the white layer.

b] The three distinct regions visible.

Figure 5.17: The Deformed Layer Taken on a 10° Taper Section at a Sliding Speed *of 2.0 ms^{-1}* (2.0 Mpa).

The actual values for the thickness of these deformed layers were difficult to establish, but were generally less than 50 microns thick. The white areas were not continuous, but formed in patches showing a distinct flow characteristic. This white layer had similar characteristics described by Rogers [65], where he found a higher carbide content of up to 50% by volume in these white layers.

This patchy white layer exhibited a hardness in the region of $1200HV_{0.2}$ to $1400HV_{0.2}$. The region adjacent to the white layer had a very fine microstructure and the hardness ranged between $600HV_{0.2}$ (AT350) and $750HV_{0.2}$ (AT250) (FIGURE 5.15). In both cases the bulk hardness values were $540HV_{0.2}$ and $820HV_{0.2}$ respectively. In general the fine matrix structure was far harder than the bulk. However, at the austempered temperature of 250°C (AT250) the fine matrix was slightly lower than the bulk.

It should also be noted that the microhardness readings were taken on the matrix of the irons whereas the bulk hardness reflects both the hardness of the matrix as well as the graphite spheroids. The difference in the bulk and microhardness values was approximately 35%, this difference is attributed to the very soft graphite spheroids influencing the bulk hardness values whereas the microhardness measurements were only taken on the matrix.

At the high sliding velocities, it was noted that the parent grade of SG60 (ferritic and pearlitic matrix) had a white layer, while the parent grade SG42 (ferritic matrix) had no white layer (FIGURE 5.18).

This white layer formed on as cast SG60 was very limited, in that the degree or amount of white layer was far less than on the austempered grades of ADI. The white layer exhibited a similar hardness to that of the white layer appearing in the austempered grades (in the region of $1300H_{V0.2}$) The fine microstructure was also evident in the adjacent layer. This layer was significantly less in thickness with a hardness of around $480H_{V0.2}$. The parent pearlite matrix had a hardness of $360H_{V0.2}$.

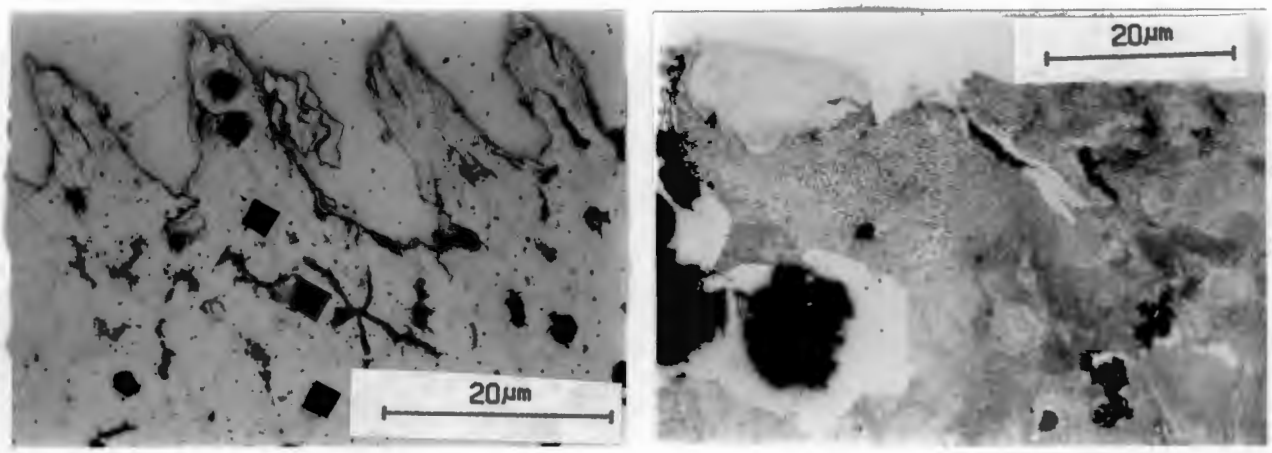

a] The surface layer of SG42 at 2.0 ms^{-1}, showing no white layer.

b] A small amount of the white layer present on SG60 at 2.0 ms^{-1}.

Figure 5.18: Evidence of Deformed Layers at 2.0 m/s for SG60 and SG42.

5.2.3 Sliding Wear Tests

Accumulative

The effect of austempering temperature on the accumulative volume loss of the irons with sliding distance is shown for the grade SG60 in FIGURE 5.19. It is apparent that the sliding wear resistance of these irons is related to the austempering temperature.

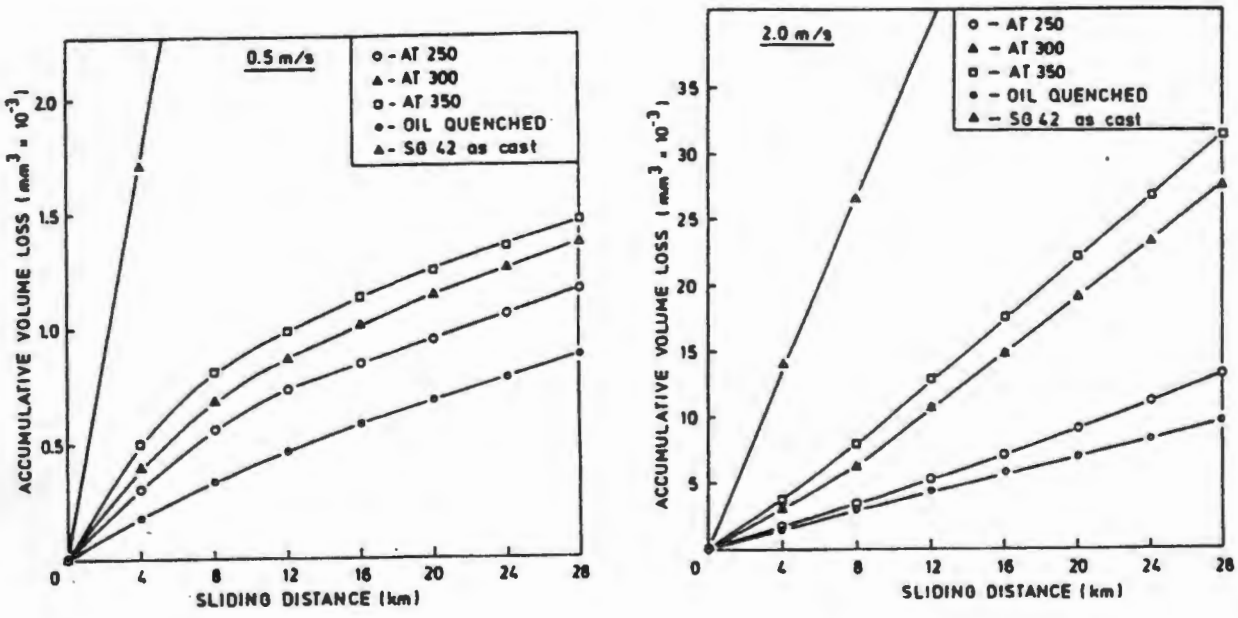

Figure 5.19: Accumulative Volume Loss vs Distance 0.5 and 2.0 ms^{-1} for SG42.

As the austempering temperature decreases from 400°C to 250°C the wear resistance increases regardless of sliding velocity. Furthermore all the austempered irons show a greater wear resistance than the parent SG iron.

It is noticeable that there is a running-in period prior to the wear rate becoming linear with sliding distance. This behaviour is illustrated more clearly in FIGURE 5.20, which shows the specific wear rate of the various irons as a function of sliding distance at the two extreme velocities.

This wear behaviour of SG42 is similar to SG60 in terms of general trends, although SG60 shows a better wear resistance at speeds of 0.5 and 1.0 ms^{-1}, while at 2.0 ms^{-1} SG42 has the better wear resistance.

Specific Wear Rate

At the lower sliding velocity of 0.5 ms^{-1} the wear rate tends to increase initially with distance and then reaches a constant value (FIGURE 5.20). This constant specific wear rate is dependent on the austempering temperature and the parent grade. A decrease in austempering temperature from 400°C to 250°C leads to an increase in the hardness, mechanical properties and the wear resistance. SG60 has the better mechanical properties for specific austempering conditions and also has better wear resistance than SG42 at 0.5 ms^{-1} (TABLE 5.2).

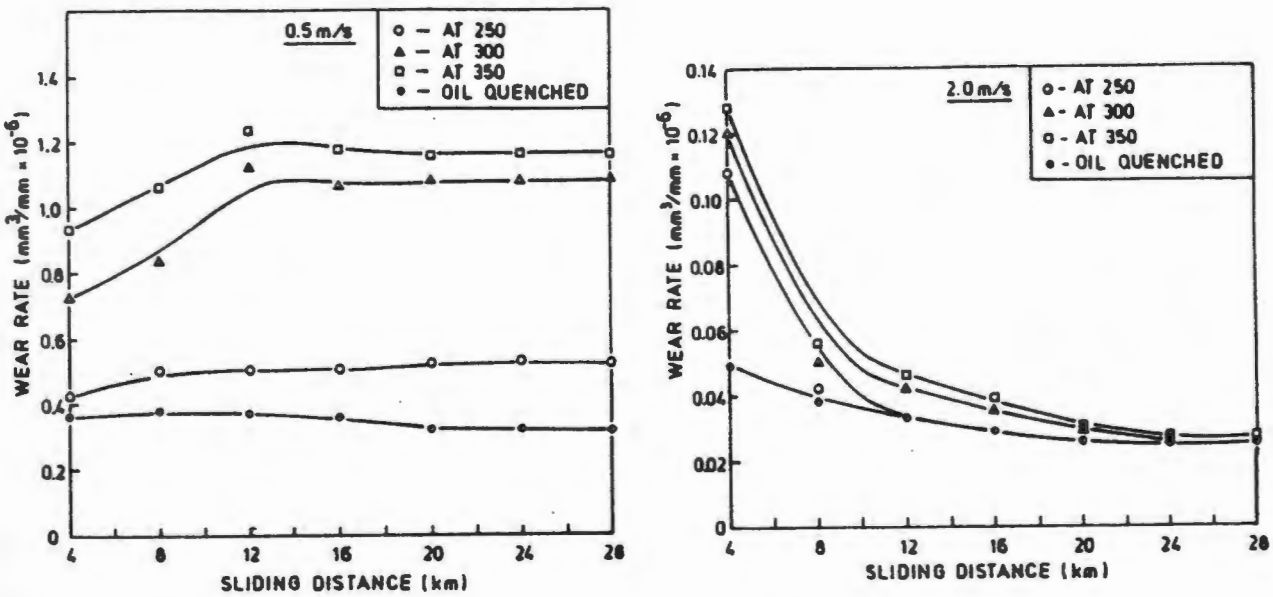

Figure 5.20: Specific Wear Rate vs Distance 0.5 and 2.0 m/s for SG42.

When sliding at a velocity of 2.0 ms^{-1}, the initial wear rate is a function of the austempering temperature, but then the wear rate tends to a constant value for all austempering temperatures for a specific parent grade. This steady state condition occurs after a sliding distance of approximately 20km. Initially the wear resistance of the SG60 grades are higher, but once the static condition is reached the wear resistance of the lower strength SG42 grades are better (TABLE 5.3).

It is significant that the ADI's are far superior to the parent material SG irons, with the wear rate decreasing in orders of magnitude. It is interesting to note that when the ADI's are compared against Steel B (850 HV) they behave extremely well. Some austempered grades perform better than Steel B at the lower velocity (0.5 ms^{-1}), and

have a similar wear rate at the higher sliding velocity of 2.0 ms^{-1} (TABLE 5.3). For example Steel B has a wear rate of 0.44 at a sliding velocity of 0.5 ms^{-1} while a SG60 AT300 grade of half the hardness has a similar wear rate of 0.65. However the SG60 AT250 grade has a lower wear rate of 0.34 while it exhibits a hardness of 530HV30, which is substantially less than the hardness of Steel B (830HV30).

Table 5.3: Wear Rates for ADI and SGI.

Material	Wear Rate $mm^3/mm \cdot 10^{-6}$			
	0.5 ms^{-1}	1.0 ms^{-1}	1.5 ms^{-1}	2.0 ms^{-1}
SG42 as cast				
OQ	6.5	3.0	1.4	0.69
AT250	0.32	0.21	0.046	0.025
AT300	0.52	0.35	0.057	0.026
AT350	1.08	0.54	0.059	0.026
	1.16	0.71	0.065	0.026
SG60				
as cast	5.9	2.7	1.1	0.48
AT250	0.34	0.22	0.050	0.039
AT300	0.65	0.33	0.051	0.041
AT350	0.72	0.34	0.052	0.041
AT400	1.06	0.53	0.054	0.041
Steel B				
Q&T 100	0.44	0.19	0.046	0.023

Sliding Velocity

The effect of increasing sliding velocity from 0.5 to 2.0 ms^{-1} is to reduce the wear rate for all austempering conditions (FIGURE 5.21).

As the speed increases from 0.5 to 2.0 ms^{-1} the wear rate decreases between 12 to 45 times for SG60 and from 8 to 26 times for SG60. The irons which have the lower austempering temperatures i.e. the harder grades, have the higher wear resistance at 0.5 ms^{-1}. At this velocity the SG60 grades have a 35% lower wear rate than for the SG42 grades, at a specific austempering temperature (TABLE 5.3).

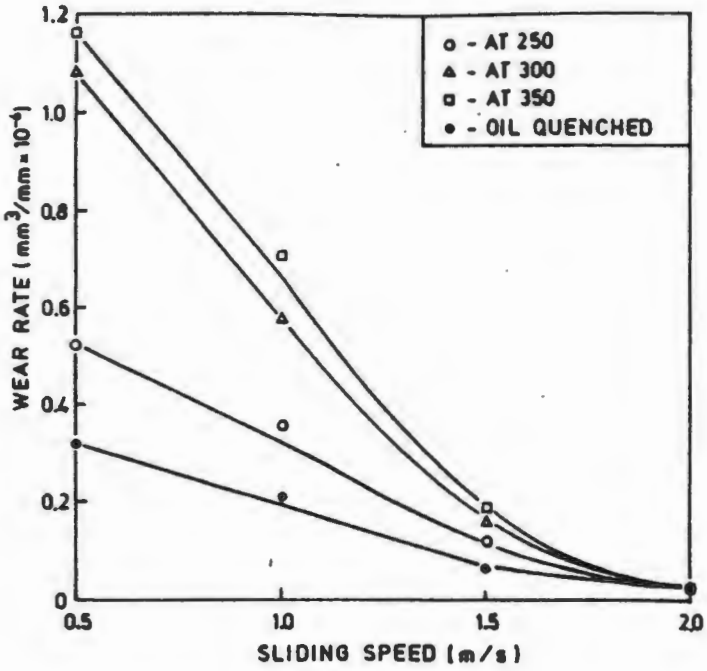

Figure 5.21: Effect of Speed on Wear Rate.

At the higher sliding velocity of 2.0 ms^{-1} the wear rate of all the irons for a specific parent grade is similar. The SG42 grades irons have a 35% lower wear rate than the SG60 grades at this speed, despite having inferior mechanical properties.

As the speed increases the coefficient of friction decreases from 0.7 at 0.5 ms^{-1} to 0.45 at 2.0 ms^{-1} (FIGURE 5.22).

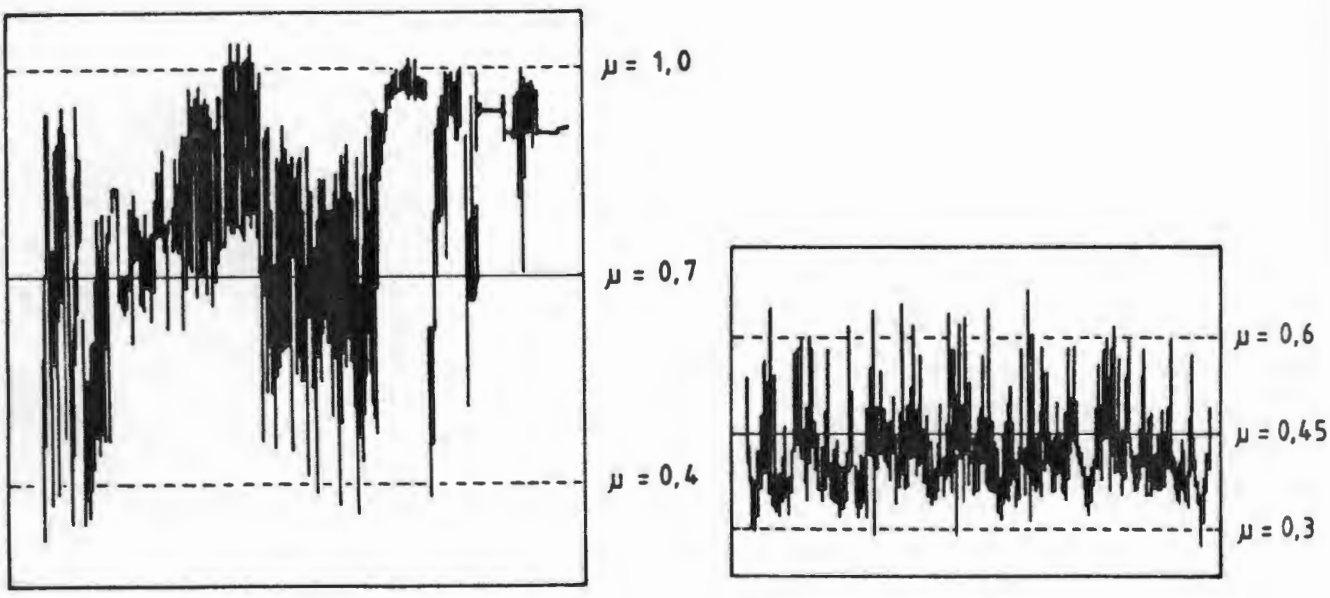

a] Typical friction trace at 0.5 ms^{-1}.

b] Typical friction trace at 2.0 ms^{-1}.

Figure 5.22: Effect on Friction as the Speed Increases

5.3 EFFECT OF LOAD

One grade each of SG60 and SG42 was austempered at 300°C and run against a SG60 oil quenched base, for loads between 0.9 and 2.8 MPa.

5.3.1 Surface Topography

0.5 ms^{-1}

As the load increases it is apparent that the general severity of the worn surfaces increases (FIGURE 5.23). When the load increases from 0.9 MPa to 2.0 MPa and finally to 2.8 MPa, the degree of surface tearing increases (FIGURE 5.24), while at the same time the abrasive secondary wear element increases (FIGURE 5.25).

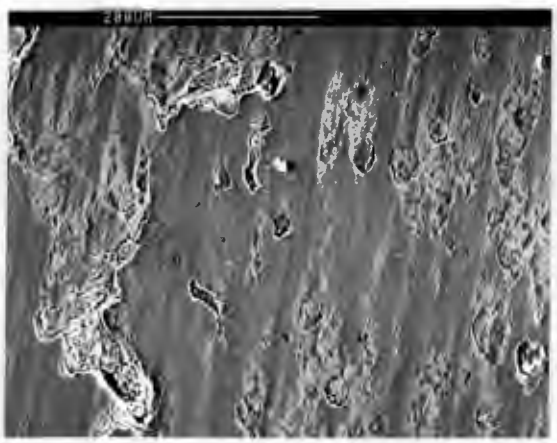

a] Surface subjected to a load of 0.9 MPa, exhibiting some degree of surface damage.

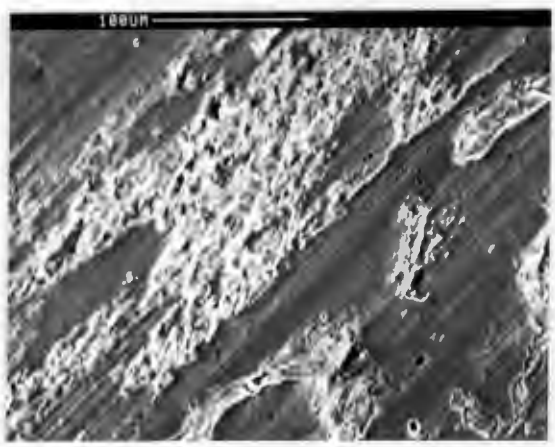

b] Surface exhibiting a greater amount of surface damage and more defined wear tracks at 2.8 MPa.

Figure 5.23: Effect of Load on the General Surface at 0.5 ms^{-1}

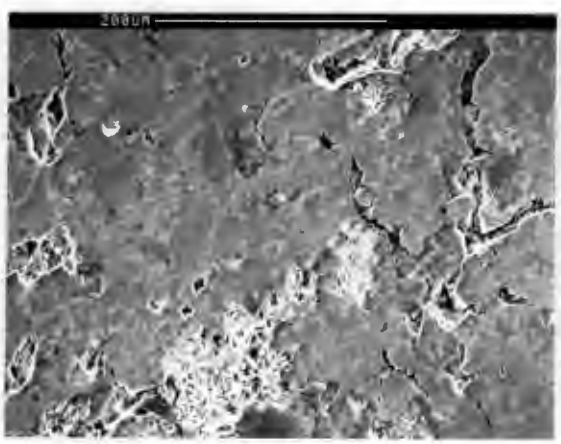

a] At a load of 0.9 MPa, small wear type pits, as a result of surface tearing.

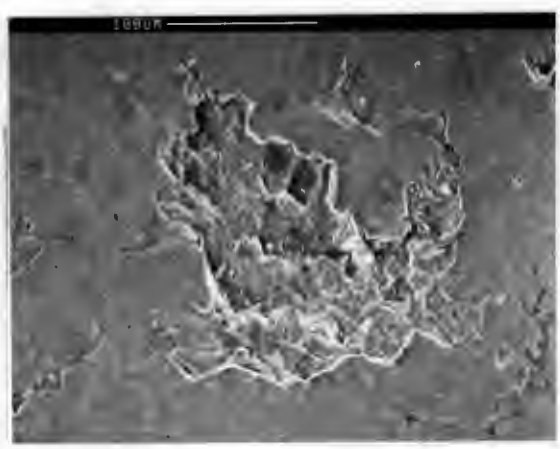

b] Increased surface tearing at a load of 2.8 MPa.

Figure 5.24: Increase in Surface Tearing With Increasing Load

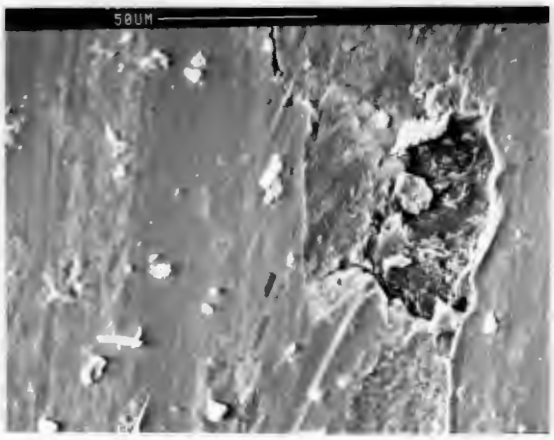

a] Surface exhibiting well defined wear tracks with a third body abrasive type wear track at an angle to the wear direction.

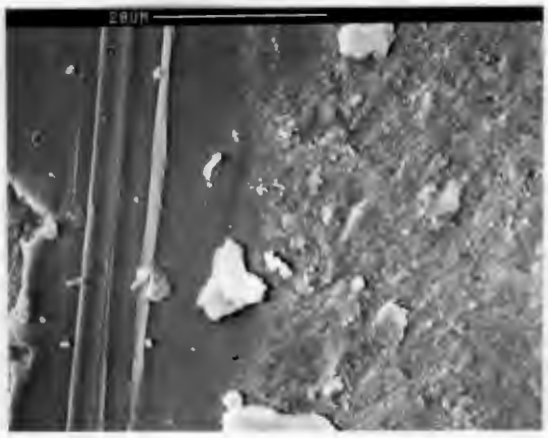

b] A distinctive abrasive type groove formed as a result of a ploughing process, due to a sharp angular debris.

Figure 5.25: Evidence of the Large Abrasive Element due to Metallic Wear at 2.8 Mpa.

At the lower loads, the surface is covered with a number of "pseudo" cracks and as the load increases these cracks decrease in number as the severity of the wearing increases (FIGURE 5.26). These "pseudo" cracks appear to be formed as a result of a non-coherent surface layer. The cracks themselves are gaps in the surface layer where the graphite from the spheroids surface. It appears that as the load or velocity increases theses "pseudo cracks act as initiation points, from which surface tearing progresses.

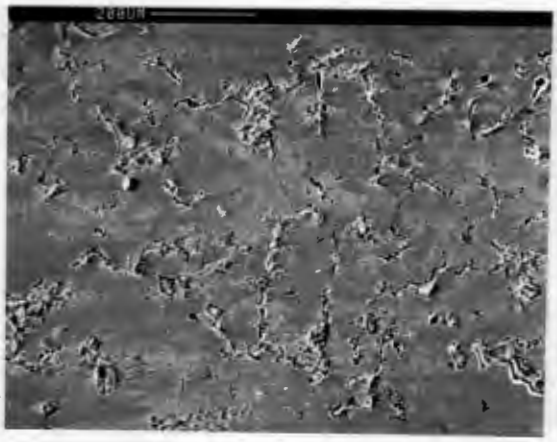

a] A general view of the surface, showing what appears to be cracks in the surface film.

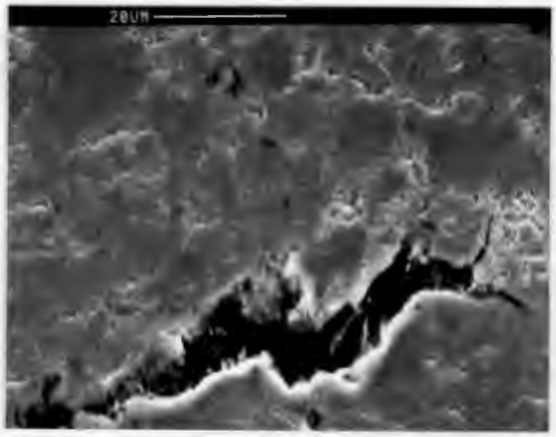

b] A close-up view of the cracks, showing the crack to be the initial point of film break down where a graphite nodule is residing.

Figure 5.26: Pseudo Cracks Found on the Surface 0.5 m/s, 0.9 MPa

2.0 ms^{-1}

At 2.0 ms^{-1} the increase of load from 0.9 to 2.8 MPa has a minimal effect on the characteristics of the surface. However the degree of smearing increases with increasing load (FIGURE 5.27). At 2.8 MPa there is some evidence of transfer and back transfer on the oxidised surface (FIGURE 5.28).

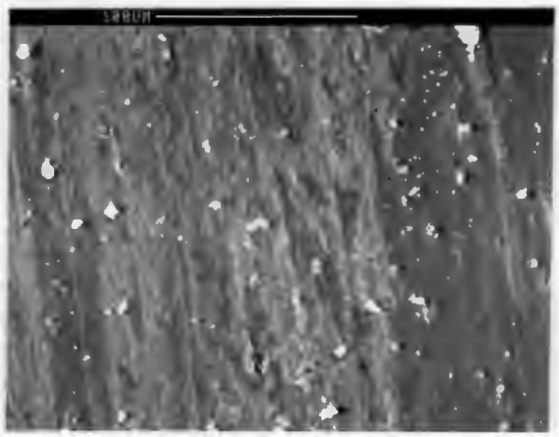

a] The surface at a load of 0.9 MPa, exhibiting some surface smearing.

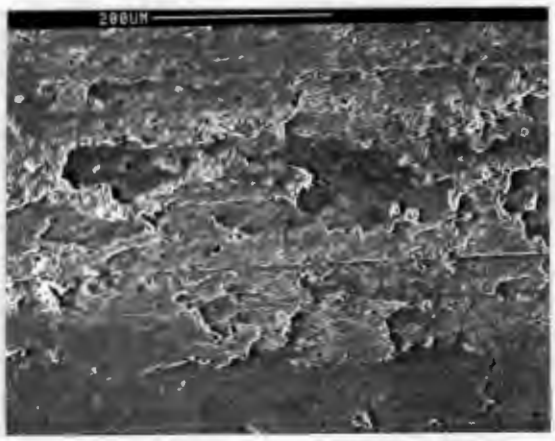

b] At a load of 2.8 MPa the surface smearing has increased slightly, with a more glazed appearance.

Figure 5.27 : Increase in Degree of Surface Smearing as the Load Increases at 2.0 m/s.

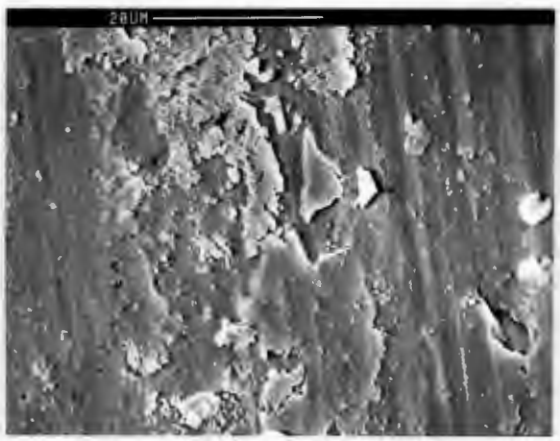

a] A number of apparently loose particles, on the surface.

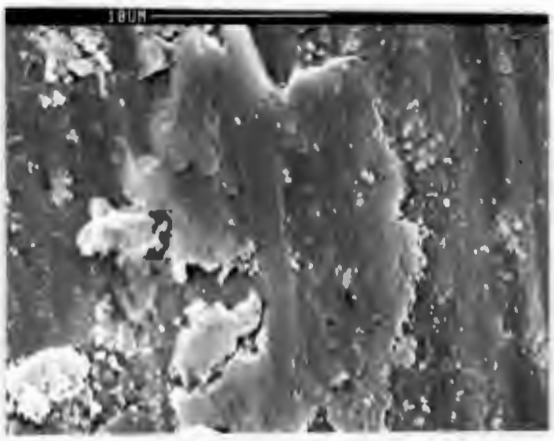

b] A more detailed view of the apparently loose particle, which has been removed else where and transferred back on to the surface.

Figure 5.28: Evidence of Transfer and Back Transfer at 2.8 Mpa 2.0 ms^{-1}.

5.3.2 Subsurface Characteristics

Microhardness

At the speed of 0.5 ms^{-1} no deformed layer was detected below 2 microns at any load tested. While at 2 ms^{-1} it was notable that the patchy white layer and characteristic three regions discussed in SECTION 5.4 was evident at all loads. The amount or degree of this white layer increased as the load increased although it was not possible to determine this quantitatively.

At the intermediate speed of 1.5 ms^{-1} the patchy white layer was evident at all loads. While at 1.0 ms^{-1} the white layer was only evident at the highest load of 2.8 MPa, it was noted that this white layer was found in a limited area and in smaller quantities.

5.3.3 Sliding Wear Tests

The effect of load on the wear rate is tabulated in TABLE 5.4 . At the lower sliding velocity of 0.5 ms^{-1} the effect of increasing the load causes a linear increase in the wear rate, while at 2.0 ms^{-1} there is a slight decrease (FIGURE 5.29).

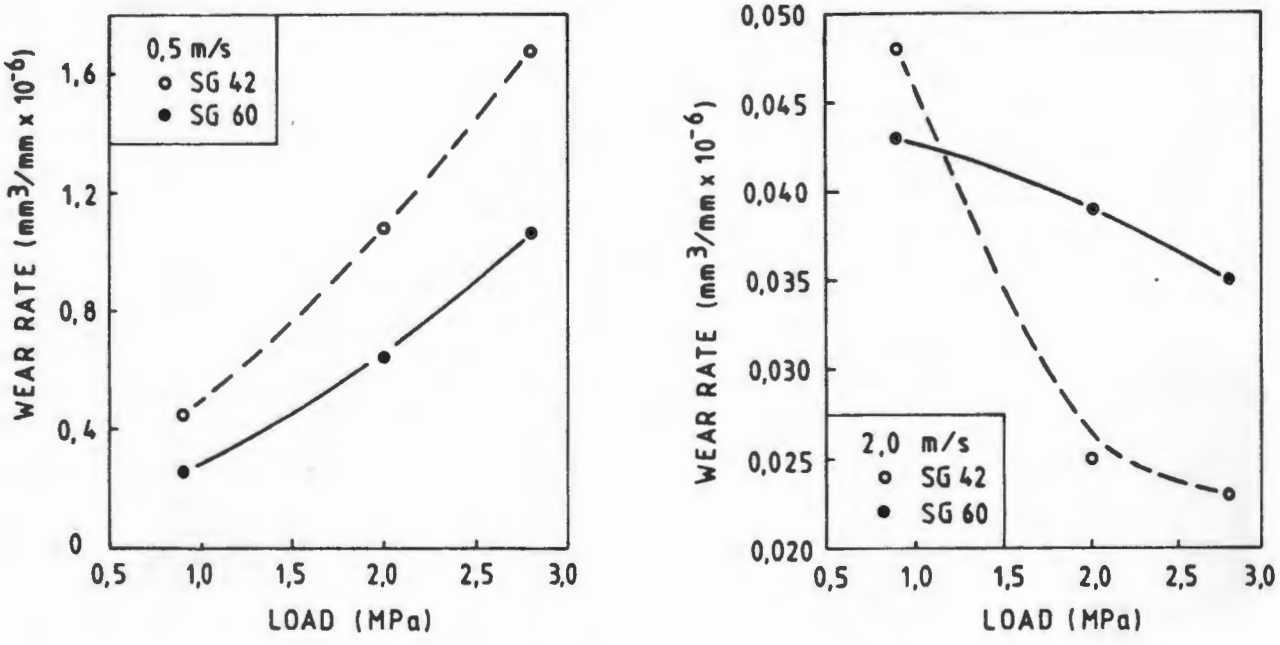

a] Effect of increasing load at 0.5 ms^{-1}. b] Effect of increasing load at 2.0 ms^{-1}

Figure 5.29: Effect of Load on Wear Rate at 0.5 and 2.0 ms^{-1}

Table 5.5 : Wear Rates of ADI in Relation to Load

Material	Wear Rate $mm^3/mm .10^{-6}$			
	0.5 ms^{-1}	1.0 ms^{-1}	1.5 ms^{-1}	2.0 ms^{-1}
SG42				
AT300				
0.9 MPa	0.45	0.57	0.122	0.048
2.0 MPa	1.08	0.54	0.059	0.026
2.9 MPa	1.68	0.40	0.051	0.023
SG60				
AT300				
0.9 MPa	0.26	0.46	0.098	0.043
2.0 MPa	0.65	0.33	0.051	0.041
2.8 MPa	1.06	0.32	0.051	0.038

When examining the difference between the two grades of SG42 and SG60 for a specific austempering condtion, the austempered grade of SG60 has a lower wear rate than the austempered grade of SG42, at all loads when sliding at a velocity of 0.5 ms^{-1}. It is apparent that the higher wear resistance of the SG60 grade is related to it's higher hardness and strength at 0.5 ms^{-1}. While at the higher sliding velocity of 2.0 ms^{-1} and load of 0.9 MPa the SG60 austempered grade has a lower wear rate, but as the load increases to 2.0 and 2.8 MPa, the SG42 grade has the lower wear rate. At 2.0 ms^{-1} there appears to be a change in the wear mechanism where the wear behaviour is no longer completely dependent the initial mechanical properties of the austempered iron. At this point the wear rates are similar for all austempered grades derived from a particular parent grade.

Sliding Velocity

The effect of load for the wear behaviour of SG42 is illustrated in terms of speed in FIGURE 5.30. At the low load of 0.9 MPa the wear rate reaches a maximum at 1.0 ms^{-1}. At the higher loads the maximum is reached at 0.5 ms^{-1}.

As the load is increased from 0.9 MPa to 2.9 MPa the difference in the wear rates between 0.5 and 2.0 ms^{-1} increase. At the low velocity of 0.5 ms^{-1} the wear rate is dependent on load, while at the higher velocity of 2.0 ms^{-1} the wear rate is similar for all three loads.

This behaviour was found to be similar for SG60, with SG60 performing better than SG42 at 0.5 ms^{-1}, similarly at 1.0 ms^{-1} and worse at 1.5 and 2.0 ms^{-1}.

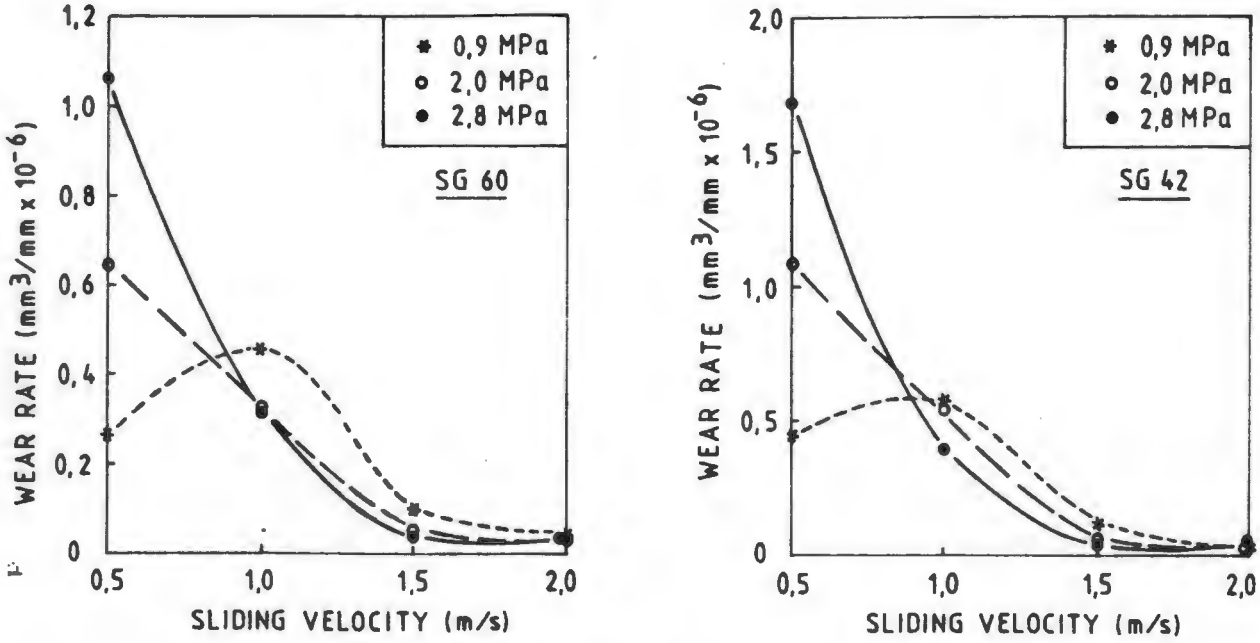

Figure 5.30: Effect of Load on Wear Rate as a Function of Speed

5.4 COMPARATIVE TEST

These tests were conducted with two grades of SG42 austempered at 250°C and 350°C, against Steel A oil quenched base, with a load of 2.8 MPa. Three quenched and tempered steels were included for a comparison.

5.4.1 Surface Topography

At 0.5 ms^{-1} the surfaces of the austempered irons had a smeared appearance similar in characteristic as that found at a sliding velocity of 2.0 ms^{-1} against a oil quenched SG60 base (SECTION 5.2). When the Austempered irons where worn against the Steel A base, all surfaces were oxidised with the surface characteristicss at 0.5 ms^{-1} and 2.0 ms^{-1} being similar in appearance (FIGURE 5.31).

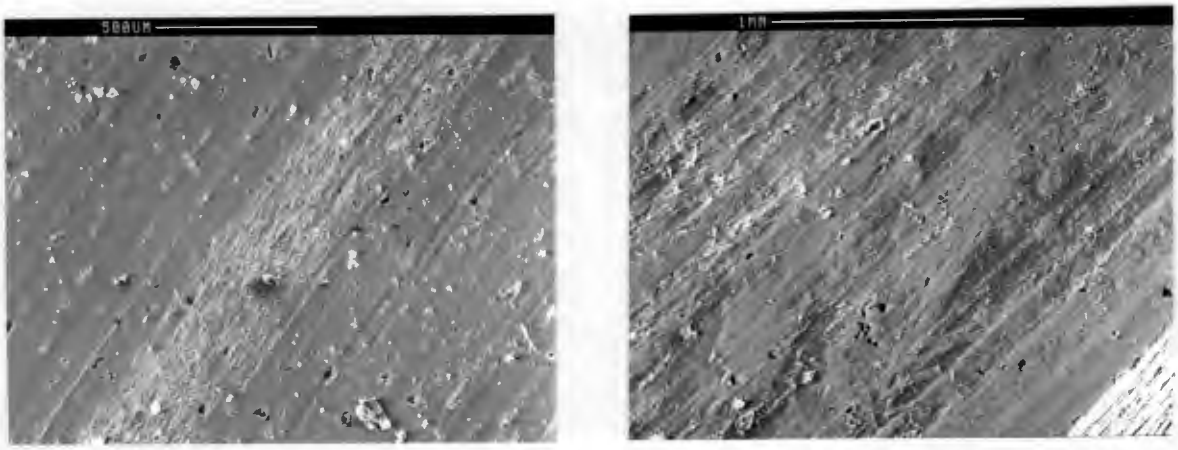

a] General surface at a sliding velocity of 0.5 ms^{-1}, exhibiting a large degree of surface smearing, with a glazed oxide surface layer.

b] The general surface at a sliding velocity of 2.0 ms^{-1} with similar characteristics as at 0.5 ms^{-1}.

Figure 5.31: General Surface at Sliding Velocity of 0.5 and 2.0 ms^{-1}

The distinction between the different sliding velocities was that at the higher velocity of 2.0 ms^{-1} the oxide or surface layer appeared to be lifting in places. This indicated a lack of coherency of the surface layer (FIGURE 5.32).

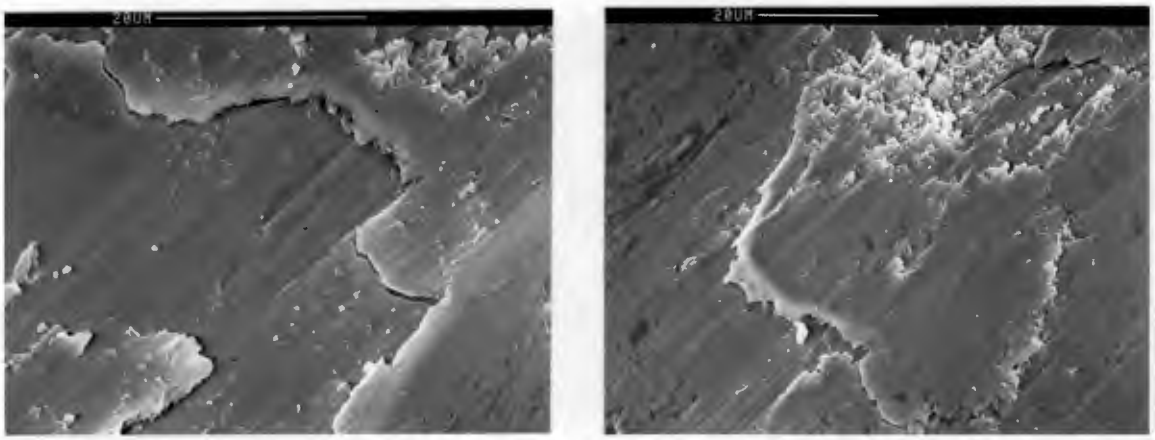

Figure 5.32: Indication of a Lack of Coherency at the Higher Velocity

5.4.2 Subsurface Characteristics

XRD

For all the speeds tested under these conditions no austenite peak was detected. This trended to indicate that the retained austenite on the surface on the wearing surface of the austempered irons had transformed completely.

Microhardness

The characteristic surface layer present at 2.0 ms^{-1} shown in SECTION 5.2 was also present, at all sliding velocities in this series of tests. The deformed layer was less than 50 microns thick, although no comparative value could be made. No quantifiable distinction in surface hardness could be made between the different sliding velocities or between the deformed layer as discussed in SECTION 5.2

5.4.3 Sliding Wear Tests

Tested under the particular conditions, the wear resistance of the austempered irons increased fairly linearly with increase in sliding velocity. The iron with the lower austempering temperature of 250°C performs better than the lower hardness and strength iron austempered at 350°C. It is notable that the difference in the upper and lower wear rates, at sliding velocity of 0.5 and 2.0 ms^{-1}, are in the same order of magnitude (FIGURE 5.33).

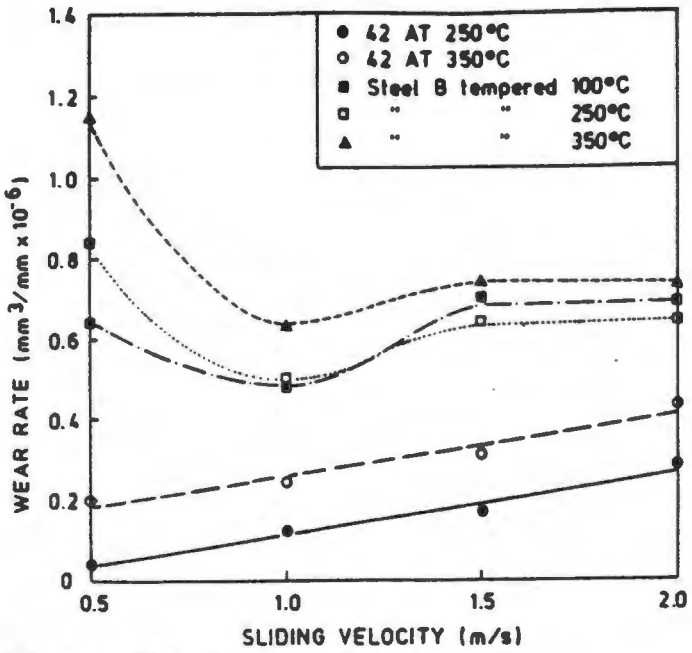

Figure 5.33: Effect of Wear Rate as a Function of Speed

It is also apparent from TABLE 5.5 that the ADI out perform the much harder steels at all velocities when sliding against a hardened steel base. This probably reflects the importance of the graphite as a lubricant, since the hardened steel performed much better when sliding against an ADI base (SECTION 5.2.1).

Table 5.5 Results of Wear Behaviour of ADI Relative to Steels

Material	Wear Rate $mm^3/mm .10^{-6}$			
	0.5 ms^{-1}	1.0 ms^{-1}	1.5 ms^{-1}	2.0 ms^{-1}
SG42				
AT250	0.04	0.12	0.16	0.28
AT350	0.20	0.24	0.31	0.43
Steel B				
Q & T				
100 (Hv850)	0.62	0.48	0.70	0.69
250 (Hv630)	0.84	0.50	0.68	0.64
350 (Hv480)	1.15	0.63	0.74	0.73

Chapter VI

DISCUSSION

It is apparent from the results of laboratory investigations that the superior properties achieved by austempering ductile irons makes them very attractive engineering materials. Furthermore, examination of the results demonstrates that austempering also improves the unlubricated sliding wear resistance of spheroidal cast irons by many orders of magnitude. The results show that these irons perform as well as a much harder steel when worn against an oil quenched spheroidal graphite iron base. However, when samples of ADI and steel are worn against a hardened low alloy steel base, the austempered ductile irons outperform the steels of much higher hardness. The remarkable performance of austempered ductile irons is clearly linked to both the microstructure and the surface characteristics which develop during sliding.

6.1 EFFECT OF VELOCITY

As the velocity of sliding increases there is a magnitudal reduction in the wear rate, with two mechanisms dominating the wear behaviour (FIGURE A). At the lower velocity an "metallic" type wear is dominant while an "oxidative" type wear is observed at the higher sliding velocity. In FIGURE A, the wear rates of the austempered irons are illustrated, exhibiting the distinction in the wear behaviour in terms of sliding velocity. At 0.5 ms^{-1} the wear resistance of these austempered ductile irons are clearly linked to austempering, with the wear rate increasing as the austempering temperature decreases. However, at 2.0 ms^{-1} the wear rate is similar for austempering conditions of a specific parent grade.

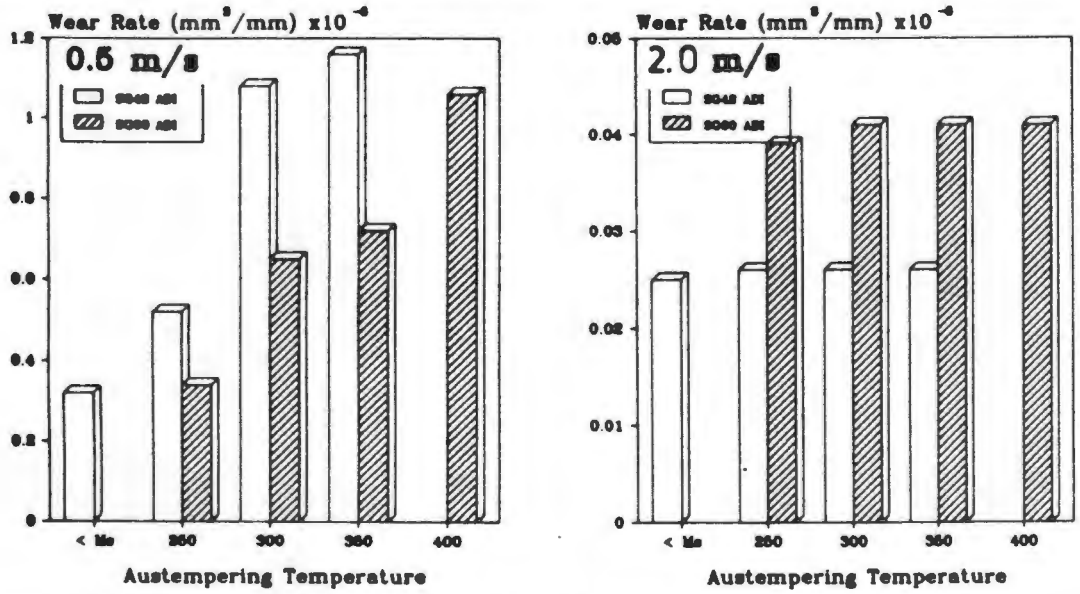

Figure A: Effect of Speed on the Wear Rate of SG42 and SG60 Austempered Irons.

Wear at the Lower Sliding Velocity

At the lower sliding velocity of 0.5 ms^{-1} metallic type wear is evident. The wear rates appear to be largely affected by the mechanical properties of the pins with surface tearing playing a major role.

The results indicate that a thin oxide film is formed at this velocity. It is believed that this film is easily displaced from the asperities resulting in metallic contacts. The prevailing oxidation kinetics and sliding velocity do not permit the majority of the asperities to reoxidise and reduce the number of metallic contacts during sliding. Thus it could be expected that a great deal of metallic interactions would persist, with welding and shearing being the dominant mechanism of wear debris formation (FIGURE B).

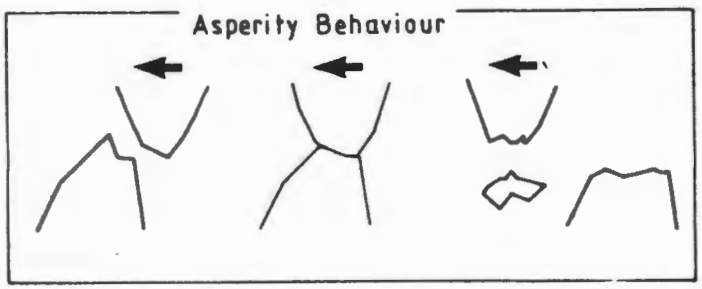

- Relatively low flash and mean temperature
- High strength junction formed
- Insufficient time for asperities to reoxidise before next asperity interaction
- Welding and shearing resulting in the formation of lump-like particles which are conducive to three-body abrasion

Figure B: The Asperity Interaction Occurring at 0.5 ms^{-1}.

The development of a thin oxide film is supported by the XPS analysis of the outer 2-4nm of the surface indicating that at this velocity the major oxide present is magnetite (Fe_3O_4), which forms at 200°C. This indicates that the majority of the surface temperature is below 200°C, with the possibility of logarithmic oxidation kinetics prevailing. This results in the development of very thin oxide films.

The SEM examination of the surface further supports the hypothesis of extensive metallic interaction with subsequent surface tearing. Associated with this tearing is the production of large angular type debris. It is thought that the abrasive type wear grooves, at angles to the wear direction, result from a three body abrasive type mechanism involving the debris. However, the well defined abrasive type wear tracks in the wear direction are formed through a ploughing mechanism from the metallic interaction of harder asperities.

At this velocity metallic type wear is predominant and the wear behaviour appears to be largely determined by the mechanical properties of the materials and their ability to resist welding and shearing.

The higher strength materials are thus expected to have a better wear resistance. The lower austempering temperatures result in a material with higher mechanical strength and thus these materials exhibit the lower wear rates. The austempered grades of SG60, for a specific austempering condition, have the better mechanical strength and also the lower

wear rate compared to the austempered SG42 grades. This indicates that microstructural parameters are the dominant factor in determining the wear behaviour under these conditions. Furthermore, when comparing the acicular ferrite and retained austenite structure to the behaviour of the as cast parent material, the austempered ductile iron outperforms the parent material by orders of magnitude.

It is expected that the adhesive force between metallic asperities for the austempered irons wearing against an austempered iron base would be higher than that for alloy steel (B) sliding against an austempered iron base. Thus it is thought that under conditions of metallic wear, the austempered iron would have a higher wear rate than Steel B at an equivalent hardness. However, a number of austempered irons which have an initial lower surface hardness than Steel B (Hv850), exhibit similar wear rates with some austempered irons outperforming Steel B, e.g. SG60 AT250 (Hv500) (TABLE [5.3]).

This remarkable wear resistance of ADI is attributed to its unique microstructure of acicular ferrite and retained austenite in conjuction with the partial transformation of austenite to martensite upon wearing. This results in an extremely hard, yet tough work hardened surface layer which appears to be confined to a thickness of less than 5 microns. Such a layer resists surface adhesion, deformation and shearing thereby resulting in a lowering of the wear rate.

Wear at Intermediate Sliding Velocities

When the sliding velocity increases to 1.0 ms^{-1} the wear process remains essentially the same as that occurring at 0.5 ms^{-1}. Metallic asperity contacts persist and metallic tearing due to welding and shearing remains the dominant mechanism. There is, however, a reduction in the wear rate as the velocity is increased from 1.0 ms^{-1} to 1.5 ms^{-1} owing to an increase in frictional heating which leads to an increase in the oxidation kinetics and a reduction in the number of metallic contacts.

As the sliding velocity increases from 1.0 to 1.5 ms^{-1} the well defined wear tracks associated with the metallic wear are steadily reduced with surface smearing becoming more evident at 1.5 ms^{-1}. The increase in the surface smearing at 1.5 ms^{-1} is an indication of a temperature increase when the sliding velocity is increased.

Wear at the Higher Sliding Velocities (2.0ms^{-1})

At a sliding velocity of 2.0 ms^{-1} the wear rate for a specific austempered ductile iron is orders of magnitude lower than that at a sliding velocity of 0.5 ms^{-1}. Associated with this reduction in the wear rate is a reduction in the frictional force as the velocity increases. It is thought that at the higher sliding velocity a thicker and more coherent oxide film (in conjunction with the formation of a white layer) results in a similar wear rate for all ADI grades for a specific parent grade. This thicker and more coherent oxide film protects the surfaces by reducing the number of metallic contacts, thus reducing the friction and the wear by acting as a boundary lubricant.

As the velocity of testing is increased, both the asperity flash temperature and the mean surface temperature increase. It has previously been noted that this type of mild wear is associated with a relatively high asperity flash temperature and a relatively low mean surface temperature [39,40]. At the sliding velocity of 2.0 ms^{-1} the predominant oxide is

wüstite (FeO) which forms at temperatures in excess of 570°C. The change in surface characteristics also leads to a change in the mechanism of material removal and a reduction in the wear rate. It is expected that a large part of the surface is at 570°C and above. The increase in temperature leads to an increase in surface oxidation rates and the development of thicker, more stable oxide layers. These conditions of increased temperature and surface oxide layer do not facilitate the formation of asperity junctions, but rather lead to deformation and smearing of the contacting surfaces with the oxide layer preventing metallic contact (FIGURE C). The mechanism of material removal is due to fatigue and delamination of the oxide and substrate, giving rise to the formation of "flake-like" debris.

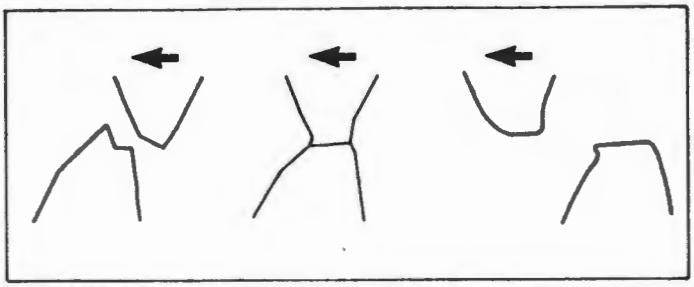

- Relatively high flash temperature but a low mean temperature
- Asperities deform easily with resultant smearing
- High oxidation kinetics prevailing and preventing metallic welding
- Debris formation mainly through fatiguing of the oxide film

Figure C: The Asperity Interaction Occurring at 2.0 ms^{-1}.

This hypothesis is supported by the nature and type of debris found as well as by the appearance of the pin surfaces at this sliding velocity. The surface appears to be smeared as a result of higher contact temperatures allowing the easy deformation of asperities, while the oxide film prevents metallic contact. It is likely that the layer geometry of the flake-like debris would be crushed into smaller particles as a result of repeated interactions between the sliding surfaces. This is in opposed to the abrasive action caused to the surface by the lump-like debris formed at the lower sliding velocity of 0.5 ms^{-1}.

The breaking down of the flake-like debris leads to further oxidation, aiding the growth of oxide films through a process coalescence. The oxidised debris is compacted to form a non-porous and adherent film which is smoothed out by asperity contacts. This process of debris coalescence occurs in conjuction with normal oxide growth. This coalescence of oxidised debris is evident by the granular-like appearance on the surface of the pins where flake particles have been removed. This film grows to a critical film thickness and with the continual cyclic stresses eventually result in the formation of the flake-like particles. As the process of flake-like debris formation is through a fatigue process of the surface film and substrate material, the fatigue strength of the oxide as well as the substrate material will have an influence on the wear rate.

It is noticeable that the wear rate of these irons decreases to a constant value as the velocity of sliding increases. It is throught that this is due to the progressive development of a wearing surface and subsurface which is similar for all austempered ductile iron grades, derived from a specific parent grade.

It is believed that at the higher velocities of testing, high asperity flash temperatures in the immediate surface regions result in the austenitisation of the duplex ferrite and very high carbon austenite matrix. Subsequent cooling gives rise to a high carbon martensitic structure containing fine carbides which are similar for all austempering irons regardless of the initial microstructure. It should be noted that the original matrix carbon content for all the austempered irons are similar for a specific grade. Furthermore, high temperatures linked to observed plastic deformation of the surface gives rise to the appearance of patchy white layers. Such white layers have been found to occur in many situations involving wear and are believed to arise generally through a thermo-mechanical process. Their extremely high hardness and resistance to tempering give rise to excellent wear properties.

The flow type characteristics found in the white layer as well as the fine matrix adjacent to the white layers tends to indicate that a thermal process is involved together with the mechanical deformation. The white layers found in the present work have similar characteristics to those discussed by Rogers [65].

The white layer formation appears to be affected by the carbon content in the matrix. White layers were found on all austempered grades of SG42 and SG60 with the degree of white layer formation being similar in all cases. However, the parent grades of SG42 exhibited no evidence of white layers, while the parent grade SG60 exhibited some evidence of white layer formation after the sliding wear tests. It should be noted that the SG60 has a higher carbon content available due to the cementite in the ferritic and pearlitic matrix, while SG42 has a low ammount of carbon available in it's ferritic matrix.

The wear resistance of SG60 was found to be far superior to that of SG42 in the as cast condition. It would also be expected that SG60 austempered grades would have a better wear resistance than the SG42 austempered grades since the SG42 austempered irons are believed to have a lower matrix carbon content than SG60 austempered irons [62]. However, the degree of white layer formation was apparent between austempered irons of SG60 and SG42 was similar. The SG42 austempered grades had the superior wear resistance, despite having the supposed lower carbon content in the matrix and the lower mechanical strength.

Prior work on the abrasive wear behaviour of these two grades showed that SG42 had a higher wear resistance than SG60 austempered grades. This was attributed to austempered grades of SG42 having a higher M_d temperature resulting in higher amounts of austenite transforming to martensite during abrasion [62]. In the present work the XRD results were inconclusive, in that no retained austenite peak was detected, owing to possible interference from white layer and oxide effects.

A possible explanation for the superior sliding wear rate exhibited by SG42 austempered ductile irons could be the highly localised effect of austenite to martensite transformation. The higher amount of austenite transforming to martensite in the SG42 austempered iron would result in a higher fatigue resistance compared with the austempered irons of SG60, and therefore the formation of (flake-like) wear debris in the substrate would be reduced with a resulting decrease in the wear rate.

Thus the variation in the original microstructure and properties of these austempered irons play little part in determining wear resistance at high velocities, since the surface and subsurface characteristics become essentially the same for all irons. These common features, together with the development of a critical oxide film thickness, leads to a steady state wear situation in which the specific wear rate is similar for all irons of a specific parent grade.

6.1.1 Model Of Wear Resistance

It is believed that as the sliding velocity increases, the wear rate follows a distinctive type of curve with three main regions (FIGURE D).

In **region 1,** mild wear changes to a severe metallic type wear as the wear rate increases from zero. This occurs because the time for asperity reoxidation steadily decreases and the time between asperity interaction decreases as the velocity increases. Thus a greater number of metallic contacts are formed as the velocity increases and a maximum wear rate is reached when a large number of high strength metallic junctions are formed. It is believed that severe metallic welding and shearing results in the formation of large angular debris which contributes to a secondary third body abrasive type wear.

In **region 2,** as the velocity increases further, severe metallic type wear reverts to a second mild wear regime. The increase in velocity contributes to an increase in frictional heating with an increase in oxidation kinetics from logarithmic to parabolic and cubic rates. This leads to a reduction in the number of metallic contacts, owing to the formation of an oxide film. At this point it is believed that the asperity flash temperature is high, while the mean surface temperature is relatively low. A minimum wear rate exists when the temperature is increased sufficiently to aid higher oxidation kinetics. It is further supposed that the low mean surface temperature results in the strength of the substrate remaining high, while the high flash temperature aids the mechanism of asperity deformation and smearing and possible white layer formation [39].

In **region 3,** as the velocity of sliding increases still further, the second mild wear regime persists with the wear rate increasing slightly with increase in velocity. It is thought that the asperity junctions oxidise as in region 2, but as the frictional heating increases there is no longer an effective increase in the oxidation kinetics. The increase in temperature above that occurring in region 2, results in a deterioration of the oxide properties of film formation, with the decohesion of the film becoming more apparent. An increase in the formation of wear particles as the temperature increases sufficiently, was predicted by EQUATION [1.25], with the growth of oxide

films under tribological conditions. According to Bill [11], with further increases in temperature, debonding of the oxide film can occur with a reversion from parabolic and cubic rates to linear oxidation rates. Although the oxide is present it is not as effective, the effectiveness decreasing as the velocity and temperature increase. An increase in the mean temperature also results in the weakening of the substrate material with a further increase in wear.

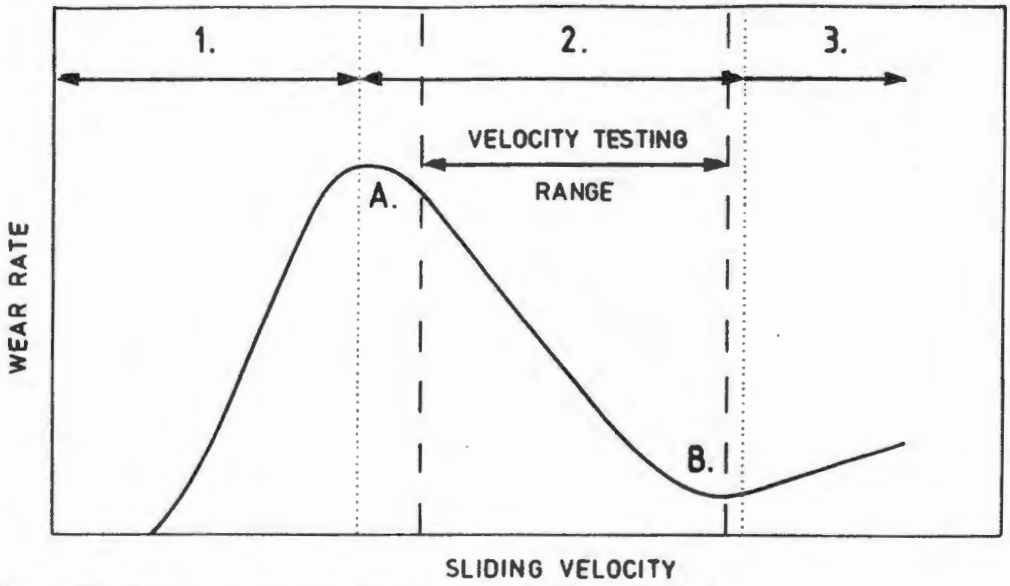

Figure D: Effect of Sliding Velocity on the Wear Behaviour

The PEAK A is related to the severity of the metallic wear regime. It is suggested that the important parameters relevant for **PEAK A** are :-

Material strength; Or an ability to resist junction shearing and welding. An increase in strength (hardness) will result in a decrease in PEAK A.

Mating material; Similar materials will result in an increase in the adhesion between the metallic junctions, thus an increase of PEAK A.

Temperatures; If the mean surface temperature is low and the junction flash temperature is relatively low, the wear rate will be at a maximum. The asperities or junctions will then have a higher strength, increasing surface tearing and abrasive effects.

The PEAK **B** is related to the minimal wear occurring during mild oxidative type wear. The important factors in determining the wear behaviour at **PEAK B** are :-

High asperity flash temperature. This results in softer, easily deformable asperity contact with cyclic fatiguing being the dominant debris formation process.

Low mean surface temperature. When the surface temperature is relatively low, it prevents the weakening of the substrate. As the temperature increases, the substrate weakens and larger particles are torn from the substrate surface.

Surface transformations. Any transformation resulting in the increase in the surface hardness leads to a reduction in the wear rate.

White layer formation. The type, hardness and degree of white layer formations leads to a reduction in wear rate.

Oxide formation. The type of oxide present, oxide coherency and thickness play an important part in the reduction of the wear and it's ability to resist metallic contacts (acting as a boundary lubricant).

6.2 THE EFFECT OF LOAD

When the load is increased at the lower sliding velocity (0.5 ms^{-1}), the wear rate increases linearly for both SG42 and SG60 austempered irons. However, at the higher sliding velocity (2.0 ms^{-1}), the increase in load did not have a significant effect on the wear rate since oxidation of the surface becomes rate controlling. This follows one of the basic tribological laws, that the wear rate is proportional to the load provided the surface characteristics remain the same.

Lower Velocity

At the lower velocity of 0.5 ms^{-1} metallic wear dominants. The severity of the wear increases as the load increases from 0.9 to 2.8 MPa. The harder, stronger austempered irons of SG60 outperforms the SG42 austempered irons. This result illustrates the importance of strength and microstructure in this wear domain.

At the low load of 0.9 MPa the combination of film formation and surface deformation results in the graphite spheroids in the ADI matrix being covered with a oxide film. On continued wearing, this film begins to breakdown resulting in the formation of pseudo cracks. These cracks are formed at localised weak points where graphite spheroids reside in the iron matrix below the surface film. When the sliding velocity or load is increased it appears that the pseudo cracks disappear as the severity of deformation increases. This is a result of these cracks being ripped apart with the material being torn out in the vicinity of the crack as a result of surface tearing, revealing the residing graphite spheroid below the surface. Associated with this increase in the surface tearing is an increase in the wear rate.

At the intermediate speed of 1.0 ms^{-1} there is a tendency towards a milder oxidative type wear, with white layer formation evident at a load of 2.8 MPa. This is indicative of the wear severity increasing as the load increases. This increase in load promotes the formation of white layers which were not present at the lower loads.

Higher Velocity

Oxidative type wear and the formation of white layers contribute to the wear becoming similar for all loads when the velocity is increased to 2.0 ms^{-1}.

The oxidative wear is dominant at all loads for velocities of 1.5 and 2.0 ms^{-1}, with the degree of white layer formation increasing as the load increased. As the white layer formation increases, the wear rate decreases.

Proposed System

A model can be proposed that follows the basic model in SECTION 5.2.4. When the load increases and the severity of the wear increases, the wear system moves to the left (FIGURE E). The increase in the severity of the wearing regime results in an increase in temperature as the load increases. The mild wear regime occurs earlier for a specific sliding velocity as the load increases. However, as the load is decreased the severity of the wearing system decreases with the curve moving to the right (FIGURE E), postponing the development of the mild wear regime. A further effect of increasing the load is that PEAK A is increased. It would be expected that during a condition of metallic wear, the surface characteristics would also remain the same and the wear rate would be related to the load. It is further expected that an increase in load at the minimum mild wear (PEAK B), will enhance white layer formation leading to a reduction in wear at this point.

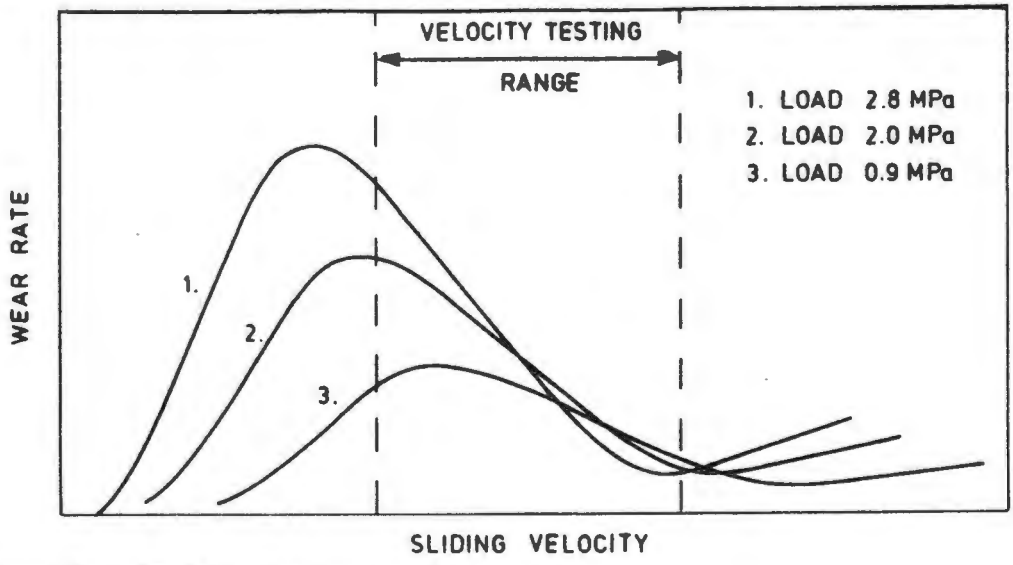

Figure E: A Model to Explain the Effect of Load

6.3 COMPARATIVE TESTING

With a change in the wear base to Steel A, the adhesive component between the mating surfaces is reduced. This occurs as a result of austempered irons now sliding against a dissimilar metal. Although the adhesive component is reduced, it will only effect the wear rate under conditions of metallic wear. The new base has no free graphite which results in a more severe wear system, with white layer formation being evident at all sliding velocities.

Wear rate increases linearly with velocity, although the increase is not very marked as is supported by the wear rates at the 0.5 and 2.0 ms^{-1} being within the same order of magnitude. This is substantiated by the similarity of the worn surfaces. At all velocities, the worn surfaces appeared similar with only the apparent degree of smearing increasing slightly as the velocity increased. Lower wear rates are experienced by the irons austempered at lower austempering temperatures.

An increase in the severity of wear results in the earlier onset of the second mild regime for a specific velocity. Corresponding to this is a parallel increase in mean and flash temperatures, with the wear behaviour being similar to region 3 discussed in SECTION [6.1.1]. It is believed that the flash asperity temperature is high enough to cause the oxidation rate to revert to linear rates because of the high decohesion of the oxide film. This degree of decohesion increases with frictional heating with the decohesion becoming more apparent at 2.0 ms^{-1}.

The mean surface temperature is also believed to increase, resulting in the weakening of the substrate material. Thus the mechanical strength of the material is expected to have an influence on the wear rate.

Proposed Model

The following model is proposed when the sliding base is changed from a ADI to a non-graphite iron. The model proposed is similar to that used to explain the the effect of sliding velocity (SECTION 5.2.4). It appears that as a result of the base change to a non-graphite producing base the severity of the wear system increases. Thus the appearance of the oxide films occurs relatively sooner, for a specific sliding velocity, as a result of higher frictional heating effects.

Illustrated in FIGURE F is the schematic demonstration of this effect, with the basic curve moved to the left as a result of the severity of the wear system increasing. The intensity of PEAK A (SECTION 5.2.4) is reduced as a result of the adhesive force being reduced when the sliding pair is not of the same material during metallic wear.

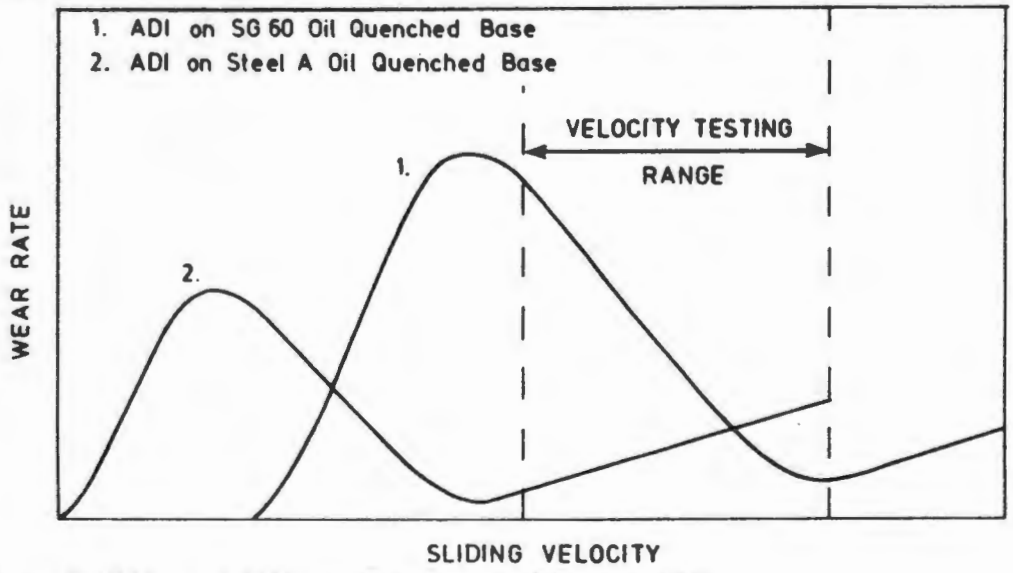

Figure F: Effect of Different Bases on the Wear of ADI.

6.3.1 Comparative Results

When compared to steels (Steel B) of higher and equivalent hardness, the austempered ductile irons perform far better at all speeds under the conditions tested. It was also noted that Steel B showed a marked reduction in the wear rate when worn against an oil quenched SGI base as opposed to a steel base (Steel A) (TABLE 5.3)

Lower Sliding Velocities

At the lower velocity tested the wear rate appeared to be linked to the mechanical properties of the material. This is illustrated when the wear resistance of the austempered irons and steel are compared as a function of hardness (FIGURE G).

The outstanding performance of ADI of SG42 and SG60 sliding against a SG60 oil quenched base is a result of the high strength of it's unique structure of acicular ferrite, austenite and free graphite with a further effect of partial transformation of the austenite to martensite. This transformation percentage is less than that which occurred in the abrasive wear of these irons [62]. Thus it is expected that the microstructure of these austempered ductile irons plays a larger role than in abrasion where a greater percentage of the surface had transformed to martensite. The higher strength properties of the SG60 austempered irons results in it's better wear resistance compared to the SG42 austempered irons. This is in fact opposed to what was experienced in abrasive wear with the greater transformation of austenite to martensite in SG42 austempered iron resulting in SG42 ADI having a better abrasive wear resistance than SG60 austempered irons.

In the present study of sliding wear, the SG42 austempered irons worn against a steel base had a far better wear resistance than the SG42 worn against a SG60 oil quenched base. This is attributed to the earlier onset of the second mild wear regime. Thus the wear occurs in an oxidative type wear regime, with development of white layers and oxide films reducing the wear rate.

Higher Sliding Velocities

Illustrated in FIGURE G, is the wear rate of the austempered ductile irons and Steel B operating at 2.0 ms^{-1}, under mild wear conditions. It is notable that under these conditions the mechanical properties have little effect on the determination of the wear rates. However, the ADI show far superior wear resistance when compared to steel (B) of an equivalent hardness.

Although no conclusive theory was found to explain the superior wear resistance of the SG42 austempered irons compared to that of the SG60 grades, is believed that austenite to martensitic transformation plays a role on a very localised scale, similar to that occurring above 5 microns at 0.5 ms^{-1}. It has previously been found that the austenite in SG42 grades is less stable and the amount of austenite transforming to martensite is greater than in SG60 [62]. This transformation will result in a reduction in wear rate due to an increase in hardness and an increase in resistance to debris formation from fatiguing.

When the austempered irons of SG42 are worn against the steel base, an oxidative wear regime persists with the formation of white layers. Furthermore, the wear resistance decreases with increasing strength. This is attributed to the mechanical properties influencing the wear rate when higher frictional temperatures result in the decohesion of the oxide film and weakening of the substrate material.

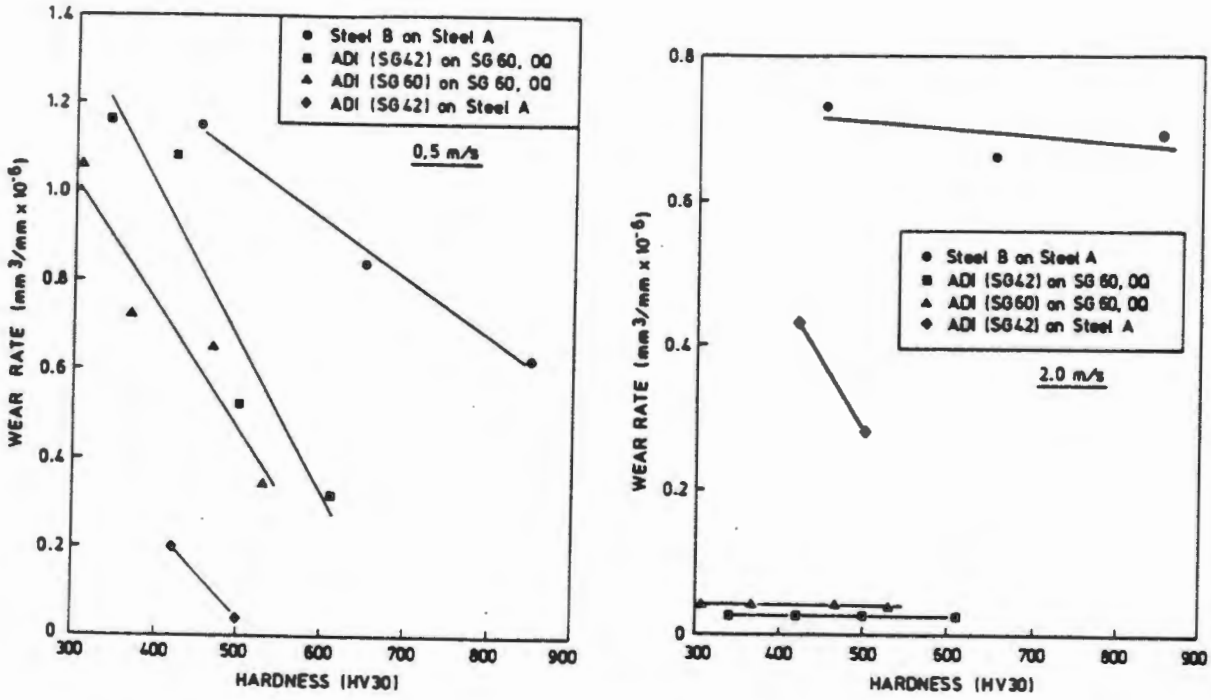

Figure G: The Effect of Hardness and Wear Rates for the Comparative Test.

Chapter VII

CONCLUSIONS

1. The unlubricated sliding wear resistance of two commercial austempered grades of spheroidal graphite iron were examined under conditions of sliding velocity and load. These irons showed a vast improvement in mechanical strength and unlubricated sliding wear resistance with austempering.

2. Two mechanisms were found to dominate the sliding wear behaviour, with the wear rate decreasing in orders of magnitude as the sliding velocity increases.
   At the low sliding velocity a metallic type wear was evident with the wear rate being influenced by mechanical properties. However an oxidative film formation in conjunction with a white layer formation are the major controlling factors in wear rate determination at the higher velocity.

3. The austempered irons show an excellent wear resistance, with the wear rate decreasing by orders of magnitude when compared with the as cast spheroidal graphite irons. Furthermore these austempered irons outperform a hardened steel of a higher hardness.

4. At the low sliding velocity of 0.5 ms^{-1}, the remarkable wear resistance is attributed to a combination of the high strength derived from the microstructure, of acicular ferrite, austenite and free graphite with the partial transformation of the austenite to martensite.

5. The development of a protective tribological oxide film in conjunction with the formation of a patchy white layer leads to a magnitudal reduction in the wear rate as the sliding velocity is increased to 2.0 ms^{-1}. The development of this surface condition which is similar for all austempered irons results in a similar wear rate persisting for all austempered irons derived from a specific parent grade.

6. It was found that at the lower velocity of 0.5 ms^{-1} the wear rate increases with load, while at the higher velocity of 2.0 ms^{-1} the wear rate decreases with load. The effect of load or speed can not be explained in terms of only the one variable. It is necessary to explain the behaviour of velocity or load in terms of each other. Thus three models of wear behaviour were proposed to explain the wear behaviour in terms of :-

   i] Sliding velocity
   ii] Effect of load on sliding velocity
   iii] Effect of base rubbing material on sliding velocity.

7. It has previously been noted that unlubricated wear under conditions when a tribological stable oxide film is present, is essentially the same as wear under boundary lubricated conditions. Therefore, if this assumption is true, the wear behaviour experienced at 2.0 ms^{-1}, when the wear rate were similar for austempered irons of a specific grade, will be similar to the behaviour expected under boundary lubrication conditions. Hence it could be possible that when choosing a grade of ADI for a component for operation under these condition, mechanical properties will be the sole criterion, as the wear behaviour is expected to be similar for all grades.
   However, under specifically dry wearing conditions the mechanical properties and thus microstructure are an essential criterion for determining the wear behaviour.

References

1. ARCHARD, J.A. (1953): "Contact and Rubbing of Flat Surfaces", J. Appl. Phys., 24, 981.

2. ARCHARD, J.F. (1953): "Contact and Rubbing of Flat Surfaces", J.Appl.Phy., 27, 1057.

3. ARCHARD, J.A. (1957): "Elastic Deformation and the Laws of Friction", Proc. Roy. Soc., A243, 190.

4. ARCHARD, J.A (1961): "Single Contacts and Multiple Encounters", J. Appl. Phys., 32, 1420.

5. ARCHARD, J.A. (1980): "Wear Theory and Mechanisms", Wear Control Handbook, ed. M. Peters and W. Winer, ASME.

6. ARCHARD, J.A. & HIRST, W. (1956): "The Wear of Metals Under Unlubricated Conditions", Proc. Roy. Soc., A236, 397.

7. ARCHARD, J.F. & HIRST, W. (1957): "An Examination of a Mild Wear Process", Proc. Roy. Soc., A238, 515.

8. ALLEN, C., QUIRKE, S. & SCHEFFLER, O. (1988): "An Evaluation of the Wear of Metallic Materials Subjected to Soil Abrasion", Soil & Tillage Research, 11, 27-42.

9. ALLEN, C. & SCHEFFLER, O. (1988): "The Abrasive Wear of Steels in South African Soils", Tribology International, 127-134.

10. BHATTACHARYYA, S. (1980): "Wear and Friction in Steel, Aluminum and Magnesium Alloys, Part I - Pearlitic and Spheroidized Steel", Wear, 61, 133-141.

11. BILL, R.C. (1981): "The Role of Oxidation in the Fretting Wear Process", Int. Conf. Wear of Materials, San Fransco, ASME, 238.

12. BOWDEN, F.P. & TABOR, D. (1954): "The Friction and Lubrication of Solids Part I:", Caredon Press, London

13. BOWDEN, F.P. & TABOR, D. (1956): "The Friction and Lubrication of Solids Part II:", Caredon Press, London

14. BOWDEN, F.P. & TABOR, D. (1973): "Friction an Introduction to Tribology", Anchor Press, New York.

15. CAMPANY, R.G. & WILSON, R.F. (1982): "The Metallurgy of Scoring and Scuffing Failure", Proc. of 9th Leeds-Lyon Symp. on Tribology, Leeds Univ., Inst. of Tribology, 201-211.

16. CORNELIUS, D.F. & ROBERTS, W.H. (1961): "Friction and Wear of Metals in Gases up to 600°C", ASLE Trans., 4, 20.

17. COCKS, M. (1954): "The Effect of Compressive and Shearing Forces on the Surfaces Films Present in Metallic Contacts", Proc. Roy. Soc. B67, 238.

18. CZICHOS, A. (1978): " Tribology a Systems Approach to the Science and Technology of Friction and Lubrication", Elsevier Amsterdam.

19. DORAZIL, E. (1979): " Zwischenstufenuwadeln von Gusseisen mit Kugelgraphit", Giesserei-Praxis, 18, 355-366.

20. DORAZIL, F. & KRAUS, E. (1970): "The Effect of Austenitisizing Temperature on Isothermal Decomposition of Austenite in Unalloyed Ductile Iron", Slevarenstri, 503-506.

21. DYSON, A. (1980): "Kinematics and Wear Patterns of Cam Follower Automotive Value Gear", Tribology International, 121.

22. EYRE, T.S. & WILSON, F. (1969): "Effect of Matrix Structure and Hardness on the Wear Characteristics of an S.G. Cast Iron", Wear, 14, 107-117.

23. EYRE, T.S. & BAXTER, A.M. (1972): "The Formation of White Layers at Rubbing Surfaces", Tribology International, 256.

24. EYRE, T.S & CRAWLEY, B. (1980): "Camshaft and Cam Follower Materials", Tribology International, 147.

25. FORREST, R.D. (1987): "The Challenge and Opportunity Presented to the S.G. Iron Industry by the Development of Austempered Ductile Iron", Proc. Conf. S.G. Irons - The Next 40 yrs, Univ. of Warwick, BCIRA, 24-1.

26. FINK,M. (1930): "Wear Oxidation - a New Component of Wear", Am.SOC. for Steel Treating, 18, 1026.

27. FRANETOVIC, V. SACHDEV, A.K. & RYTNZ, E.F. (1987): " A Transmission Electron Microscopy Study of Austempered Lower Bainitic Nodular Iron", Metallography 20, 15-36.

28. GOOD, J.N. & GODFREY, D. (1947): "Changes Found on Run in Scuffed Surfaces of Steel, Chrome Plate and Cast Iron", NASA Tech. note, 1432.

29. GRIFFITHS, B.J. (1983): "White Layer Formation at Machining Surfaces and their Relationship to White Layer Formation at Worn Surface", Brunel Univ. UK.

30. HARDING, R.A. (1986): "Heat Treatment Plant for Austempering Ductile (SG) Iron", BICRA Report 1650.

31. HAMILTON, G.M. (1980): "The Hydrodynamics of a Cam Follower", Tribology International, 133.

32. HARRIS, D.A. & MAITLAND, R.J. (1970): " The Effect of Austenitizing of Lower Bainite in a Spheroidal Cast Iron", Iron and Steel, 325-238.

33. HURRICKS, P.L. (1974): "The Fretting Wear of Mild Steel from 200°C to 500°C", Wear, 30, 189.

34. ISHIHARA, Y. (1986): " Mechanical Properties of Austempered Ductile Iron at Elevated and Low Temperature", Proc. Conf. 2nd International Conference on Austempered Ductile Iron, Univ. Michigan, ASME, 237-236.

35. JANOWAK, J.K. & GUNLACH, R.B. (1983): "Development of a Ductile Iron for Commercial Austempering:, AFS Transactions, 499-508.

36. JANOWAK, J.K. & GUNLACH, R.B. (1984): "A Review of Austempered Ductile Iron Metallurgy", Proc. Conf. 1st International Conference on Austempered Ductile Iron, ASM, Chiicago, 1-12.

37. JOHANSSON, M. (1977): "Austenitic-Bainitic Ductile Iron", AFS Transactions 85, 117-122.

38. KARSAY, S.I. (1976): "Ductile Iron Production Part I", Quebec Iron and Titanium Corporation.

39. KAWAMOTO, M. & OKABAYASHI, K. (1979): "Study of Dry Sliding Wear of Cast Iron as a Function of Surface Temperature", Wear, 58, 59.

40. KAWAMOTO, M. & OKABAYASHI, K. (1980): "Reply to Comments on The Unlubricated Wear of Cast Iron", Wear, 65, 399.

41. KAYABA, T. & IWABUCHI, A. (1981): "The Fretting Wear of 0.45 Percent Carbon Steel and Austenitic Stainless Steel From 20 C up to 650 C in Air",Int. Conf. Wear of Materials, San Fransico, ASME, 229.

42. KERRIDGE, M. (1955): "Metal Transfer and the Wear Process", Proc. Roy. Soc., B68, 400.

43. KUBASCHEWSKI, O. & HOPKINS, B.E. (1962): "Oxidation of Metals and Alloys", Butterworths London.

44. LIM, S.C. & BRUNTON, J.H. (1986): "The Unlubricated Wear of Iron", Wear, 113, 383.

45. MILLS, P. & SULLIVAN, J.L. (1983): "A Study of the Core Level Electrons in Iron and Its Three Oxides", J.Phy.D., 16, 723.

46. MOLGAARD, J. & SRIVASTAVA, V.K., (1975): "The Activation Energy of Oxidative wear", Wear, 41, 263-270.

47. MONTGOMERY, R.S. (1969): "Run-In and Glaze Formation on Gray Cast Iron Surfaces", Wear, 14, 99.

48. MOORE, D.F. (1975): "Principles and Applications of Tribology", International Series on Materilas Science and Technology, 14, Pergamon Press, Oxford.

49. MORROGH, H. (1987): "S.G. Irons - in Retrospect and for the Future", Proc. Conf. S.G. Irons - The Next 40 yrs, Univ. of Warwick, BCIRA.

50. MORTON, P.A. " Unpubliced Researched" Climax Molybedenum Co.

51. OXX, G.D. (1958): "Which Coating at High Temperature", Prod. Eng., 29 (1958), 61.

52. PEACH, P.W. & BORLAND, D.W. (1982): "The Unlubricated Wear of Flake Graphite Cast Iron", Wear, 85, 257.

53. QUINN, J.F. (1962): "The Role of Oxidation in the Mild Wear of Steel", Brit. J. Appl. Phys., 13, 33.

54. QUINN, J. F. (1967): "The Effect of 'Hot Spot' Temperatures on the Unlubricated Wear of Steel", ASLE Trans., 10, 158.

55. QUINN, T.F. (1971): "The Application of Modern Physical Techniques to Tribology", Newnwes-Butterworths London, 1-33.

56. RABINOWICZ, E. & TABOR, D. (1951): "Metallic Transfer Between Sliding Metals", Proc. Roy. Soc., A208, 455.

57. RABINOWICZ, E. (1953): "A Quantitative Study of the Wear Process", Proc. Roy. Soc., B66, 929.

58. ROLLANSON, F.C. (1973): "Metallurgy for Engineers", 4th Edition, Edward Arnold Ltd.

59. ROSENBERG, S.J. & JORDAN, L. (1935): "The Influence of Oxide Films on the Wear of Steels", Trans.Am.Soc.Metals, 23, 577

60. ROYLANCE, B. J. & POCOCK, G. (1983): "Wear Studies Through Particle Size Distribution, Part I: Application of Weibull Distribution to Ferrography", Wear, 90, 113.

61. RUNDMAN, K.B. & KLUG, R.C. (1982): "An X-Ray and Metallurgical Study of an Austempered Ductile Cast Iron", AFS Transactions, 499-508.

62. SHEPPERSON, S. & ALLEN, C. (1988): "The Abrasive Wear of Austempered Spheroidal Cast Irons", Wear, 121, 271-287.

63. STEED, J. (1918): "Micro-Metallurgy and its Pratical Application", J.West. Scot. Iron and Steel Ind.,19,169.

64. SUGISHITA, J. & FUJIYOSHI, S. (1981): "The Effect of Cast Iron Graphites on Friction and Wear Performance, Part I: Graphite Film Formation on Grey Cast Iron Surfaces", Wear, 66, 209.

65. SULLIVAN, J.L. (1987): "The Role of Oxides in the Protection of Tribological Surfaces - Part 1", Proc. Conf. Tribology, Friction, Lubrication and Wear - Fifty Years on, Vol. 1, IMechE, 283-295.

66. SULLIVAN, J.L. (1987): "The Role of Oxides in the Protection of Tribological Wear Surfaces, Part 2", Proc. Conf. Tribology, Friction, Lubrication and Wear - Fifty years on, Vol. 1, 293.

67. TIMOSHENKO, S. (1934): "Theory of Elasticity", Mc Graw Hill, New York.

68. TOA, F.F. (1969): "A Study of Oxidation Phenomena in Corrosive Wear:", ASLE Trans., 12, 97.

69. WELSH, N.C. (1964): "The Dry Wear of Steels, Part I - The General Pattern of Behaviour", Phil. Trans. Roy. Soc., 257A, 31.

70. WELSH, N.C. (1964): "The Dry Wear of Steels, Part II - Interpretation and Special Features", Phil. Trans. Roy. Soc., 257A, 51.

71. WELSH, N.C. (1975): "Frictional Heating and its Influence on the Wear of Steels", Proc. Roy. Soc.,A259, 228.

72. YOSHIMOTO, G. & TSUKIZOE, T. (1957): "On the Mechanism of Wear Between Metal Surfaces", Wear 1, 472

APPENDIX 1: Method for the Determination of the Quantilty of Retained Austenite in ADI

DETERMINATION OF RETAINED AUSTENITE IN A MARTENSITE MATRIX USING X RAY DIFFRACTION

The Problem

Austenite is a solid solution of iron with a cubic structure. When cooled rapidly there is a metastable shear transformation which yields matensite. Depending on the composition and applied cooling rate, austenite may be retained in the composition. Since the mechanical properties of a steel depend on the ratio of martensite (-body centred tetragonal phase) and austenite (γ-FCC phase) determination of the amount of retained austenite is essential.

Methods of Determining Retained Austenite

Both austenite and martensite have the same chemical composition and their solubility in any known solvent is identical. Hence a determination of their quantities by chemical means is not possible.

Optically the microstructure of retained austenite and martensite are indistinguishable. However, the physical properties of austenite and martensite are different e.g. the magnetic behaviour and the coefficient of expansion differ. These properties can be used in estimates of the retained austenite content.

More commonly used methods are those that are able to distinguish between the two crystal structures of austenite and martensite. Two such successful methods are Mossbauer spectrography and X-ray diffraction. By far the simplest method is X-ray diffraction and was used in this study.

Theory

Quantitative X-ray diffraction analysis for determination of the relative amounts of two phases in a mixture requires the comparison of the intensities of two suitable reflections (hkl) of both phases. These reflections must not coincide with any other K_α reflection. They should also be fairly close to each

other to avoid systematic errors. For the austenite/martensite mixture the diffraction lines best meeting these requirements are the (200) reflection of the martensite, and the (220) reflection of the austenite.

Integrated intensities are used to compare the two peaks i.e. the area under the diffraction peaks. The integrated intensity of a reflection (hkl) can be expressed as follows :

$$I\,(hkl) = K.FF.LP.\ m.\ e^{-2m}.A(\theta)\left(\frac{V}{v^2}\right) \qquad (1)$$

where

- K = Proportionality constant, depending on the intensity of the radiation used and the crystal size of the sample.
- FF = The product of the structure factor and its complex conjugate for the reflection (hkl).
- LP = Lorentz-polarisation factor, for sample without texture, this factor can be simply tabulated as a function of the Bragg angle.
- m = Multiplicity factor for the (hkl) plane
- e^{-2m} = Debye-Waller temperature factor
- $A(\theta)$ = Absorption factor, the irradiated volume and hence the absorption factor are constant for every angle (θ) if the specimen surface is plane.
- V = The relative volume of the phase to be analysed.
- v = The volume of the elementary cell of the component which gives the reflection (hkl).

The proportionality constant and the absorption factor have the same value for the intensities $I_\gamma(220)$ and $I_\alpha(200)$. For the ratio P of these intensities the formula becomes

$$P = \frac{I\ (220)}{I\ (200)} = \frac{FF.\ LP.\ e^{-2m}\ \frac{V_\gamma}{v_\gamma^2}\ m\ (220)}{FF.\ LP.\ e^{-2m}\ \frac{V_\alpha}{v_\alpha^2}\ m_\alpha(200)} \qquad (2)$$

The numerical values using Mo radiation for these factors are as follows :

	Austenite	Martensite
FF	$(536)^2$	$(288)^2$
LP	23	30
e^{-2m}	0.80	0.84
m	12	6
v	$(3.58)^3$	$(2.86)^3$

Substituting these values yields

$$P = \frac{1.31V_\gamma}{V_\alpha} \qquad (3)$$

This method is reliable where only the 2 phases, martensite and austenite exist. If a third phase such as ferrite is present it cannot be used. For the partial volumes V_α and V_γ the following equation applies

$$V_\alpha + V_\gamma = 1 \qquad (4)$$

Combining (3) and (4) yields the following expression for the partial volumes of the austenite phase

$$V_\gamma = \frac{P}{P + 1.31} \qquad (5)$$

If carbides are present their quantity may be estimated from metallographic investigations. Equations (4) and (5) will then be slightly different. As X-rays only penetrate a thin layer beneath the surface of a specimen (2 um for Mo radiation) and the volume examined is comparatively small, the physical condition of the surface layer is of great importance. Care must be taken to prevent undue heating of the austenite. To prepare the surface for X-ray diffraction the specimen is mechanically polished down 0.25 um and then lightly etched with 2.5% nital to remove any strained material.

Diffractometer conditions

For this study, the conditions used for the determination of retained austenite are listed. These conditions were based on information taken from a Philips Scientific report and experience on the diffractometer.

Radiation	Mo K_α
Voltage	45 Kv
Current	30 MA
Range	10^3
Window	40
Time constant	1 sec
Bragg angle (200)	28.6°
Bragg angle (220)	32.5°
Filter	Zr
Divergence slit	1°
Receiving slit	0.2 mm
Scatter slit	1°
Scanning speed	2°/minute
Chart speed	4cm/minute

Calculation

A trace (fig. A) consists of two peaks, the (220) and the (200) peaks. To find the integrated intensity ratio, it is necessary to divide the total integrated intensity of the (200) peak by that of the (220) peak. In order to do this, the integrated intensity for each peak separately must be known i.e. the total intensity above the background intensity. Thus the average counts of the background taken over the same angular spread as the peak is subtracted from the total counts under the peak. Having calculated this for each peak, the integrated intensity ratio can be calculated, i.e.

$$P = \frac{(220)_\gamma \text{ total counts - background counts}}{(200)_2 \text{ total counts - background counts}}$$

$$P = \frac{\text{Austenite peak counts}}{\text{Martensite peak counts}}$$

then $V_\gamma = \frac{P}{P + 1.31}$ where V = volume fraction of retained austenite

Example

Background 1	Martensite	Background 2	Austenite	Background 3
26.85-27.65	28.10-29.70	30.20-31.00	31.00-32.66	32.60-33.40
= 0.80°	= 1.6°	= 0.80°	= 1.6°	= 0.8°
27067	75573	22902	49338	24437

Martensite Peak = 75573 - (27067 + 22902) = 25604

Austenite Peak = 49338 - (22902 + 24437) = 1999

$$P = \frac{1999}{25604} = 0.078$$

$$V_\gamma = \frac{0.078}{1.31 + 0.078} = 0.562$$

= 5.62% retained austenite

The sensitivity, reproducability and accuracy of X-ray diffraction measurements are discussed by Averbach and Cohen (56). Sensitivity depends largley upon the radiation used and monochromatic is necessary for maximum sensitivity. Reproducability is high with standard deviation as good as 0.2%. Supposedly the lower limit of determination of retained austenite by XRD. The standard deviation for the reproducability for this investigation was ± 0.8%. Accuracy however is more difficult to measure due to the problem of obtaining relaible standards, but Averbach and Cohen (56) indicate that it is adequate above 1% retained austenite.

X.R.D. TRACE FOR MARTENSITE, RETAINED AUSTENITE STRUCTURE